

بِسْمِ اللَّهِ الرَّحْمَنِ الرَّحِيمِ



Sudan University of Science and Technology



College of Graduate Studies

**Preparation of NiO / Cobaltite Nanosheets and their Application in
Cathode of High-Performance Lithium-Sulfur Batteries**

تحضير الصفائح النانوية من أكسيد النيكل / الكوبالتيت وتطبيقها في كاثود بطاريات الليثيوم
والكبريت عالية الأداء

**A thesis Submitted for the Fulfillment of the degree of Doctor of
Physics**

By:

Salma Abualela Aldirdiri Abuadhab

Supervisor: Prof. Mubarak Dirar Abdalla

Co-supervisor: Dr. Sohad Saad Elwakeel

June 2022

الآية

قال تعالى:

بسم الله الرحمن الرحيم

اقرأ باسم ربك الذي خلق (1) خلق الإنسان من علق (2) اقرأ وربك الأكرم (3) الذي علم بالقلم (4) علم الإنسان ما لم يعلم (5) كلاً إنَّ الإنسان ليطغى (6) أن رآه استغنى (7) إنَّ إلى ربك الرجعى (8) أرايت الذي ينهى (9) عبداً إذا صلى (10) أرايت إن كان على الهدى (11) أو أمر بالتقوى (12) أرايت إن كذب وتولى (13) ألم يعلم بأن الله يرى (14) كلا لئن لم ينته لنسفعا بالناصية (15) ناصية كاذبة خاطئة (16) فليدع ناديه (17) سندع الزبانية (18) كلا لا تطعه واسجد واقترب (19).

سورة العلق

Dedication

Every challenging work needs self-efforts as well as guidance of elders especially those whom are very close to our heart.

I wish to dedicate this humble effort to the best Mum in the world, my beloved father, my husband and my children and to all my brothers and sisters, for their continuous love, encouragement and support.

Acknowledgment

First and foremost, I would like to thank Almighty God for granting me the capability and providing me health and opportunity to finish this work,

I offer my sincerest gratitude to my supervisor, Professor Mubarak Dirar Abdalla, Xiong Jie for the patient guidance, encouragement. Despite their many research projects, but they are with me in every step I have done with guidance and care. I consider myself very fortunate for being able to work with a very considerate and encouraging professors like them.

I will never ever forget my assistant supervisor, Dr Sohad Saad Elwakeel, Xiaoxue Lv, and Yin Hu, for his kind care, patient guidance, worthy advice and encouragement. Indeed, this study would not be possible to be done if it was out of their support in different parts

Also, I would like to thanks all my lab-mates for the great effort and valuable advices and support in many sectors of this work,

I would like to thank the University of Electronic Science and Technology of China Authority for giving me access to their facilities used during this research.

Abstract

Lithium sulfur batteries Li-S Lithium-sulfur (Li-S) batteries are under intense investigation for nearly three decades as one of the most promising energy storage devices due to its high theoretical capacity of 1675 mAh/g and the theoretical high theoretical density of 2567 Wh/kg. Other advantages include natural abundance, low cost and environmental dignity, and the characteristics of long cycling, making sulfur more attractive such as cathode for rechargeable batteries. However, lithium and sulfur batteries are not used in industries due to some critical issues, such as the disintegration of the polysulfide during cycling which causes the so-called "shuttle effect" with its associated fast loss of power and the low capacity of Coulomb's efficiency and expansion in the large volume of 80% ~ Generation of sulfur elements to Li_2S . In order to achieve the superior electrochemical performance of (Li-S), this thesis focused on addressing the above issues by designing and manufacturing new cathode materials. Transition metal oxides have a great promise as the high-performance electronic cathode material for lithium batteries. In this study, NiO nanosheets on carbon cloth (CC) was prepared via a simple chemical bath method, it is the hierarchy matrix and used as a cathode material for LSBs. And also, the hybrid nanostructure (NiCo_2O_4) was manufactured via a facile atmospheric and water-based method, and designed as cathode additive for Li-S batteries. The nano structures of CC and NiO/CC composite and also NiCo_2O_4 were probed using X-ray diffraction (XRD) technique and scanning electron microscope (SEM). Cyclic voltammetry (CV) and galvanostatic charge/discharge measurement were performed on CHI660c electrochemical

workstation. The relationship between current and voltage of the working electrode were measured by Cyclic Voltammetry (CV) at different scan rates.

The compound (CC / NiO/S) containing sulfur content is 80% by weight. The compound pole provides a high discharge capacity of 1154.8 mAh/g at 0.1C, a specific capacity of 661.9 mAh/g can be obtained, with a low decay rate of 0.07% per cycle over 300 cycles. At the current densities of 0.5, 1, 2, 3, 4 and 5 mA cm², the specific capacities of 1008.8, 761.6, 596.5, 526.2, 442.2 and 416.9 mAh/g can be achieved, respectively, indicating excellent rate performance. Besides, a capacity of 1004.4 mAh/g is observed when the current density reduces back to 0.5 mA cm², indicating high reversibility of the NiO/CC/S composite electrode after high-rate cycling. Excellent capabilities and periodic stability arise from many unique functional features of the cathode. Carbon fiber works to improve the transfer of ion / electron with the absorption of expanding size, NiO nanosheets play an important role in limiting the dissolution of polysulfides by chemical bonds with sulfur. And also, electrochemical measurements reveal that the NiCo₂O₄ electrode exhibits an initial specific capacity of 1399.8 mAh/g at the current density of 0.1C. The mesoporous NiCo₂O₄ nanoparticles can provide abundant adsorption sites to confine polysulfides and facilitate the ionic transport. This work may provide a promising method for preparing high-performance cathodes of Li-S batteries.

المستخلص

بطاريات الليثيوم الكبريتية (Li-S) قيد التحقيق المكثف لما يقرب من ثلاثة عقود كواحدة من أكثر أجهزة تخزين الطاقة الواعدة نظرًا لقدرتها النظرية العالية البالغة 1675 مللي أمبيرساعة / جرام والكثافة النظرية العالية لـ 2567 واط / كغم تشمل المزايا الأخرى الوفرة الطبيعية والتكلفة المنخفضة والكرامة البيئية وخصائص ركوب الدراجات الطويلة ، مما يجعل الكبريت أكثر جاذبية مثل الكاثود للبطاريات القابلة لإعادة الشحن. ومع ذلك ، لا يتم استخدام بطاريات الليثيوم والكبريت في الصناعات بسبب بعض المشكلات الحرجة ، مثل تفكك البولي سيفيد أثناء ركوب الدراجات مما يتسبب في ما يسمى بـ "تأثير الموك" وما يرتبط به من فقدان سريع للطاقة والقدرة المنخفضة لكفاءة كولوم والتوسع في الحجم الكبير بنسبة 80٪ ~ توليد عناصر الكبريت إلى Li_2S . من أجل تحقيق الأداء الكهروكيميائي المتفوق لـ (Li-S)، ركزت هذه الأطروحة على معالجة القضايا المذكورة أعلاه من خلال تصميم وتصنيع مواد كاثود جديدة. تتمتع أكاسيد المعادن الانتقالية بوعد كبير باعتبارها مادة الكاثود الإلكترونية عالية الأداء لبطاريات الليثيوم. في هذه الدراسة ، تم تحضير صفائح NiO النانوية على قطعة قماش كربونية (CC) بطريقة حمام كيميائية بسيطة ، وهي عبارة عن مصفوفة هرمية وتستخدم كمادة كاثودية لـ LSBs. وأيضًا ، تم تصنيع البنية النانوية الهجينة ($NiCo_2O_4$) عبر طريقة سهلة في الغلاف الجوي والماء ومصممة كاثود مضاف لبطاريات Li-S. تم فحص الهياكل النانوية لمركب CC و NiO / CC ، وأيضًا $NiCo_2O_4$ باستخدام تقنية حيود الأشعة السينية (XRD) ومسح المجهر الإلكتروني (SEM). وتم إجراء قياس الفولتية الدوري (CV) وقياس الشحن / التفريغ الجلفانيساتاتيكي على محطة العمل الكهروكيميائية CHI660c. وتم قياس العلاقة بين التيار والجهد الكهربائي للقطب العامل عن طريق قياس الفولتميتر الدوري (CV) بمعدلات مسح مختلفة. وفر القطب المركب (CC/NiO/S) المحتوي على الكبريت بوزن 80٪ سعة تفريغ عالية تبلغ 1154.8 مللي أمبيرساعة / جم عند 0.1 كولوم، وتم الحصول على سعة محددة تبلغ 661.9 مللي أمبيرساعة / جرام ، مع معدل تضاؤل منخفض يبلغ 0.07٪ لكل دورة على مدى 300 دورة. عند الكثافات الحالية البالغة 0.5 ، 1 ، 2 ، 3 ، 4 ، 5 مللي أمبير سم² ، يمكن تحقيق السعات المحددة 1008.8 ، 761.6 ، 596.5 ، 526.2 ، 442.2 و 416.9 مللي أمبيرساعة / جرام ، على التوالي ، مما يشير إلى أداء معدل ممتاز. إلى جانب ذلك ، يتم ملاحظة سعة 1004.4 مللي أمبير / جرام عندما تنخفض الكثافة الحالية مرة أخرى إلى 0.5 مللي أمبير سم² ، مما يشير إلى قابلية انعكاس عالية للقطب

المركب NiO / CC / S بعد ركوب الدراجات عالي المعدل. تنشأ القدرات الممتازة والاستقرار الدوري من العديد من الميزات الوظيفية الفريدة للكاثود. تعمل ألياف الكربون على تحسين نقل الأيونات / الإلكترون مع امتصاص الحجم المتوسط ، وتلعب الصفائح النانوية NiO دورًا مهمًا في الحد من انحلال polysulfides بواسطة الروابط الكيميائية مع الكبريت . وأيضًا ، تكشف القياسات الكهروكيميائية أن القطب الكهربائي NiCo₂O₄ يعرض سعة أولية محددة تبلغ 1399.8 مللي أمبير ساعة / جرام عند الكثافة الحالية البالغة 0.1 كولوم. يمكن للجسيمات النانوية المسامية من NiCo₂O₄ توفير مواقع امتزاز وفيرة لحصر البولي كبريتيد وتسهيل النقل الأيوني. قد يوفر هذا العمل طريقة واحدة لإعداد كاثودات عالية الأداء لبطاريات Li- S.

Contents

Items	Page No.
الأية	I
Dedication	II
Acknowledgement	III
Abstract (English)	IV
Abstract (Arabic)	VI
Contents	VIII
List of tables	XI
List of figures	XII
List of Abbreviations	XVI
Chapter one: Introduction	
1.1 Background of Energy Storage Researches	1
1.2 Rechargeable Batterie	1
1.3 Principles of Operation of Rechargeable Batteries	3
1.4 Lithium-Ion batteries	5
1.4.1 Operating Principles	5
1.4.2 LIB Limitations	6
1.5 Lithium Sulfur Batteries	7
1.5.1 The Mechanism of Discharge and Charge	8
1.5.2 Lithium-Pure Sulfur Batteries	10
1.5.3 Problems	12
1.5.3.1 Sulfur Blocking Issue in Cathode	13
1.5.3.2 The Spread of Polysulfide between Cathode and Anode	14
1.5.3.3 Erosion of Lithium Metal	15
1.6 Research problem	15
1.7 Project Objective	16
1.8 thesis Layout	17

Chapter two: Literature Review	
2.1 High-Performance Anodes	18
2.2 Compound Cathodes	19
2.3 Electrolytes	34
2.4 Modified Separators	40
Chapter three: Material Characterizations and Electrochemical Measurements	
3.1. The Chemicals and Materials	44
3.2 Experimental Steps	46
3.3 Material Synthesis	47
3.4 Material characterizations	48
3.4.1 X-Ray Diffraction	48
3.4.2 Scanning Electron Microscope	49
3.4.3 Brunauer-Emmett-Teller	52
3.5 Electrochemical Measurements	54
3.5.1 Electrode Fabrication	54
3.5.2 Electrochemical and Cell Assembly Testing	54
3.5.3 Electrochemical Characterizations	55
3.5.3.1 Cyclic Voltammetry	55
3.5.3.2 Galvanostatic cycling measurement	55
3.5.3.3 Electrochemical Impedance Spectroscopy	56
Chapter four: NiO Nanosheets Grown on Carbon Cloth as Mesoporous Cathode for High Performance Lithium-Sulfur Battery	
4.1 Introduction	57
4.2 Experimental	58
4.2.1 Materials	58

4.3.1 Synthesis of NiO Nanosheets/Carbon Cloths	58
4.3.2 Preparation of NiO/CC/S	59
4.3 Results and Discussions	59
4.3.1 Physicochemical Properties of the Materials	59
4.3.2 Electrochemical Performance of the S/NiO/CC and S/CC Composite	62
4.4 Conclusion	68
Chapter five: Mesoporous NiCo₂O₄ nanoparticles as cathode additive for high-performance lithium sulfur battery	
5.1 Introduction	70
5.2 Experimental Section	71
5.2.1 Materials Synthesis	71
5.2.2 Materials Characterization	72
5.2.3 Electrochemical Measurements	72
5.3 Results and Discussion	73
5.4 Conclusion	77
5.5 Recommendations for Study Future	79
References	80

List of Tables

Table	Item	Page No.
1.1	Cell voltages, theoretical specific energies and densities for several kinds of batteries.	3
2.1	Table shows In LSBs, comparison of electrochemical performance of pure sulfur cathodes.	12
3.1	Table shows Chemicals and materials for Synthesis and Electrochemical tests.	44
3.2	Table shows Used on the instrument's experiments.	45

List of Figures

Figure	Item	Page NO.
Figure 1.1	Specific practical capacities of some rechargeable batteries, with estimated driving distances and package prices side by side.	2
Figure 1.2	Schematic of a discharge plan in a general rechargeable battery.	4
Figure 1.3	(a) Schematic illustrating the operating principle of a rechargeable LIB with graphite as the anode material and LiCoO_2 as the cathode material	5
Figure 1.4	Schematic of the configuration and operation of lithium-sulfur batteries.	7
Figure 1.5	Schematic illustration of a typical lithium-sulphur (Li-S) cell.	8
Figure 1.6	(a) Schematic of a LSB consisting of lithium anode, electrolyte and sulfur cathode and (b) the typical discharge/charge curves (c) The voltage profile and chemistry of sulphur cathode in the organic electrolyte.	10
Figure 1.7	Electrochemical performance of a lithium-pure sulfur battery. (a) The Charge/discharge curves in the first cycle and (b) the cyclic performance at 0.1C (1C= 1675 mA/g).	11
Figure 2.1	Hierarchical designs of carbon-based sulfur composites: (a) microporous carbon spheres, (b) spherical ordered mesoporous carbon nanoparticles, (c) porous hollow carbon, (d) graphene oxide sheets, (e) porous carbon nanofibers, and (f) hollow carbon nanofibers.	21
Figure 2.2	The polymer summary shows the conductivity applied in Li-S batteries.	23
Figure 2.3	Polymer-sulfur composites: (a) PEDOT: PSS spheres(b) PPy tubes(c) PT spheres and (d) PANI nanofibers, to encapsulate sulfur.	24
Figure 2.4	(a) Schematic of preparation of S/PANI yolk-shell nanoparticles, (b) TEM image of nanoparticles with SEM image in inset and (c) cyclic tests at 0.2 and 0.5 C.	24
Figure 2.5	(a) Schematic preparation process and (b) cyclic performance of the sulfur- TiO_2 yolk-shell composite.	25
Figure 2.6	SEM images of active materials: (A) neat NiO; (B) NiO/C composite.	26

Figure 2.7	(a) Profiles of the NiO/S, RFG/S and RFG–NiO/S electrodes for the first cycles under a current density of 0.1C, (b) Cyclic voltammograms of Capacity retention and Coulombic efficiency at a current density of 0.1C (c) Rate performance of NiO/S, RFG/S and RFG–NiO/S composite electrode at various current densities and (d) Cyclic voltammograms of Capacity retention and Coulombic efficiency at a current density of 0.5 C.	27
Figure 2.8	(a, b) SEM and TEM micrographs of the nickel hydroxide and after annealing at 400 C ° GCD. Profiles of (c) the S and (d) NiO (400 C °)/S electrodes for the first three cycles under a current density of 0.2C.	28
Figure 2.9	(a) SEM images of NiO–graphene composite. (b) Cyclic voltammograms of Capacity retention and Coulombic efficiency at a current density of 200 mA g ⁻¹ .	29
Figure 2.10	(a) SEM image of sheet-like Ni-based precursor; (b) SEM image of NNN sample; (c), the cycle numbers are 1 st , 2 nd , 5 th , 10 th , 20 th , 30 th and 50 th from right to left, respectively (d) Long-term discharge stability tests of NNN-S80 and S cells at 2C and 5C.	30
Figure 2.11	(a) Charge and discharge voltage profiles of (NCO-NFs/S) and S composite electrodes for the first cycle at 0.2 C. (b) Cyclic voltammograms of Capacity retention and Coulombic efficiency at a current density of 1 C.	31
Figure 2.12	Characterization of the NiCo ₂ O ₄ nanofibers and S/ NiCo ₂ O ₄ composite. a, b) Scanning electron microscope (SEM) images NiCo ₂ O ₄ nanofibers. c) TEM image of NiCo ₂ O ₄ nanofibers and the corresponding SAED pattern. d) HRTEM image of NiCo ₂ O ₄ nanofibers. Electrochemical characterization of e) Long-term cycle performance of the S/ NiCo ₂ O ₄ and S/CNF composites at 1 C rate.	32
Figure 2.13	(a) and (b)The constant discharge/ charge profiles of the hollow NiCo ₂ O ₄ /S composites and pure sulfur electrode at 0.2 C, respectively. (c) and (e), (f)TEM images Hollow NiCo ₂ O ₄ Nano cages and NiCo ₂ O ₄ /S composites.	33
Figure 2.14	(a and b) SEM images of NiCo ₂ O ₄ hollow microtubes, (b) Cyclic voltammograms of Capacity retention and Coulombic efficiency at a current density of 0.5 C.	34
Figure 2.15	(a) Schematic illustration of the Pyr _{1,201} TFSI/TEGDME electrolyte with LiTFSI as lithium salt in LieS cell; b) Cross-section SEM image of lithium metal cycled in 50% I L containing electrolyte for 100 cycles at 0.2 C. c) Cycling performance of the Li–S batteries with the LiTFSI-P _{1,201} TFSI/ (30 wt%) TEGDME electrolyte.: (d) Molecular structures and sizes of the electrolyte components: Pyr _{1,201} TFSI, TEGDME, LiTFSI, and LiODFB.	37

Figure 2.16	The schematic cell configuration of rechargeable Li-S: (a) traditional Configuration with severe shuttle effect and Li ₂ S poison problems and (b) new configuration with an interlayer.	39
Figure 2.17	SEM images of interlayers made from (a) PPy nanotubes, (b) carbonized eggshell membrane, (c) CNTs, (d) reduced graphene oxide, (e) mesoporous carbon, and (f) nickel foam.	39
Figure 2.18	(a) Schematic of a Li-S cell with a bifunctional microporous carbon interlayer inserted, (b) Prototype LiS coin cell configuration with a carbon interlayer in the cathode region. (c) Electrochemical performance of the LiS cell with a MWCNT interlayer at 0.5 C rate.	40
Figure 2.19	(a) Schematic and SEM images of the single-wall carbon nanotube modulated separator configuration. Cross-section SEM images of various samples b)) N-doped porous carbon nanowire-modified separator c) cell with the C-coated separator, d) N-doped mesoporous carbon-coated separator e, f) TiO ₂ -Super P coated separator-cathode interface and the Al ₂ O ₃ -Super P coated separator-cathode interface g) Integrated sulfur electrode with the G@PP separator and corresponding EDS spectrum and h) fluoro-functionalized reduced graphene oxide separator.	42
Figure 2.20	Schematic configuration of the Li-S with (a) a pristine separator; (b)mesoporous carbon-coated separator; SEM images of (c) top surface of the mesoporous carbon-coated separator and (d) cross-section and.	43
Figure3.1	Comprehensive procedures and techniques.	46
Figure 3.2	Schematic of a chemical bath deposition.	47
Figure 3.3	Illustration of X-ray diffraction and Bragg equation.	48
Figure 3.4	Schematic illustrating the operation and layout of a SEM.	51
Figure 3.5	Schematic illustrating the interaction between the incident electron beam and the sample.	51
Figure 4.1	Schematic illustrating the Synthesis of NiO nanosheets/carbon cloths.	59
Figure 4.2	X-ray diffraction (XRD) patterns of (a) Ni (OH) ₂ and (b) NiO on the carbon cloth.	60
Figure 4.3	Nitrogen adsorption/desorption isotherms and pore size distribution (inset) of the (a) CC and (b) NiO/CC composite.	61

Figure 4.4	SEM images of (a) Pure carbon cloth, (b) NiO Nanosheets grown on carbon cloth (inset, low magnification image), and (c) micro structure of NiO Nanosheets. (d) Typical SEM image for a selected region of the NiO/CC composites, and the corresponding elemental mapping of (e) O and (f) Ni.	62
Figure 4.5	(a) Charge and discharge voltage profiles of NiO/CC/S and CC/S composite electrodes for the first cycle at 0.1C. (b) Rate performance of NiO/CC/S composite electrode at various current densities. (c) Cycle capacity and Coulombic efficiency of NiO/CC/S and CC/S composite electrodes at a current density of 2.0 mA cm ² (~1C).	64
Figure 4.6	Electrochemical performance of the S/NiO/CC and S/CC composites (sulfur loading: 1.5–3.0 mg cm ⁻²). (a, b) Comparison of discharge–charge profiles of the S/NiO/CC and S/CC composites at 0.2 C rate. (c) Cycle capacity and Coulombic efficiency of NiO/CC/S and CC/S composite electrodes at a current density of 1.5 mA cm ² . (d) Cycle capacity and Coulombic efficiency of NiO/CC/ at a current density of 2.5 mA cm ² . (e) Cycle capacity and Coulombic efficiency of NiO/CC/S at a current density of 3.0 mA cm ² and (f) Cycle capacity and Coulombic efficiency of CC/S composite electrodes.	65
Figure 4.7	CVs of the NiO /CC /S electrodes at a scan rate of 0.1 mV s ⁻¹ between 1.7 and 2.7 V	66
Figure 4.8	EIS of the hollow NiO/CC/S composites electrode.	67
Figure 5.1	SEM images of NiCo ₂ O ₄ nanoparticles. The scale bars are (a) 1 μm and (b) 300 nm, respectively.	73
Figure 5.2	(a) XRD patterns and (b) N ₂ adsorption-desorption isotherm and pore size distribution curve (inset) for NiCo ₂ O ₄ sample.	74
Figure 5.3	Electrochemical performances of the NiCo ₂ O ₄ /sulfur composites electrode. (a) The discharge/charge profiles. (b) Rate capability. (c) Cycle performance at 0.5 C. (d) CV curves at different scan rate.	76

List of Abbreviations

Abbreviation	statement
CC	Carbon Cloth
CBP	Cobalt Based Precursors
PMMA	Poly- (Methyl Methacrylate)
PET	Polyethylene-Terephthalate
EtOH	Ethanol
EG	Ethylene Glycol
PEG	Polyethylene Glycol
Co (NH ₂) ₂	Urea
CH ₄ N ₂ S	Thiourea
TETA	Triethylenetetramine
PVDF	Polyvinylidene Fluoride
NMP	N-Methyl-2-Pyrrolidone
LiTFSI:	Lithiumbis (Trifluoromethanesulfonyl)Imide
S.C	acetylene black
CBD	Chemical Bath Deposition
LSB	Lithium- Sulfur Batteries
EDL	Electric Double Layer
BET	Brunauer–Emmett–Teller
BJH	Barrett–Joyner–Halenda
EDX	Energy-Dispersive X-ray spectroscopy

PVDF	Poly (Vinylidene Difluoride Source Axial Distance technique)
CV	Cyclic Voltammogram
SAED	Selected-Area Electron Diffracts
XRD	X-ray Diffractometry
EDS	Energy Dispersive Spectroscopy
SEM	Scanning Electron Microscope

Chapter one

Introduction

1.1 Background of Energy Storage Researches

As life evolves and population increases, our demands for energy consumption in the form of fossil fuels are increasing to achieve an advanced lifestyle, leading to severe environmental problems, such as air pollution and global warming. To mitigate this problem, renewable sources and new energy technologies, such as solar, wind, and geothermal energy, must be used. However, given these alternative energy forms continuously, energy storage is a useful topic. Rechargeable batteries are one of the most viable options. Battery technology must be improved to meet the growing power requirements of electronic devices and applications, portable electronics and smart networks are common examples of applications that require improved battery technology. In commercial terms, electric vehicles will become more efficient, reducing reliance on gasoline-powered vehicles and thus reducing carbon emissions associated with these vehicles. Thus, this optimization will have a beneficial effect for many different technological applications [1].

1.2 Rechargeable Batteries

Among energy storage devices, rechargeable (or secondary) batteries have shown to be more promising as they can convert chemical energy into electrical energy and vice versa, including lithium batteries, nickel metal hydride, lead acid, nickel, cadmium and sodium [2]. Lithium has the highest theoretical energy density in all solid electrodes, so lithium batteries advance among all

types of batteries. Its advantages in high energy density, high voltage and light weight result in its success [3]. However, even with its full development to achieve its highest value the energy density of LIBs cannot meet long-term demand. To achieve the development of new energy storage devices, research has been carried out in (Li-S). (Li-S) is one of the most promising candidates for next-generation energy storage devices. Provided specific and high-power operation of about 600 W / kg, equivalent to 4 to 5 times the power of current LIBs. In Table 1.1, Lithium-Sulfur Batteries (Li-S) show their advantages over the specified theoretical voltage, power and density. In addition, in Figure 1.1, the specific practical capacities, driving distances and package prices are compared for some rechargeable batteries [2].

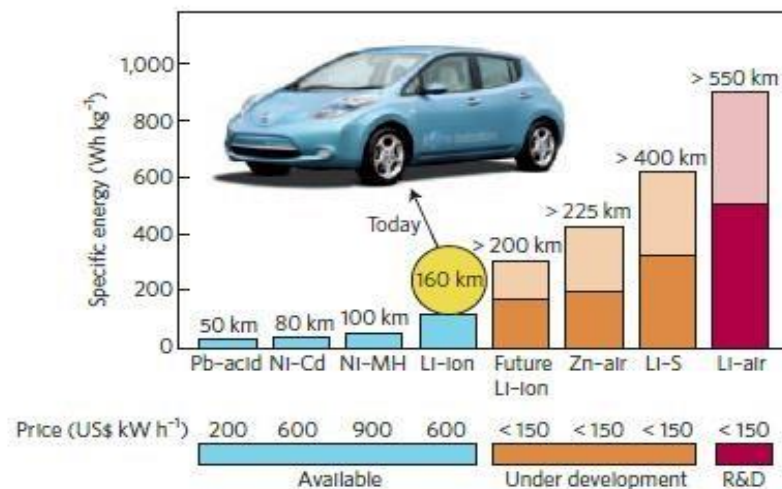


Figure 1.1 Specific practical capacities of some rechargeable batteries, with estimated driving distances and package prices side by side [2].

Table 1.1 Cell voltages, theoretical specific energies and densities for several kinds of batteries [2] .

Battery	Cell voltage (V)	Theoretical specific energy (Wh/kg)	Theoretical energy density (Wh/L)
Li–O ₂ (aqueous) 2Li + O ₂ + H ₂ O ↔ 2LiOH	3.2	3582	2234 (Li+H ₂ O+LiOH)
Li–O ₂ (non-aqueous) 2Li + O ₂ ↔ Li ₂ O ₂	3.0	3505	3436 (Li+Li ₂ O ₂)
Li–S 2Li + S ↔ Li₂S	2.2	2567	2199 (Li+Li₂S)
Zn–air Zn + 1/2O ₂ ↔ ZnO	1.65	1086	6091 (ZnO)
Li-ion 1/2C ₆ Li + Li _{0.5} CoO ₂ ↔ 3C+LiCoO ₂	3.8	387	1015

1.3 Principles of Operation of Rechargeable Batteries

The improvement of rechargeable battery technology at present is powered by cheap, powerful and sustainable new energy supplies. Batteries are made of two poles with different electrically separated electrodes, which are ionic conductors. Electrons flow automatically from the positive pole to the cathode when an external load is applied to connect the poles [4]. Ions are propagated across the electrolyte in order to maintain the charge balance, which in turn leads to the acquisition of electrical energy by the external circuit [5]. For rechargeable

batteries, when the battery is recharged, the electrons flow from the cathode to the anode when the voltage is applied in the opposite direction. Figure 1.2 shows a discharge plan in a general rechargeable battery. Battery performance depends on the chemical composition of the battery. The theoretical capacity of the cell in the battery is defined as the "total amount of electricity (in hours of ampere) involved in the electrochemical reaction" occurring inside the battery.

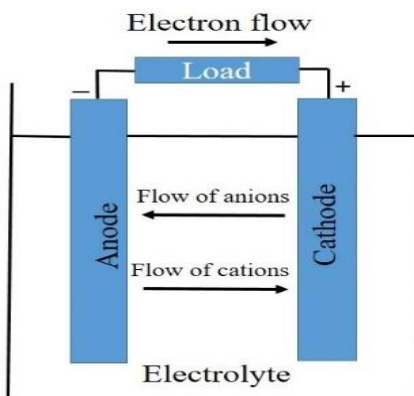


Figure 1.2 Schematic of a discharge plan in a general rechargeable battery [4].

The theoretical power can be calculated by the equivalent weight of fines in the material, and the molecular weight of the active substance in fines divided by the total number of electrons involved in the reaction. The specific theoretical energy of a cell can be defined as the amplitude multiplied by the voltage or standard voltage of the cell. Theoretical ability has not been fully realized in practice due to many factors contributing to the reduction. For example, the excess amount of the active component of the active electrode material reduces the ability. Furthermore, non-reactive materials (unreacted electrode components, spacers, and electrolyte) are essential for proper battery operation. These non-reactive substances add weight to the battery, reducing cell capacity.

Finally, the battery usually does not completely discharge to zero volts which reduces the amount of electricity the battery provides [4].

1

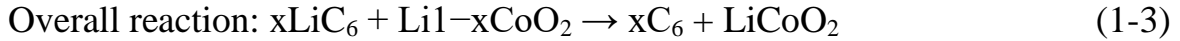
1.4 Lithium-Ion Batteries

The lithium-ion battery is a type of rechargeable battery where the lithium ions move in the direction of the negative electrode to the positive when discharged and vice versa when charging. Lithium Batteries lead among all battery types. For the first time by SONY in 1991 using the LiCoO_2 /graphite chemistry the concept of Lithium-Ion Batteries (LIBs) was introduced. Since that time, it has remained in the main markets for years in an important position it has been successfully used in many portable electronic devices, such as mobile phones and laptops. Presently, these types of rechargeable batteries account for a market share of over \$ 30 billion and are currently indisputable as the preferred power source for consumer electronics [3].

1.4.1 Operating Principles

The lithium-ion battery consists of a lithium-based electrode and a negative electrode usually made of carbon. Lithium metal oxides, are a popular choice for anode due to their stability and high performance, such as LiMn_2O_4 and LiCoO_2 . Diagram 1-3a shows the LiCoO_2 /graphite system as an example to explain the principle of operation of widely used lithium ion batteries [6]. The mechanism of production and energy storage of beneficial action is the transfer of lithium ions from the anode material (negative electrode, “reductant”) to become partitioned with the cathode material (positive material, “oxidant”). During the discharge process, the cationic lithium ions move from the anode (usually carbon-based as graphite, C_6) and enter on the (lithium cobalt oxide

(LiCoO₂) as the cathode. The reactions that occur during discharge of the battery are:



Against this process (Upon charging), the lithium is extracted from the cathode and re-inserted into the anode. As shown when the charge is discharged, the next reaction occurs in the charging process.

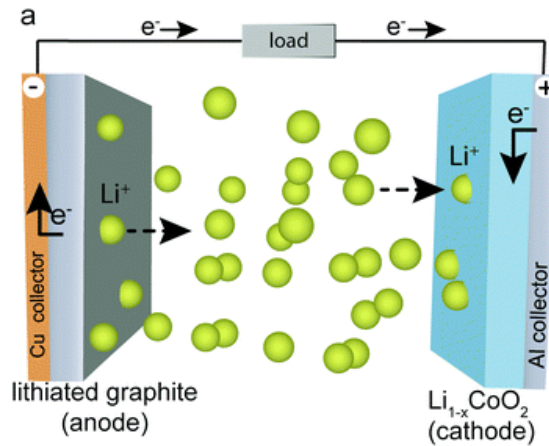


Figure 1.3 (a) Schematic illustrating the operating principle of a rechargeable LIB with graphite as the anode material and LiCoO₂ as the cathode material [6].

Through this mechanism, electrons are synchronously transferred with lithium ions and convert the chemical potential gradient into electrical energy. This adjusts to effectively charge the battery and prepare it for another discharge cycle. An external voltage is required for the charging process to occur in order to push the lithium ions at the cathode from a low chemical voltage to a higher

chemical voltage. To separate the anode from the cathode in the cell, a Li^+ ion conductive dielectric membrane is placed, and this is known as a separator. The separator ensures the transfer of ionic charge carriers while preventing short circuits between electrodes. In addition, in lithium-ion cells lithium ions are usually readily delivered through the use of a solvent-based organic electrolyte.

1.4.2 LIB Limitations

For Lithium-Ion batteries there are many disadvantages including low shelf life, high cost, and low thermal stability, and many more things. Despite this, its high energy density is highly desirable. The battery with a higher energy density allows the device to work for a longer period before needing to be recharged. With lithium-ion battery technology, it is clear that we have reached the maximum theoretical energy density of the materials commonly used in LIBs. In Lithium-Ion Battery, LiCoO_2 (LCO) is used as the cathode material due to its high theoretical capacity of 273 mAh/g [7], however we are approaching the theoretical capacity of this material. The innate ability to absorb Li^+ in the metal oxide and carbon anode structure is effectively limited the capacity by preventing Li^+ species from undergoing oxidation and reduction reactions. Moreover, upon examining LiCoO_2 , we can determine the mass ratio of useful lithium metal to lithium oxide. This ratio is approximately 1:13 (Li: Li-Oxide) as the lithium metal represents about 7% of the total mass of the cathode. This effect can be seen when calculating the theoretical capacity of the metal oxide material (274 mA g^{-1}) and compared with the practical capacities often reported in the literature (150 mA g^{-1}) [8]. To improve cathode performance, a new lithium host must be developed allowing for a much higher density of lithium to be stored. Sulfur based cathodes represent an attractive strategy for increasing the lithium-to-host ratio [9].

1.5 Lithium Sulfur Batteries

Lithium and Sulfur Batteries, one of the most promising filters in the energy storage system, meet the growing demands of electric vehicles, electronic devices and large-scale power storage for nearly three decades under intense investigation. The traditional lithium-sulfur battery is simply composed of sulfur-based cathode (usually mixing with carbon conductor and polymer binder) and anode of Lithium metal, which are immersed in an electrolyte and physically separated by a porous membrane or separator, through which ions diffuse, as displayed in Figure 1.4 [10].

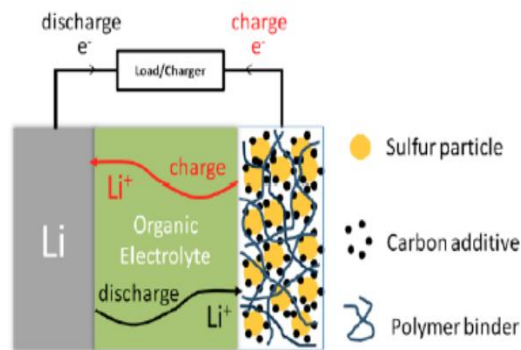


Figure 1.4 Schematic of the configuration and operation of Lithium-Sulfur Batteries [10].

The operation of rechargeable Li-S batteries is simply based on the theory of Li ions migrating between the cathode and the anode through the electrolyte. In order to achieve high cycling efficiency and long life, the movement of Li ions in anode and cathode hosts should not change or damage the host crystal structure. Figure 1.5 shows a typical Li-S cell, in which the cathode consists of sulphur (yellow) and a conductive additive (black; for example, carbon black), and a metallic lithium anode which is separated by an organic electrolyte [2],[11].

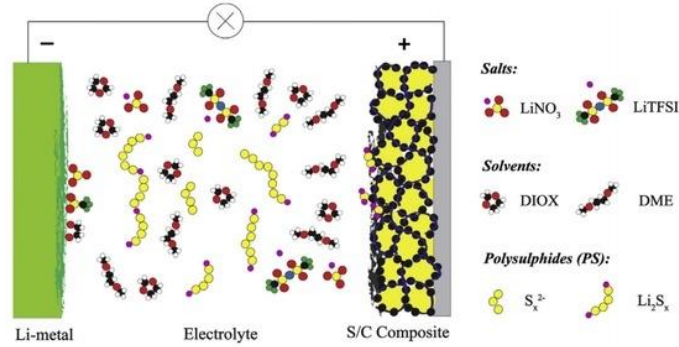


Figure 1.5 Schematic illustration of a typical lithium–sulphur (Li–S) cell [11].

Sulfur is a plentiful, environmentally friendly, and cost-effective sulfur material that offers a high theoretical cathode capacity of 1,675 mAh/g and a high energy density of 2,600 Wh /Kg theoretically. Lithium is the most electropositive sensitive of 3.04 volts as well as the lightest 46.94 g/mol. Therefore, lithium metal is used as a negative pole [12]. Although the promising advantages of lithium-sulfur battery systems, there are some existing problems that hinder the practical application of this battery in the current industry. Because sulfur is an ionic and electrically insulating material, additives such as conductive carbon and polymer are used to maintain an intimate contact with the structure of the sulfuric cathode so that reversible electrolysis can occur [13]. Besides, transfer of lithium polysulfide's, changing morphology during the cycling process are all factors affecting cell performance.

1.5.1 The Mechanism of Discharge and Charge

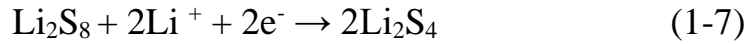
The electrochemical mechanism of lithium sulfur batteries is based on the oxidation-reduction reaction of the polysulfide [12].

The redox reaction of Li-S is described as $S_8 + 16Li \rightarrow 8Li_2S$ is located at about 2.2V voltage with respect to Li^+ / Li^0 [2]. In the discharge process, metallic

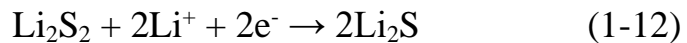
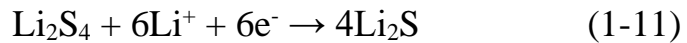
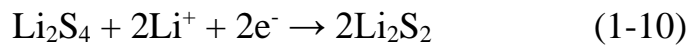
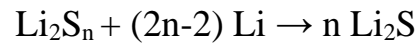
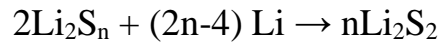
lithium is oxidized directly to Li^+ on the anode, while the reaction on the cathode is gradual and complex. The first phase of the discharge involves reducing the insoluble primary sulfur to high-order polysulfide's (Li_2S_x , $x = 4-8$) and dissolves in the electrolyte solution, which occurs in the possible range 2.5-2.0 volts [11] described in Eq.(1-6).



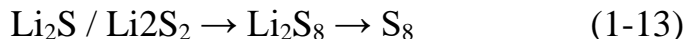
The second phase of the unloading process involves a decrease in the length of the S-S series, reducing long-soluble polysulfide's (Li_2S_x) to low-grade polysulfides, Li_2S_2 and Li_2S . Which is mentioned in Equation 8. The existence of rapid mobility because it remains in the liquid.



The final phase is the reduction and formation of solid products ($\text{Li}_2\text{S}_2 / \text{Li}_2\text{S}$), described in Eq. (1-1)2. Due to the insoluble and non-conductive properties of Li_2S_2 and Li_2S , the reduction process suffers from extreme polarization and takes very slow of places and even disappear. In general, the reduction is done in two stages. Reducing the two-phase liquid in two phases of low-grade polysulfide, described in Eq. (1-9) and Eq. (1-10). Overall, the process of reduction takes places in the 1.9-2.1 V potential range and contributes to the main capacitance of the Li - S cell.



The charging process is much simpler. The reaction products are oxidized Li_2S / Li_2S_2 into long-chain lithium polysulfide's and then are converted back to the initial sulfur:



Typical discharge / charge curves of the LSB are described in Figure 1.6. [2]

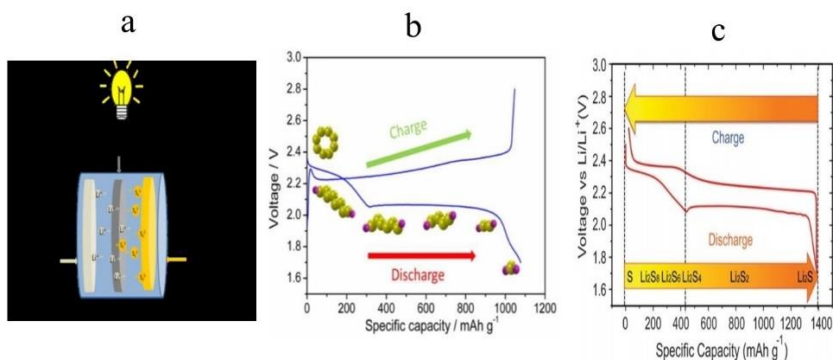


Figure 1.6 (a) Schematic of a LSB consisting of lithium anode, electrolyte and sulfur cathode and (b) the typical discharge/charge curves [2] (c) The voltage profile and chemistry of sulphur cathode in the organic electrolyte [14] .

1.5.2 Lithium-Pure Sulfur Batteries

The pure lithium sulfur battery is composed of lithium metal anode, separator, liquid organic electrolyte, and sulfur cathode. The separator is used to prevent a short circuit and allow the migration of lithium ion and it is usually a polymer material of polyethylene. The electrolyte contains of an organic solvent and a lithium salt. The most suitable lithium salts are LiCF_3SO_3 , LITFSI ($\text{LiN}(\text{SO}_2\text{CF}_3)_2$), LiClO_4 and LiNO_3 is a common addition in the electrolyte because it greatly improves Coulombic efficiency [15-17]. The most suitable lithium salts are LiCF_3SO_3 , LITFSI ($\text{LiN}(\text{SO}_2\text{CF}_3)_2$), LiClO_4 and LiNO_3 is a

common addition in the electrolyte because it greatly improves Coulombic efficiency. Mostly 1,3-dioxolane (DOL) and -dimethoxyethane (DME) are solvents in the electrolyte of LSBs. Sulfur cathodes are typically synthesized by of the mixing commercial sulfur powders, conductive (carbon black) and binder of polymer (Polyvinylidene Fluoride, PVDF), and using aluminum foil as the current collector. Given to the above challenges, pure lithium sulfur batteries do not exhibit decent electrochemical behaviors even under the density of very low current. In Figure 1.7a, in Huang's work of a pure lithium sulfur battery the charge/discharge curves of the first cycle presented an initial discharge capacity of only 371 mAh/g, much lower than theoretical (1675 mAh/g) [18]. Also, in Figure 1.7b the cyclic performance is presented with very weak capacity and recyclability.

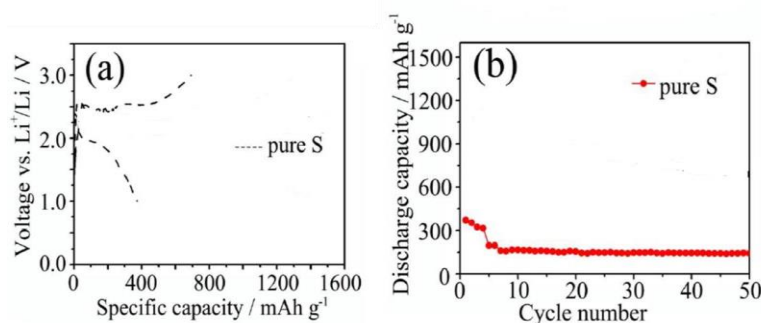


Figure 1.7 Electrochemical performance of a lithium-pure sulfur battery.

(a) The Charge/discharge curves in the first cycle and (b) the cyclic performance at 0.1C (1C= 1675 mA/g) [18].

Also presented similar works to pure sulfur cathode batteries, most of which presented dissatisfied electrochemical manners, such as columbic efficiencies, low capacitances, rapid power wear and short life cycle in Table (1.2).

Table 1.2 In Li-S, comparison of electrochemical performance of pure sulfur cathodes

Cathode Materials	Discharge current rate	Initial discharge capacity (mAh/g)	Cycle number	Residual capacity (mAh/g)	References
Sulfur	0.1 C	371	50	<150	[18]
Sulfur	0.1 mA/cm ²	400	50	100	[19]
Sulfur	0.4 mA/cm ²	710	50	230	[20]
Sulfur	0.1 mA/cm ²	<750	80	208	[21]
Sulfur	160 mA/g	1094	80	<150	[22]
Sulfur	100 mA/g	680	100	374	[23]

1.5.3 Problems

Although the promising advantages of the lithium sulfur battery, still a number of challenges in developing a the process of commercialization lithium-sulfur battery [24]. First, due to poor electronic conductivity of sulfur, it leads to sacrifices overall density of cathode energy in general with the use a large amount of carbon conductive in the sulfur-based cathode [25] .Second, during charging and discharging process, the intermediate lithium polysulfide's can decompose in the organic liquid electrolytes, leading to loss of effective material and the impact of polysulfide shuttle, which causes in in capacity fading and efficiency of the poor Coulombic [26] .

1.5.3.1 Sulfur Blocking Issue in Cathode

Primary sulfur has relatively low electrical conductivity, which is 5×10^{-30} S cm^{-1} . The low conductivity by its nature impedes the full use of the active substances, causing the specific capacity to decrease. The sulfur density is 2.07 g/cm^3 , while the Li_2S density is 1.66 g/cm^3 . The expansion volume of sulfur to Li_2S during the cycles is as large as $\sim 80\%$, and may lead to mechanical malfunction of the electrodes. Formation of Li_2S is insoluble and non-conductive and Li_2S_2 during cycling fetches more problems. Usually, the formation of polysulfide results to the following problems of cell performance,

1. Expansion of volume may lead to deterioration of carbon structure and affect cycling performance in the future.
2. The deposition of Li_2S and Li_2S_2 on the cathode structure results to low conductivity and poor cycling life.

According to previous access, in the oxidation process the expansion and contraction due to the change of liquid solid phase leads to a 76% approximation of the volumetric increase in the carbon cathode structure [27]. While cycling, the morphological change may reduce in active electric carbon the surface area of contact between sulfur and carbon, and decrease the size of pores to hold sulfur and agglomerate of sulfur particles. As a outcome, in the host matrix the sulfur loses intimate contact with carbon, making it difficult to activate and therefore inactive with respect to the isolation of Li_2S and Li_2S_2 in the subsequent cycle of cycling [26]. Li_2S may remain inactive on the cathode, even when the cell is fully charged due to lack of communication with the connected media.

Importantly, the non-conductive thickness of Li_2S and Li_2S_2 that are attached to the electrodes limits the full electrolyte penetration of the entire electrode,

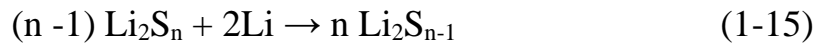
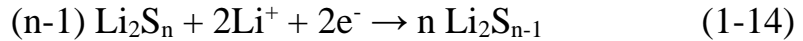
which is also explained by the rapid dissipation of amplitude [28]. The issue of blocking polysulfide by the cathode is critical to the performance of cell cycling [29]. Polysulfide blocking and loss of intimate contact between active ingredient and conductor leads to incomplete cycling in each cycle and in turn reduces battery capacity [30].

1.5.3.2 The Spread of Polysulfide between Cathode and Anode

As shown in the charging and discharging process, high soluble polysulfide is formed during the reduction discharging process of element sulfur or the oxidation charge of low-grade polysulfide. High order polysulfide buildup increases the concentration of polysulfide on the positive side. Polysulfide is spread from the anode to the negative electrode that contains lithium metal, depending on the accumulation of concentration gradient. The higher order polysulfide's continuously diffuse from cathode to anode and react with the lithium metal and form lower order polysulfide. As a result of reaction and diffusion process, lower order polysulfides accumulate on negative side of the cell. Therefore, these lower order polysulfide's diffuse back to positive side of the cell with the concentration potential [31]. During the charging process in the subsequent cycle, the lower order polysulfides will be oxidized to form higher order polysulfides and the whole process will be repeated. The back-and-forth diffusion process of polysulfide is known as "polysulfide shuttle effect", during which both reduction reaction with lithium metal and redox reactions with sulfur on cathode take place. Therefore limiting the shuttling diffusion is crucial to solve the problem of capacity fading of the cell [31].

1.5.3.3 Erosion of Lithium Metal

That the effect of the shuttle not only leads to the loss of active sulfur on the cathode, but also corrodes the lithium metal in the anode. On Li Anode, dissolved polysulfide goes under the electrochemical and chemical reduction, as illustrated by Eq (1-14) and (1-15) [17].



During a polysulfide shuttle, lithium metal is consumed and insulating a $\text{Li}_2\text{S} / \text{Li}_2\text{S}_2$ layer is formed on the surface of the lithium metal. This thick passivation layer increases cell resistance. It slows down or completely inhibits the additional interaction between metallic lithium and electrolyte components. In addition, during the $\text{Li}_2\text{S} / \text{Li}_2\text{S}_2$ configuration, these insoluble particles tend to stack and form a dendrite on the lithium surface. Since the insulate Li_2S blocks the contact between electrolyte and metallic lithium, the insoluble Li_2S actually promotes the formation of dispersion. The dispersion formed on the metal surface that grows and breaks through the separate part causes a short circuit within the batteries [17].

1.6 Research problem

Modern (Li-S) meet the increasing demands of electronic devices, electric cars, and large-scale energy storage. Research of the intense efforts have been made for developing new materials for various components (Li-S) to improve the electrochemical performance. Despite the accomplishments, some important dilemmas still need to be resolved:(1) The complexity and high cost of synthesis the material process hinder their widespread implementation; (2) Reduced content of sulfur in the cathode reduces the specified working energy

and (3) Grasp polysulfide degradation restriction by novel Nano carbon materials is not sufficiently obvious.

1.7 Project Objective

In search host of sulfur capable of providing high electronic conductivity, strong structure with high electrolytic high surface area, strong poly sulphide uptake, while maintaining low composite volume. The cathode is one of the main elements of the lithium sulfur battery, it the serves as the host material for the sulphur that ultimately governs cell performance. The objective of this project is to develop a strategy that will effectively increase the performance of the sulfur electrode using a simple and efficient method. The approach to this design is to use nickel metal oxides such as NiCo_2O_4 and NiO planted on carbon cloth with unique structures and porous texture and increase their porosity to increase the additional sulfur packaging and thus increase performance, to help the lithium -sulfur battery achieve low capacity decay rates are lower than 0.10% per cycle under several hundred cycles (> 200) at different current rates specified, high specific capacities of the electrode at different specified current rates, and loading relatively high surface sulfur greater than $3.5 \text{ mg} / \text{cm}^2$. In chapter 3, a polar host designer used the NiO nanosheets leaf sown on the carbon cloth by a simple chemical bath method. The carbon cloth supported NiO Nanosheets deliver to be like a conductive matrix and at the same time and stable reservoir to restrict the solution of the polysulfides. Thus, it has exhibited excellent cycle performance.in chapter 4, the metal oxide nanoparticle molecules (NiO_2Co_4) are introduced as an additive for the introduction of polysulfides, thus suppressing the shuttle effect. To further understand the roles of additives in the cathode, the content of NiO_2Co_4 is improved and mechanisms of polysulfide entrapment between oxides and polysulfides are discovered.

1.8 thesis Layout

In Chapter 1, a brief introduction is provided on the background of rechargeable batteries and the principles of their operation,, and we talked about the lithium-ion batteries and operating principles to them and LIB limitations, followed by an introduction to lithium and sulfur batteries and the charge and discharge mechanism, followed by challenges and problems in developing the lithium sulfur battery marketing process followed by research problem, followed by doctoral motives and the objectives of this research, followed by thesis layout. Some literature reviews are summarized and we talked about the current solution to them in Chapter 2. In Chapter 3, it reviews several diffuse methods to characterizing of the materials and to the electrochemical evaluation. Chapter 4 illustrates the growth of NiO nano sheets on a relatively small carbon cloth and electrochemical performance is evaluated. The obtained NiCo₂O₄ is presented and is also investigated in the electrochemical performance assessment, the conclusion of this thesis, and some ongoing work has been suggested for to work in the future in Chapter 5.

Chapter two

Literature Review

To solve these challenges, new methods have been developed to prevent polysulfide dissolution and the effect of shuttles. According to the cell installation, breakthroughs in lithium sulfur batteries can be classified into three aspects: lithium anode protection, electrolyte modification / separator, and sulfur cathode composition.

2.1 High-Performance Anodes

Metallic lithium is used as an anode in Li-S. Lithium metal is an ideal anode for the development of high-energy Li-S batteries due to its high theoretical capacity (3860 mAh /g), its light weight and its negative electrical potential (-3.04 V versus the standard hydrogen electrode) [32]. However, the metallic lithium anode is highly reactive in the electrolyte and easily reacts with the shuttle's soluble medium lithium polysulfides to form an unstable solid electrolyte interface (SEI) layer. During cycling, unstable SEI cannot prevent the change in the shape and size of lithium anode, resulting in dendritic growth of Li metals. Moreover, due to the unstable SEI breakdown, the pure lithium surface was exposed to the electrolyte and parasitic reactions that make up the new SEI layer, which reduces the efficiency of lithium riding [33]. The metallic lithium anode causes low Coulombic efficiency due to stray and fossilized mineral deposits resulting from the use of metallic lithium as anode in non-aqueous electrolyte, short life cycle, and safety. In addition, in fact because of the presence of polysulfide's, the relative volumetric variation of lithium anode is not final, and the degradation of lithium anode in Li-S is much more complex than LIBs [32]. Therefore, the success of Li-S batteries depends on a reliable

lithium metal anode. Metallic lithium is used as an anode in Li-S. In order to reduce lithium anode corrosion, many of substitutional anodes have been found for sulfur-based batteries rechargeable. An attempt was made to use graphite as anode and lithium sulfide in situ / carbon-cathode of the full-sulfur lithium battery in the Zheng study [34]. The whole modified cell showed much better stability for the cycle, effectively delaying the anode corrosion ,due to a stable solid electrolyte interphase (SEI) layer formed on the surface of the anode during the first few cycles, [32]. Carbon a hard was used as replacement anode for in a Li-S cell. The specific capacity of up to 753 mAh/g, and high Coulombic efficiency of about 99% on 550 cycles, with a current rate of 334 mA in 1 between 2.6 and 1.0 volts. Moreover to carbon -based anodes , silicon anodes [35], boron [36] and tin [36] were also introduced into Li-S. It has enticed large interest in the field of Li-S batteries in last year's owing to its low weight, large theoretical specific energy, high conductivity, and theoretical stone energy density. These advanced anodes can inhibit the formation of lithium dendrite and show better stability over the long term. Although significant advances have been made in the design and synthesis of new cathode materials, the development of advanced anode materials to prevent degradation of anodes appears to be equally important to enhance the practical application of Li-S.

2.2 Compound Cathodes

A disadvantage of sulfur is that it is a non-conductive material. To improve the electrochemical performance of the Li-S battery system, sulfur is always combined with other materials. The ideal sulfur carrier should have high electrical conductivity, as well as confining lithium polysulfide to bypass the shuttle problem.

The majority of studies in Li-S research are based on sulfur cathode materials. The use of sulfur carbon compounds has been the most common and effective way to improve electrochemical performance, since Jie et al. Reported in 2009 by sulfur impregnation in high-volume nanoparticles where given high specific capacity [13]. Carbon-based materials including black carbon [37] micro porous/mesoporous carbon[38, 39], carbon nanotubes [40] , grapheme [41] , hollow carbon spheres [42], hierarchical porous carbon [43], carbon nanofibers [44] , are the most popular pillars of sulfur fusion. Peled and co-workers introduced the original concept of sulfur packaging in porous carbon [45]. Since then, through the use of many carbon materials as a host has been making significant progress in improving the carbon materials. Porous carbon substrates serve as a suitable matrix for the compound because of its absorbability of soluble polysulfides. The idealism carbon matrix for carbon sulfur compounds needs the next characteristics [46]:

1. High electrical conductivity
2. Electrochemical converge of sulfur
3. Small porous cells to absorb polysulfides
4. Possibility of Liquid electrolyte access to active substance
5. Stable tire to maintain pressure due to volume changes of active substance during cycling

During the cycling process heterogeneous contact between conductive carbon and sulfur may occur; hence the hierarchical design is important in the composition of the sulfur-carbon compound cell. Hierarchical carbon provides enough space to load the active substances, because it has a high surface area and a large pore size, which greatly improves the electrical conductivity of the cathode. Such as microporous carbon spheres (Figure 2.1 (a), It has a large space. Due to adsorption limited lithium polysulfides within the structure, the

sulfur load is not sufficient for high performance. Spherical ordered mesoporous carbon nanoparticles (Figure 2.1(b)) it has larger pores compared with micropores so that more active sulfur can be loaded. porous hollow carbon (Figure 2.1(c)) Porous carbon is used to encapsulate primary sulfur to reduce the spread of polysulfide. Another option is to immobilize the intermediate polysulfide, graphene oxide sheets (Figure 2.1 (d)). porous carbon nanofibers (Figure 2.1 (e)), also show good performance [31].

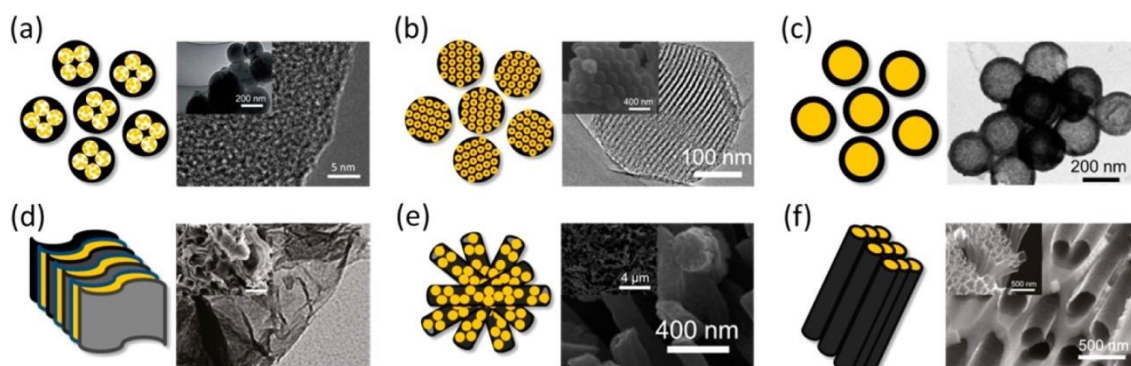


Figure 2.1 Hierarchical designs of carbon-based sulfur composites: (a) microporous carbon spheres, (b) spherical ordered mesoporous carbon nanoparticles, (c) porous hollow carbon, (d) graphene oxide sheets, (e) porous carbon nanofibers, and (f) hollow carbon nanofibers [31].

These porous structures have provided ample space for sulfur formation, making sulfur well connected with the conductive matrix, which effectively promotes the full use of active substances. To incorporate sulfur into carbon, the most common method is diffusion method. Sulfur is mixed in a certain amount with the carbon matrix and heated in an atmosphere at 155 C° for hours because at this temperature the sulfur has a lower viscosity, which facilitates liquid sulfur into the pores [47]. Chemical reactions arising from sulfur precursors ($\text{Na}_2\text{S}_2\text{O}_3$, Na_2S) and acids for in situ sulfur planting are carried out in carbon hosts [41] [48]. The other active materials are also integrated into

carbon matrix, such as the final discharge product of Li_2S [49] , and intermediate polysulfides Li_2S_4 [50] and Li_2S_6 [50] .

Depending on the buffer nature of the sulfur and $\text{Li}_2\text{S}_2 / \text{Li}_2\text{S}$, the polymer procedure will be a promising material for sulfur encapsulation. The polymers used in the Li-S system can be divided into two types: conductive polymers and non-conductive polymers. Conducting polymers such as Polyaniline (PANI) [51], polypyrrole (PPy) [52] , poly (3, 4-ethylenedioxythiophene) (PEDOT) [53] and polythiophene (PT) [54] , and have been widely used in Li-S, we can see part of that in the Figure 2.2. It can facilitate electron transport, improve the use of active substances. Furthermore, the polymer coating acts as a barrier to inhibit the dissolution of polysulfide in the electrolyte. Non-conductive polymers, such as polyacrylonitrile (PAN) [55], polyvinylpyrrolidone (PVP) [53], polyethylene glycol (PEG) [13] ,and poly(propylene oxide) (PPO) & poly(ethylene oxide) (PEO) block copolymer [56], were used as a coating material in the cathode, and thus effectively improved the stability of the Li-S cycle as they were used as a barrier to effectively restrict the degradation of polysulfides during the charging / discharging process. Conducting polymers with different structures (Figure 2.3), like PANI nanotubes/ nanofibers [57],[58] , PEDOT shell [59], tubular PPy [21] and PT shell [54] ,employed to incorporate sulfur and all these studies have achieved great improvements with high capacity and good cycle ability. In Zhou's study, the a yolk-shell structure of PANI-coated sulfur composite was swimmingly developed [60]. Unique nanostructure has played a very important role by developing electrochemical performance of Li-S (Figure 2.4). Conductive PANI shells expedited ion/electron transfer and prevent the spread of polysulfides from the shells, effectively blocking the shuttle impact. Supreme, due to the presence of free space inside the polymer shell to expand the generated volume from sulfur to

Li₂S during cycles, yolk-shell nanostructures have been shown much improved cyclability compared with S/PANI core-shell isotopes. So, the yolk-shell electrode delivered a stable capacity of 765 mAh/g at 0.2 C after 200 cycles.

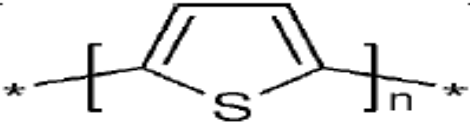
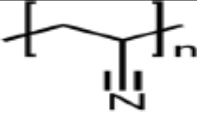
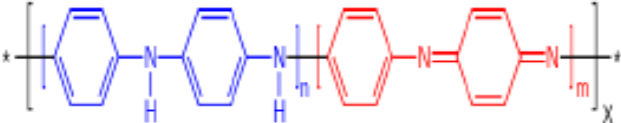
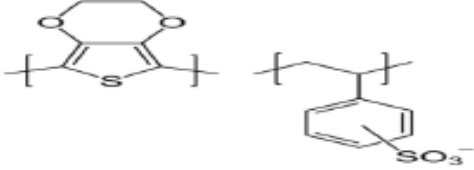
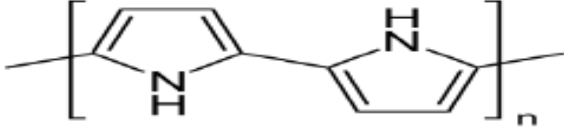
Polymer Name	Chemical Structure	Reference
Polythiophene		[61, 62]
Polyacrylonitrile (PAN)		[63, 64]
Polyaniline (PANI)		[48, 65]
PDOT: PSS		[66]
Polypyrrole		[67, 68]

Figure 2.2 The polymer summary shows the conductivity applied in Li-S batteries [48, 61-68]

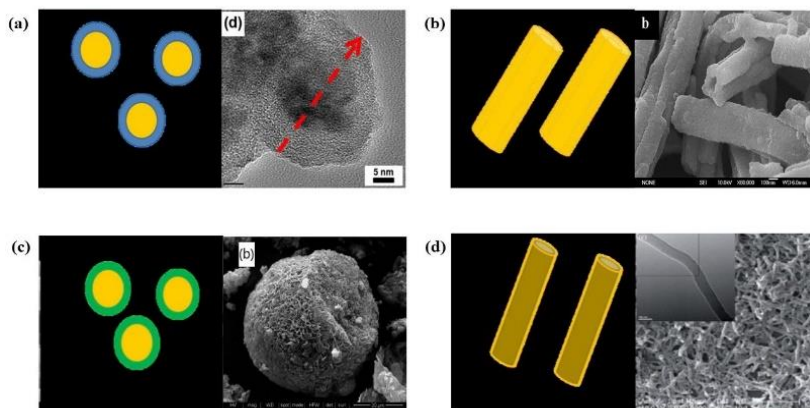


Figure 2.3 Polymer-sulfur composites: (a) PEDOT:PSS spheres[59], (b) PPy tubes [21] (c) PT spheres[54] and (d) PANI nanofibers[58] , to encapsulate sulfur.

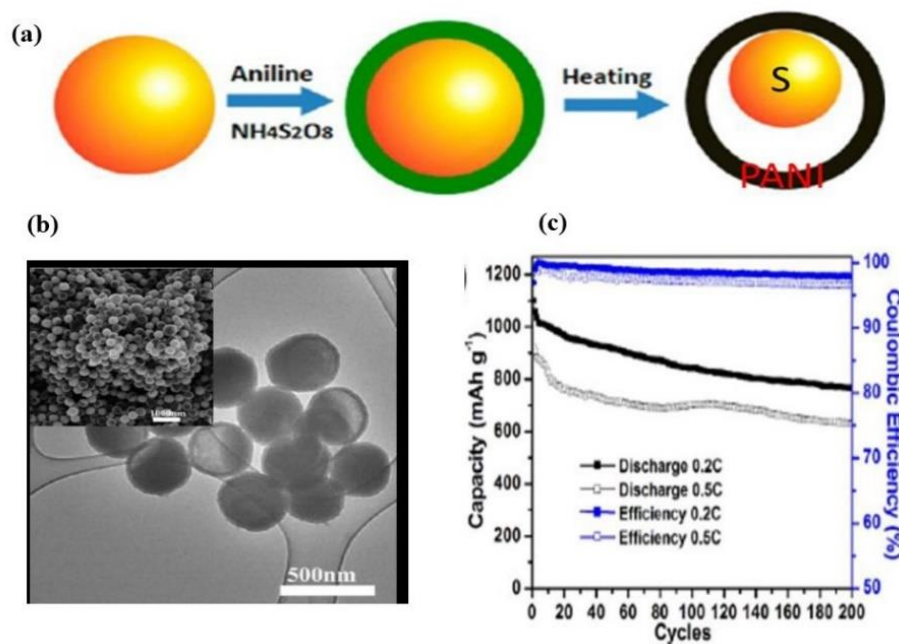


Figure 2.4 (a) Schematic of preparation of S/PANI yolk-shell nanoparticles, (b) TEM image of nanoparticles with SEM image in inset and (c) cyclic tests at 0.2 and 0.5 C.

Metal oxides such as TiO_2 [69] and TiO_{2n-1} [70] have been reported to load sulfur as substrates materials for Li-S. The sulfur- TiO_2 yolk-shell composite was successfully constructed in the study of Seh [69]. The shell it can prevent the solubility of polysulfides into the electrolyte, and this internal Nano-architecture with vacant space has been able to accommodate the change in the volume of active substances, avoiding cracking and breaking shells. As an outcome, the composite novel yolk showed a very stable cycle of more than 1000 cycles at 0.5 C as shown in Figure 2.5. Significant success was achieved by forming TiO_{2n-1} with sulfur. Both experiments and theoretical simulations were conducted to investigate the interaction between the oxides and active materials. The study revealed that the surface of TiO_{2n-1} with well-coordinated Ti-low sites is favorable for adsorption and selective deposition of sulfur types [70]. Add to that, other Nano-sized metal oxides such as MnO_2 [50], SiO_2 [71], SnO_2 [72], MgO [73], ZnO [73] and Al_2O_3 [74] were insert as additives in the cathode.

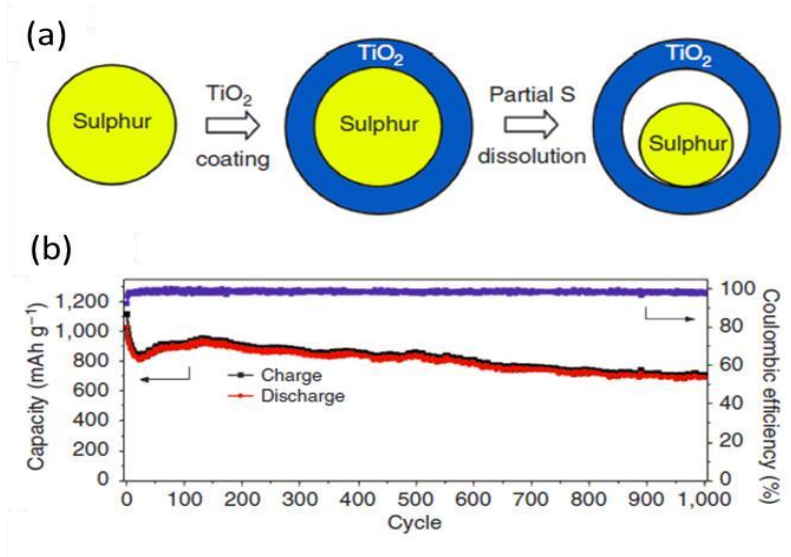


Figure 2.5 (a) Schematic preparation process and (b) cyclic performance of the sulfur- TiO_2 yolk-shell composite [69].

Nickel oxide has attracted considerable interest in electrochemical devices due to its low cost, environmental friendliness, and natural abundance [75]. for Nano-structured Nano molecules the synthesis of nickel hydroxides with new structures is an easy and straightforward method, by heating nickel hydroxide products at elevated temperatures in the air where NiO materials can easily be obtained. Nickel oxide (NiO) nanoparticles have been prepared via sucrose-derived carbon sphere as a soft template derived from the hydrothermal treatment of sucrose. The size of the carbon sphere template is around 2–4 μm , by P. Preetham et al, (Figure 2.6) [76].

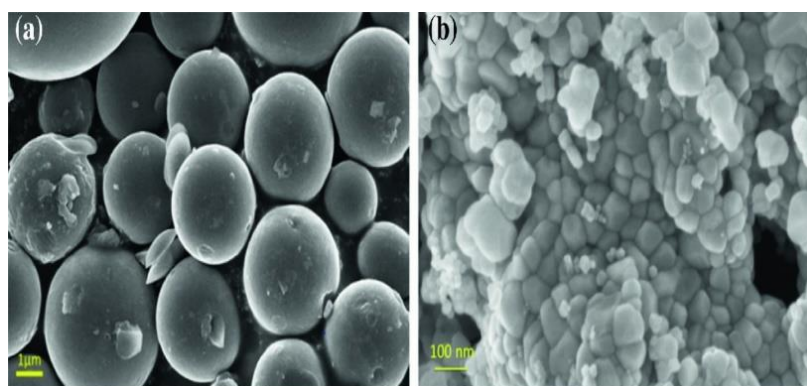


Figure 2.6 SEM images of active materials: (A) neat NiO; (B) NiO/C composite [76].

A highly wrinkled NiO Nanosheet-based hierarchical structure were successfully prepared by Hongda Li et in figure 2.7, that can efficiently restrain the polysulfide shuttle via physical and chemical confinement. Reduced fluoro graphene–NiO/S (RFG–NiO/S) composites are also prepared by hydrothermal method and thermal treatments. Their results show that the developed hybrid composite of RFG–NiO/S, which provides better initial reversible discharge capacity of 995 mAh/g, retains 640 mAh/g after 110 cycles at 0.1 C, and the

specific capacity of 381 mAh/g after 200 cycles at the higher current rate of 0.5 C [77].

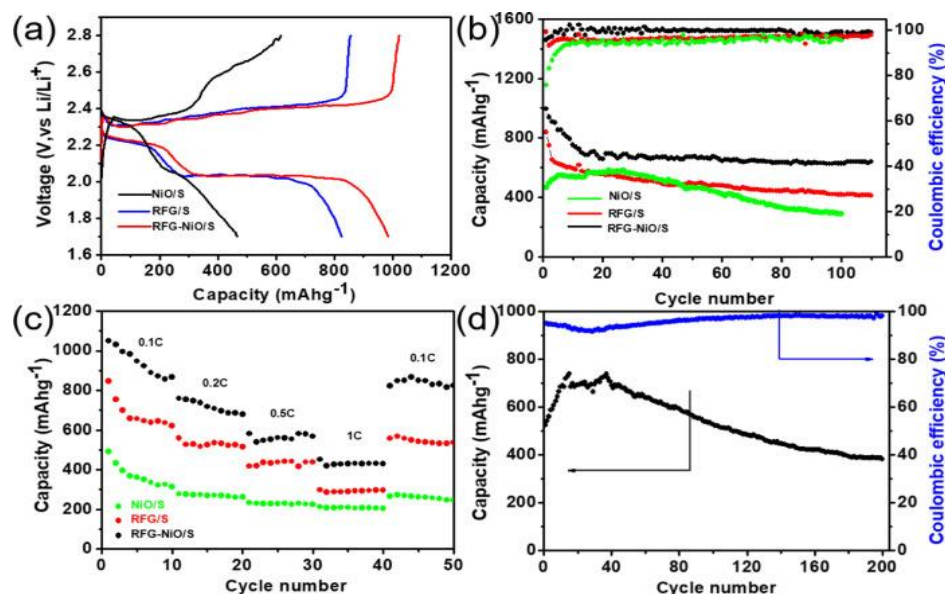


Figure 2.7 (a) Profiles of the NiO/S, RFG/S and RFG–NiO/S electrodes for the first cycles under a current density of 0.1C, (b) Cyclic voltammograms of Capacity retention and Coulombic efficiency at a current density of 0.1C (c) Rate performance of NiO/S, RFG/S and RFG–NiO/S composite electrode at various current densities and (d) Cyclic voltammograms of Capacity retention and Coulombic efficiency at a current density of 0.5 C [77].

Jyun-Wei Guo et al, was able to obtain nickel oxide hollow globules constructed from nanoparticles by hydrothermal synthesis in the presence of glycine. After heating the nickel hydroxide at 400 C ° in air. The obtained sulfur-filled hollow NiO pellets were loaded into carbon paper as (NiO / S) cathodes of the lithium sulfur batteries. The NiO / S cathode provided a large specific capacity of 1300 mAh/g at 0.2 C (335 mAh/g), much larger than the

bare sulfur loaded in carbon paper (1000 mAh/g). In addition, the NiO / S cathode showed superior power recovery after testing the C rate and coulombic efficiency see in Figure 2.8 [78].

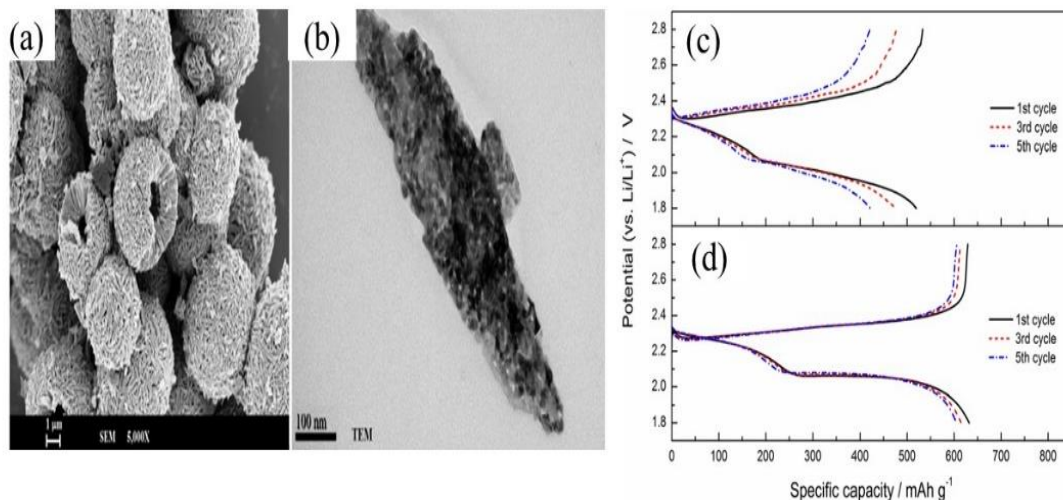


Figure 2.8 (a, b) SEM and TEM micrographs of the nickel hydroxide and after annealing at 400 C ° GCD. Profiles of (c) the S and (d) NiO (400 C °)/S electrodes for the first three cycles under a current density of 0.2C [78].

Recently, Dong Xie et al. It provides an easy synthesis of the graphene compound through a combination of a solution-based method and a subsequent solid through the subsequent calcination process. The compound shows highly improved electrochemical performance and provides an initial discharge speed of 2169.6 mAh/g and a reverse power of up to 704.8 mAh/g with a current of 200 mA g⁻¹ after 50 cycles, shown in Figure 2.9 [79]. Here in work done by Jie Wang et al, network NiO nanosheets have been successfully prepared as an intermediate for a Li-S battery, which is coupled to a carbon layer at the cathode side of the separator.

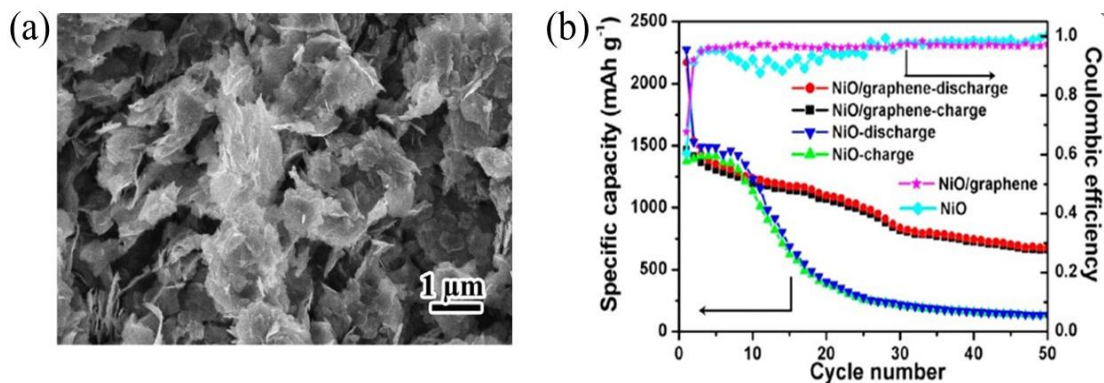


Figure 2.9 (a) SEM images of NiO-graphene composite. (b) Cyclic voltammograms of Capacity retention and Coulombic efficiency at a current density of 200 mA g⁻¹ [79].

During battery operation, the carbon layer prevented the polysulfides from shuttle movement, which effectively enhanced the cycle stability. The nanoparticle NiO sample of the grid with 80% of mass S at 0.2 C showed the highest capacity and excellent retention power, compared to the sample of the NiO Nano scale sheets of the grid with loading S at 60%, 40%, 20% and S. In add, maintain steady cycling performance at 2 C and 5 C, over 300 cycles with nearly 100% Colombic efficiency in figure (2.10) [80]. Trioxide transition metal oxides such as NiCo₂O₄ have attracted great interest in electrochemical energy storage. The NiCo₂O₄ trio is one of the most promising high-performance electrodes for energy storage due to its low cost, natural abundance, environmental friendliness, high electrical conductivity and electrochemical activity compared to NiO and Co₃O₄ [81, 82]. have been the Widely verified [83] . In recent years, tremendous efforts have been made to prepare NiCo₂O₄ nanostructures in various forms using different methods [84, 85], that have been reported.

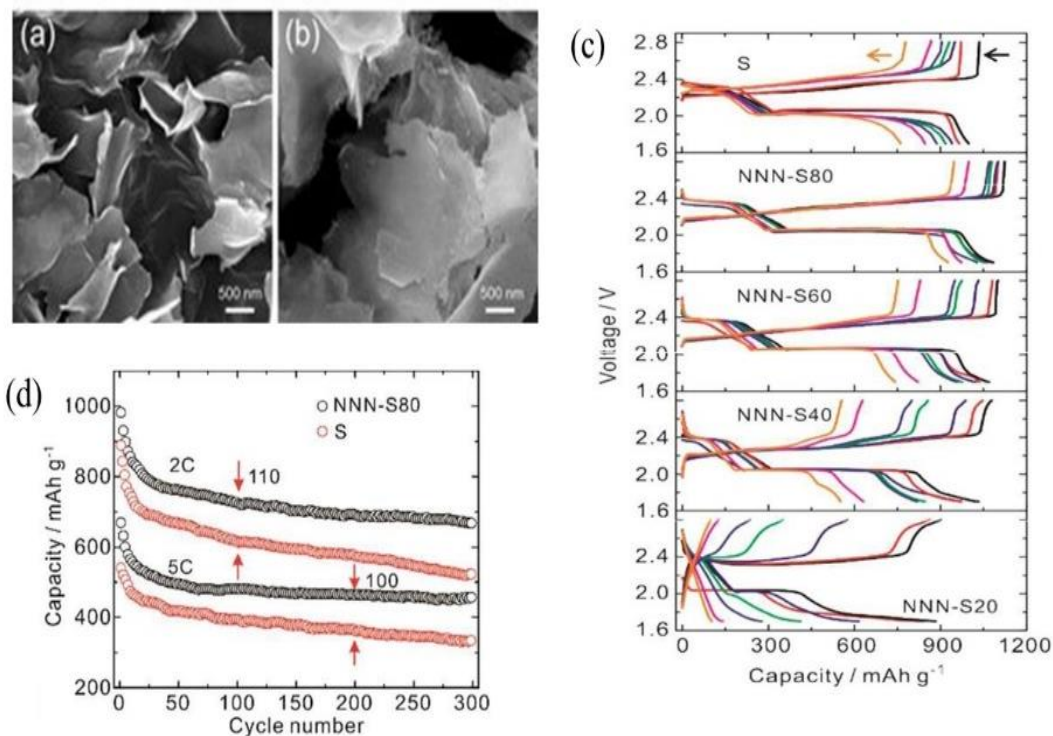


Figure 2.10 (a) SEM image of sheet-like Ni-based precursor; (b) SEM image of NNN sample; (c), the cycle numbers are 1st, 2nd, 5th, 10th, 20th, 30th and 50th from right to left, respectively (d) Long-term discharge stability tests of NNN-S80 and S cells at 2C and 5C [80].

For example, in this work by Dengji Xiao et al on-sulfur hosts based on interwoven NiCo₂O₄ Nanosheet/carbon nanotube composites are designed and synthesized by using a solvothermal reaction and subsequent annealing. As a result, the Li-S batteries based on this sulfur host exhibit high specific capacity, excellent cycling stability, and good rate capability. The discharge capacity of NiCo₂O₄ nanosheets can reach 575 mAh/g are achieved at rates of 2 C [86]. In the work done by Jie Luo et al, the NiCo₂O₄ nanofibers were successfully synthesized through electro spinning method and designed as sulfur host materials. Figure 2.11, the results showed that NiCo₂O₄ /S (NCO-NFs/S) nanofibers prepared for composite cathodes for lithium-sulfur batteries with

high-performance enhanced capacitance, exhibit excellent electrochemical performance with a high specific capacity of 1238 mAh/g at 0.2 C, and the specific capacity of 706 mAh/g after 500 cycles at 1C [87].

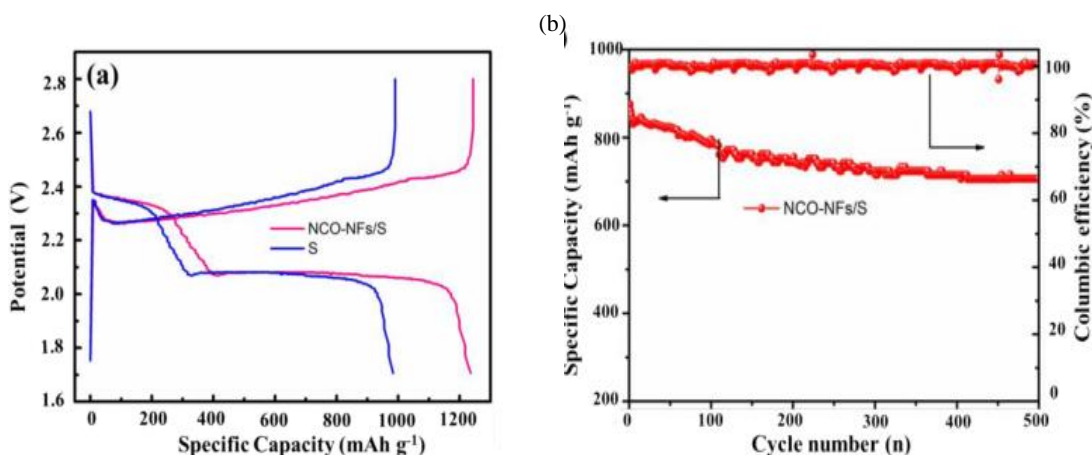


Figure 2.11 (a) Charge and discharge voltage profiles of (NCO-NFs/S) and S composite electrodes for the first cycle at 0.2 C. (b) Cyclic voltammograms of Capacity retention and Coulombic efficiency at a current density of 1 C[87].

In addition, through NiCo₂O₄ nanofibers as carbon-free sulfur immobilizers are introduced to fabricate sulfur-based composites, successfully prepared by Ya-Tao Liu et al, NiCo₂O₄ can leading to a good cycle stability of sulfur cathodes. Where this S/NiCo₂O₄ composite provides high capacity and high stability cycling, it's a high gravimetric capacity of 1125 mAh/g at 0.1 C rate, see in Figure (2.12) [88]. In the work done by Xiangchun Xia et al, NiCo₂O₄ nanoparticles were successfully synthesized through and by heating method (Figure 2.13). The results showed that hollow NiCo₂O₄/S composites prepared for Li-S batteries with high superior cycle stability and, enhanced capacitance, which is ascribed to the presence of the hollow NiCo₂O₄.

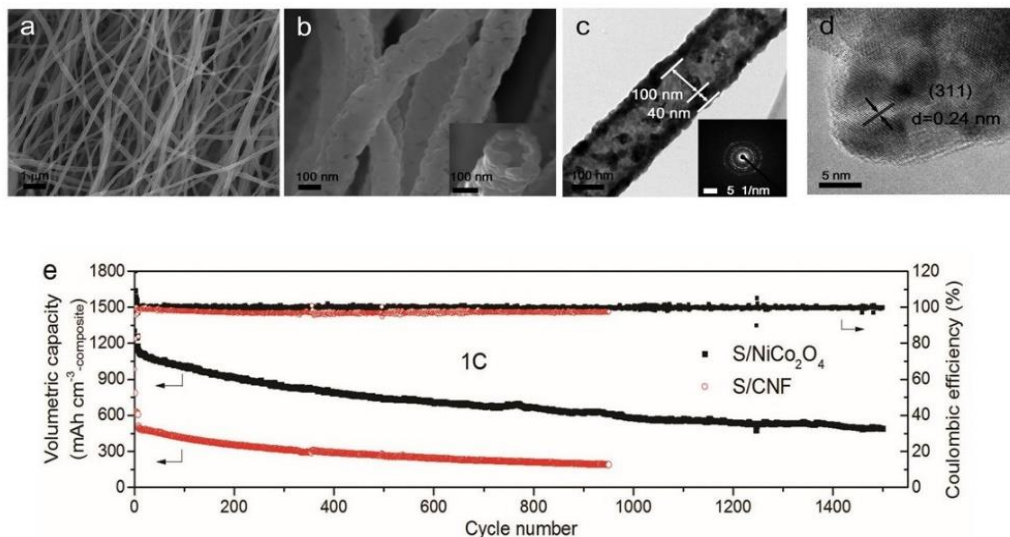


Figure 2.12 Characterization of the NiCo_2O_4 nanofibers and $\text{S}/\text{NiCo}_2\text{O}_4$ composite. a, b) Scanning electron microscope (SEM) images NiCo_2O_4 nanofibers. c) TEM image of NiCo_2O_4 nanofibers and the corresponding SAED pattern. d) HRTEM image of NiCo_2O_4 nanofibers. Electrochemical characterization of e) Long-term cycle performance of the $\text{S}/\text{NiCo}_2\text{O}_4$ and S/CNF composites at 1 C rate [88].

Compared with pure sulfur electrode, as the cathode materials for the Li-S batteries the hollow $\text{NiCo}_2\text{O}_4/\text{S}$ composites show more excellent electrochemical performance. The initial specific capacity of the $\text{NiCo}_2\text{O}_4/\text{S}$ cathode is 1006 mAh/g at the current density of 0.2C [82]. In addition, Azhar Iqbal et al successfully synthesized a highly efficient sulfur host namely NiCo_2O_4 hollow microtubes/sulfur composite ($\text{NiCo}_2\text{O}_4/\text{S}$) and used in lithium-sulfur batteries as an electrode for high-performance. The hollow interior cavity providing structural integrity while sufficient self-functionalized surfaces of NiCo_2O_4 chemically bind polysulfides to prevent their dissolution in the organic electrolyte.

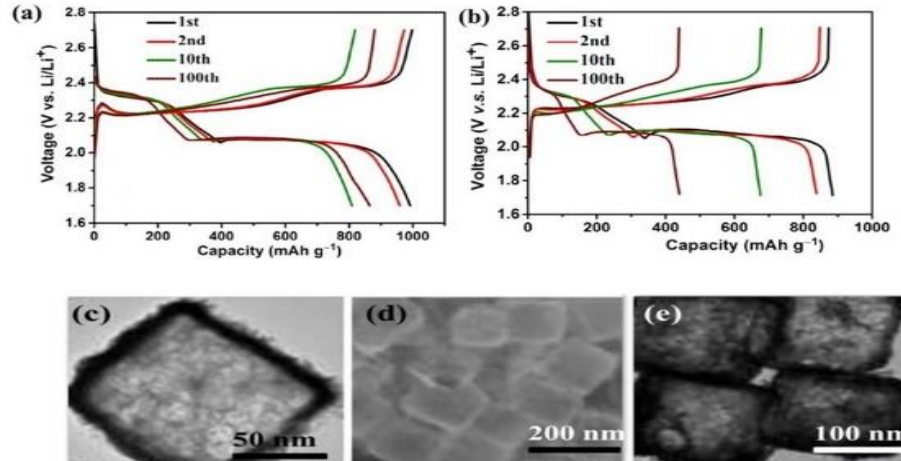


Figure 2.13 (a) and (b) The constant discharge/ charge profiles of the hollow NiCo₂O₄/S composites and pure sulfur electrode at 0.2 C, respectively. (c) and (e), (f) TEM images Hollow NiCo₂O₄ Nano cages and NiCo₂O₄/S composites [82].

where this the synthesized NiCo₂O₄/S cathode delivers high specific capacity (1274 mAh/g at 0.2 C) and good rate capability at high current rates (Figure 2.14) [89]. Recently stated Ya-Tao Liu et al, for the manufacture of sulfur-containing composite materials, NiCo₂O₄ nanofibers is introduced as carbon-free sulfur-free stabilizers. NiCo₂O₄ can stabilize a good cycle of sulfur cathodes. In particular, the S / NiCo₂O₄ compound provides a high gravitational capacity of 1125 mAh/g at 0.1 C rate with the compound as an active substance, and a low fade rate of 0.039% per cycle over 1500 cycles at a rate of 1 C [88]. Electrochemical performance was greatly enhanced by the strong chemical convergence between these nanoparticles and sulfur-containing species, which were able to capture polysulfides and mitigate the effect of the shuttle. And sulfides are considered the best options as additives, because they can act as an intermediary in the electrochemical oxidation system of Li-S.

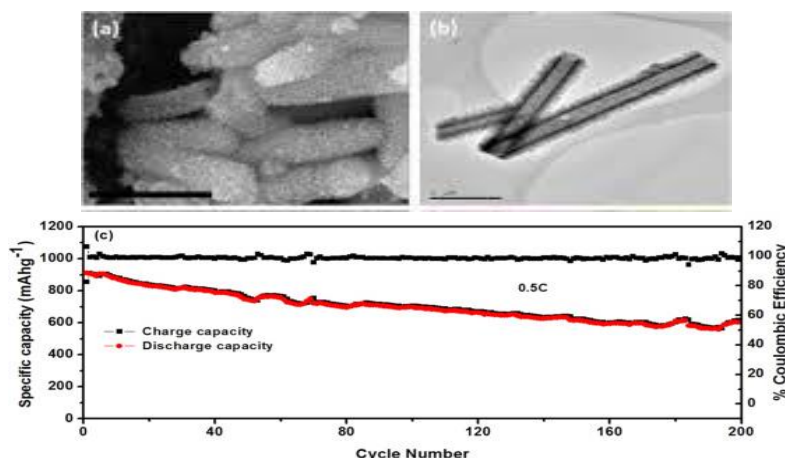


Figure 2.14 (a and b) SEM images of NiCo₂O₄ hollow microtubes, (b) Cyclic voltammograms of Capacity retention and Coulombic efficiency at a current density of 0.5 C [89].

All results indicate that the electrochemical properties of electrode materials are highly dependent on their size and shape. Therefore, it is necessary to develop an easy, low-cost, scalable method to assemble high-performance nanostructure materials in the desired shape and size.

2.3 Electrolytes

Electrolyte is the means used to connect the cathode and anode and transfer lithium ions between them. The electrochemical behaviors of Li-S batteries can be radically different in different electrolytes, arising from the various solubility of polysulfides in different electrolytes. So, much attention has been paid to exploration the occasion electrolytes for Li-S batteries [12]. Several special electrolytes have been developed, for example, ionic liquid electrolyte, organic liquid electrolytes, solid electrolytes and polymers. Liquid organic liquids containing lithium salts such as lithium bis (trifluoromethanesulfonyl) imide

(Li[N(S O₂CF₃)₂] or Li(TFSI), Li[SO₃CF₃]), and LiClO₄, and a mixture of organic solvents including DME, DOL, tetraethylene glycol dimethyl ether (TEGDME), tetrahydrofuran and fluoroethylene carbonate, are often used in Li-S for easy availability, high ionic conductivity, reasonable polysulfides solubility, low viscosity to fill in the micropores of the sulfur cathode, excellent wettability to sulfur cathodes and lithium anodes, low interfacial resistance, and chemical stability. Yet, polysulfides interact during the reaction process with most common electrolyte solvents, like esters, carbonates and phosphates. So, ether based solvents, like DME and DOL, are preferably suitable organic solvents in Li-S due to their persistence with metallic lithium and their compatibility with Sulfur of Cathode [17], [32]. For the selection of lithium salts, the highest priority is chemical compatibility with polysulfides. Until now, LiCF₃SO₃ and LITFSI (LiN) SO₂CF₃ and LiClO₄ have been reported to be the most suitable salts, where LITFSI excels in providing high ionic conductivity and less corrosion of the aluminum substrate [17]. The solubility of lithium polysulfides in these liquid electrolytes, which acts on the effect of shuttle and the formation of dendrite on the surface of the metal anode Li is inevitable. To reduce the dissolution of polysulfides in liquid electrolytes additives were developed. The most important results on the electrolyte are that lithium nitrate (LiNO₃) is an exceptionally strong electrolyte additive and is effective in inhibiting the polysulfide shuttle, which improves the efficiency of Coulombic, and can contribute to increasing the ionic conductivity of electrolytes, from 0.8 to 1.4 m sec⁻¹ [16]. Studies have shown that LiNO₃ acts as an oxidizing agent, a critical component to form a protective film for the lithium anode surface, improving the life cycle of LSBs [16, 90]. Other additives, such as phosphorus pentasulfide (P₂S₅) [91], copper acetate (Cu(OOCCH₃)₂) [92], LiB [93], LiBOB (lithiumbis (oxalato) borate) [94] and lithium oxalyldifluoroborate (LiODFB)

[95], were used to enhance the formation of the surface passivation layer on the lithium electrode and improve the electrochemical performance of Li-S [16, 90]. In addition, high viscosity and low conductivity of focused electrolytes with less free solvent molecules can effectively prevent the dissolution of polysulfide, reduce side reactions between Li metal and polysulfide types, protect Anode Li, and suppress the formation of Li dendrite [96]. In another aspect, the researchers studied the possibility of reducing the dissolution and shuttle of polysulfides using ionic liquid electrolyte or electrolyte polymers / solid state. Ionic fluids with high electrochemical stability, wide potential window and low vapor pressure are a new type of electrolyte material for Li-S batteries because they can saving low solubility energy towards polysulfides and detracton shuttle effect (Figure 2.15) [97, 98]. A series of ionic liquid electrolytes ,such as LiTFSIPyr_{1,201}TFSI/TEGDME/ LiTFSI [99], a hybrid electrolyte of N-methyl-N butylpyrrolidinium bis (triuoromethylsulfonyl) imide (Py₁₄TFSI) and LiTFSI dissolved in a mixture of DOL and DME[100] ,and Pyr_{1,201}TFSI (N-methoxyethyl-N-methylpyrrolidinium bis-(trifluoromethanesulfonyl)-imide)/TEGDME electrolyte with Lithium difluoro(oxalate)borate (LiDFOB)/ LiTFSI binary lithium salts [98], have been prepared to promote the formation of a SEI layer on the Li anode surface during charging and discharging. The smooth surface of an anode Li coated with a compact and uniform film was observed during cycling. For example, it has been shown that enhancing thermal stability and reducing the flammability of electrodes is made by the additive Py₁₄TFSI [100]. Py₁₄TFSI high viscosity ion liquid combined with conventional electrolyte contributes to the formation of a more stable and higher quality SEI layer on the surface of Li metal to protect Li anode [101] .Stable charge and discharge can be maintained by TFSI anion,

and the ether group in the cation of ionic liquid effectively improves conductivity of electricity.

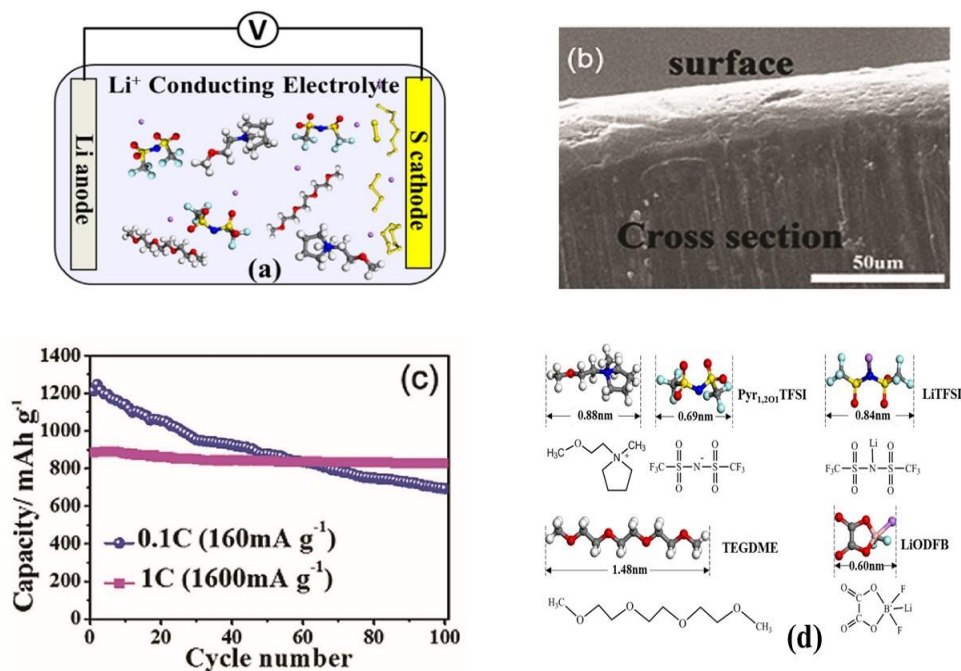


Figure 2.15 (a) Schematic illustration of the Pyr_{1,2O1}TFSI/TEGDME electrolyte with LiTFSI as lithium salt in LieS cell[98]; b) Cross-section SEM image of lithium metal cycled in 50% I L containing electrolyte for 100 cycles at 0.2 C [100]. c) Cycling performance of the Li–S batteries with the LiTFSI-P_{1,2O1}TFSI/ (30 wt%)TEGDME electrolyte[99]. : (d)

Molecular structures and sizes of the electrolyte components:

Pyr_{1,2O1}TFSI, TEGDME, LiTFSI, and LiODFB [98].

In general, the application of polymeric electrolytes in Li-S batteries suffers from low ionic conductivity at room temperatures. Reducing the dissolution and cubation of polysulfides, and reducing safety concerns associated with liquid electrolyte by gel polymer and solid-state electrolytes can be more effective than liquid electrolyte [102]. To enhance the ionic conductivity and mechanical properties of polymeric electrolytes many polymer structures have been

developed. For example Poly(ethylene oxide) (PEO) with lithium salts containing Nano particular scattered ceramic fillers including SiO_2 [103], ZrO_2 [104], and Al_2O_3 [105], these electrolytes display high ionic conductivity, excellent thermal stability, and good interstitial stability. For Li-S batteries, various other solid electrolytes with high ionic conductivity were examined at room temperature, such as $\text{Li}_2\text{SP}_2\text{S}_5$ /hydroxyterminated perfluoropolyether (PFPE-diol)/ (LiTFSI) [106], $\text{Li}_{3.25}\text{-Ge}_{0.25}\text{P}_{0.75}\text{S}_4$ [107, 108], $\text{Li}_2\text{SP}_2\text{S}_5$ [109, 110], $\text{Li}_2\text{S-GeS}_2\text{-P}_2\text{S}_5$ [111], and $\text{Li}_{10}\text{GeP}_2\text{S}$ [112]. Solid electrolytes can effectively eliminate the problem of dissolving polysulfide and blocking Li dendrite, although the main challenges remain the achievement of smooth electrode / electrolyte interfaces and a significant decrease in impedance between the resulting solid-state electrolyte and solid electrode in Li-S batteries. Most studies focused on the development of advanced cathode materials. So, to ease the most important challenge is the so-called "shuttle effect". As mentioned above, during the charging and discharging process, intermediate lithium polysulfide can be decomposed into organic liquid electrolytes, resulting in loss of active substances and the effect of shuttle polysulfide. Another promising solution is to introduce an interlayer that blocks the polysulfide between the Li anode and the cathode S to prevent corrosion of the Li anode, and to prevent the efficient transmission of polysulfides from the S cathode to the Li anode thus greatly reducing the passivation of the Li anodes into the Li-S battery. For the first time, single-walled carbon nanotubes were presented in the form of an inner layer and the new Li-S formation shown in Figure (2.16)[113]. The interstitial layer can effectively prevent the transmission of polysulfides by capturing and facilitating the optimal use of inhibitory active substances, thereby improving the stability of cycling in Li-S cells, and a number of carbon-based interlayers have been found. (Figure 2.17),

including porous carbon paper[114], membrane Carburetor [115, 116] , low graphite oxide [117], nickel foam [118] and polymers [119] interfaces for Li-S. Based on the improved electrochemical performance of the Li-S, the introduction of an interstitial layer between the separator and cathode is an attractive method.

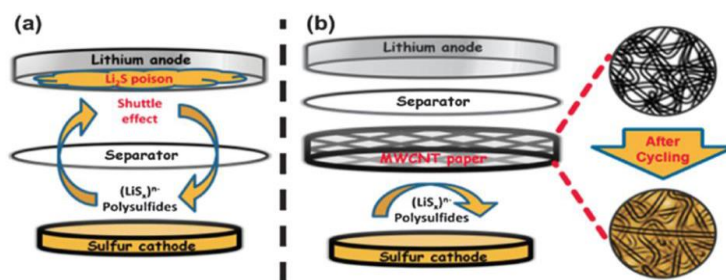


Figure 2.16 The schematic cell configuration of rechargeable Li-S: (a) traditional Configuration with severe shuttle effect and Li_2S poison problems and (b) new configuration with an interlayer[113].

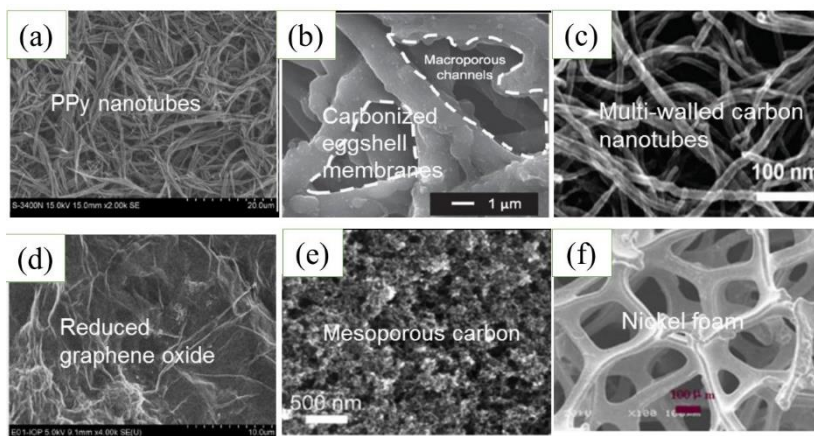


Figure 2.17 SEM images of interlayers made from (a) PPy nanotubes [119] ,(b) carbonized eggshell membrane [116],(c) CNTs[113], (d) reduced graphene oxide [117], (e) mesoporous carbon [120], and (f) nickel foam [118].

For the first time, a small carbon paper (MCP) was introduced between the cathode and separator by the Manthiram group [121], as shown in Figure (2.18). With MCP dual-function between the cathode and the separator, a significant improvement was achieved in the use of active substances, also in the capacity retention, the cycle was maintained at a rate of 1C over 1000 mAh/g after 100 cycles, conversion to 85% retention rate with Average Coulombic efficiency of 97.6%. Since then, all types of porous carbon are used interchangeably [46].

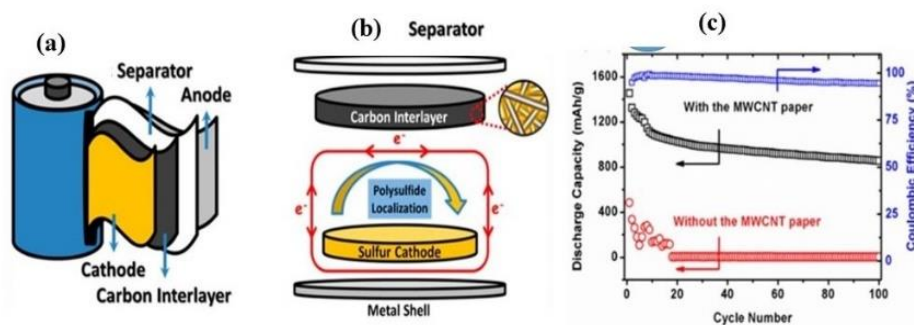


Figure 2.18 (a) Schematic of a Li–S cell with a bifunctional microporous carbon interlayer inserted,(b) Prototype LiS coin cell configuration with a carbon interlayer in the cathode region [121].(c) Electrochemical performance of the LiS cell with a MWCNT interlayer at 0.5 C rate [46].

2.4 Modified Separators

Despite the various successes in the new interfaces discussed above, the thickness of these films is unnecessarily large (hundreds of millimeters) and the weight (several milligrams), which results in low battery power density. Also, the ideal interlayer usually requires a stand-alone structure, which makes the material more complex. The separator is an essential part of the electrochemical cell, which provides paths for the transport of ions and prevents the inner short circuit. The approach of exploring modified joints appears to be more effective

to promote electrochemical behaviors with (1) functions similar to the thinner and lighter coating layer. (2) Prevent the transmission of polysulfide to the anode, suppress the effect of the shuttle; and (3) protect the surface of the lithium metal from the side reactions with Propagation of polysulfides. Functional layers have been applied to adjust the separator for high battery performance, like various carbon materials [122, 123], polymers [124, 125], metal oxides / sulphides [126, 127] , and their compounds [128, 129] . These modified spacers have been very successful in improving the performance of Li-S batteries. The most popular material for modifying lithium-sulfur battery separators is carbon materials such as carbon nanotubes [130], N-doped porous carbon nanowires [131], carbon black [122], nitrogen-doped mesoporous carbon [129], and grapheme [132, 133], (Figure 2.19) [134], because they have a porous structure, large conductive surface area or sufficient pathways to absorb dissolved polysulfides and regulate polysulfides, and also have high electrical conductivity to provide a fast, short-distance electron transfer. In the study of the conclusion of the manufacture of a modified carbon-encapsulated carbonate separator [123] . The thinner and lighter layer of the separation coating was much lighter than most of the interlayer, with a thickness of about 27 microns and a weight of 0.5 mg / cm² (Figure 2.20). The carbon layer provides a material place for settling dissolved soluble polysulfide and maintaining it as active substances within the cathode side, achieving outstanding performance with a high residual capacity of 723 mA / g after 500 cycles at 0.5 C. Modified separators using metal oxides and their compounds, including MnO/ Ketjen Black [135], Al₂O₃ [136], Mg_{0.6}Ni_{0.4}O/Ketjen Black composite [137], and V₂O₅ [138], have improved the electrochemical performance of Li-S batteries because their strong effect on the binding of

polysulfide of oxygen-rich metal oxides helps suppress the spread of polysulfides along of lithium anode . To solve the problem of the impact of shuttle lithium polysulfides and corrosion in Li anodes, multimedia separators were prepared, including three-layer separators of sulfur/graphene/polypropylene [132], carbon/lithium aluminum germanium phosphate/Celgard [139], and carbon nanotube/polypropylene/ Al_2O_3 [140]. Graphene/ polypropylene / Al_2O_3 separator [140], presented by blade coating process, shows dual function .

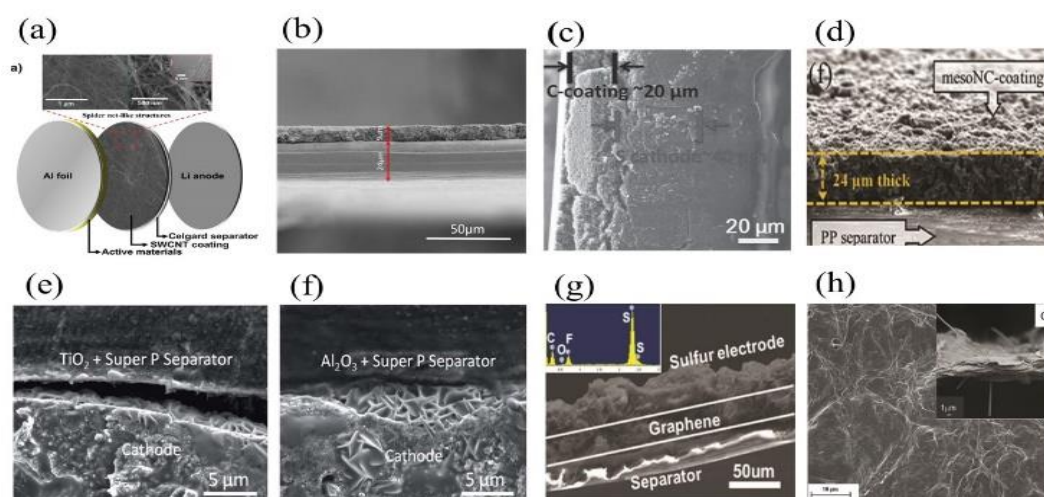


Figure 2.19 (a) Schematic and SEM images of the single-wall carbon nanotube modulated separator configuration. Cross-section SEM images of various samples [130] b) N-doped porous carbon nanowire-modified separator [131]. c) cell with the C-coated separator, [122] , d) N-doped mesoporous carbon-coated separator [129], e, f) TiO_2 –Super P coated separator–cathode interface and the Al_2O_3 –Super P coated separator–cathode interface [134], g) Integrated sulfur electrode with the G@PP separator and corresponding EDS spectrum [132], and h) fluoro-functionalized reduced graphene oxide separator [133].

Graphene coated on one side of the polypropylene separator represents an electrostatic depot and a conductive layer to allow for rapid transfer of ions and electrons, the coated Al_2O_3 molecules on the other side operate on the safety and thermal stability of the cell. The modified polymer separators such as a polydopamine layer [141], a mixture of Nafion and super P [142], and ion selective Nafion membrane layer [143], can confine polysulfide anions into the sulfur cathode side and prevent them from spreading along the lithium anode, and also maintaining the stability of the electrode structure and blocking the transport path of dissolved polysulfides.

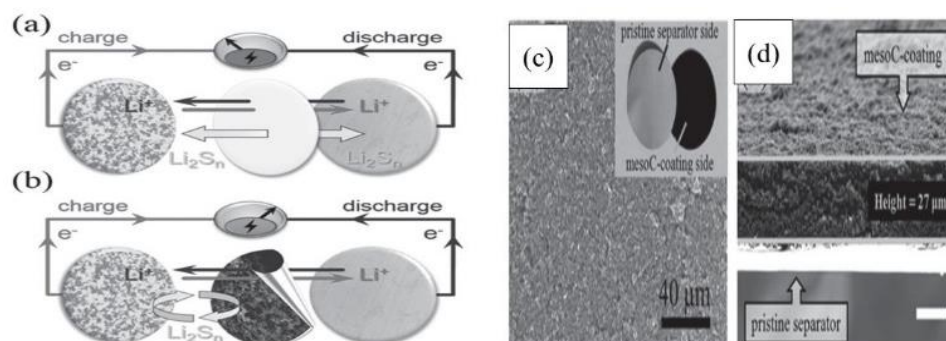


Figure 2.20 Schematic configuration of the Li-S with (a) a pristine separator; (b) mesoporous carbon-coated separator; SEM images of (c) top surface of the mesoporous carbon-coated separator and (d) cross-section and [123].

Chapter Three

Material Characterizations and Electrochemical Measurements

3.1 The Chemicals and Materials

In table 3.1 summarizes the chemicals and materials used to Characterizations, Synthesis and Electrochemical Measurements used in my PhD studies.

Table 3.1 Chemicals and materials for Synthesis and Electrochemical tests

Item	Chemicals and materials	Formula	Purity	Supplier
1	Ethanol	C_2H_5OH	Reagent	Sigma Aldrich
2	Nickel Chloride Hexahydrate	$NiCl_2 \cdot 6H_2O$	99	Sigma Aldrich
3	Ammonium persulfate	$(NH_4)_2S_2O_8$	>98	Sigma Aldrich
4	ammonium hydroxide	NH_4OH	99	Sigma Aldrich
5	Nickel (II) nitrate hexahydrate	$Ni(NO_3)_2 \cdot 6H_2O$	99	Sigma Aldrich
6	hexamethylenetetramine (HMT)	$C_6H_{12}N_4$	99	Sigma Aldrich
7	trisodium citrate dihydrate (TSC)	$C_6H_5Na_3O_7 \cdot 2H_2O$	98	Sigma Aldrich
8	Cobalt (II) nitrate hexahydrate	$Co(NO_3)_2 \cdot 6H_2O$	99.9	Sigma Aldrich
9	carbon cloths	CC	N/A	Sigma Aldrich
10	acetylene black	s.c	99	Sigma Aldrich

11	Polyvinylidene fluoride (PVDF)	$(\text{CH}_2\text{CF}_2)_n$	N/A	Sigma Aldrich
12	N-methyl-2-pyrrolidone (NMP)	$\text{C}_5\text{H}_9\text{NO}$	99.5	Sigma Aldrich
13	lithiumbis(trifluoromethanesulfonyl)imide	LiTFSI in DOL/DME	99.95	Sigma Aldrich
14	Lithium nitrate	LiNO_3	99	Sigma Aldrich
15	(CR2016) coin-type cells	N/A	N/A	Sigma Aldrich
16	Celgard 3501	N/A	N/A	Sigma Aldrich
17	Lithium Metal	Li	99.9	Sigma Aldrich

The equipment's used in the experiments on shows the table 3.2. Table 3.1 was adopted to assemble the sulfur lithium batteries. The typical instruments for physical characterization of the samples, show in items 1-9. While items 10-17 are used during the exploration of electrochemical properties of the products.

Table 3.2 used on the Instruments experiments

Item	Instruments	Model	Brand
1	glove box	(CR2016)	Chenhua, Shanghai
2	SEM	SU8010	HITACHI
3	X-ray diffraction	XRD-6000	Shimadzu
4	BET Analyzer	3000	NOVA
5	Battery Tester	LAND CT-2001A	Wuhan, China
6	Electrochemical Workstation	CHI660c	Chenhua, Shanghai

3.2 Experimental Steps

In this research used two topics of main; the part of first is the active Material characterizations and composite electrode fabrication, and the second part it applies to use of the active Material of electrochemically as electrode on the lithium sulfur batteries.

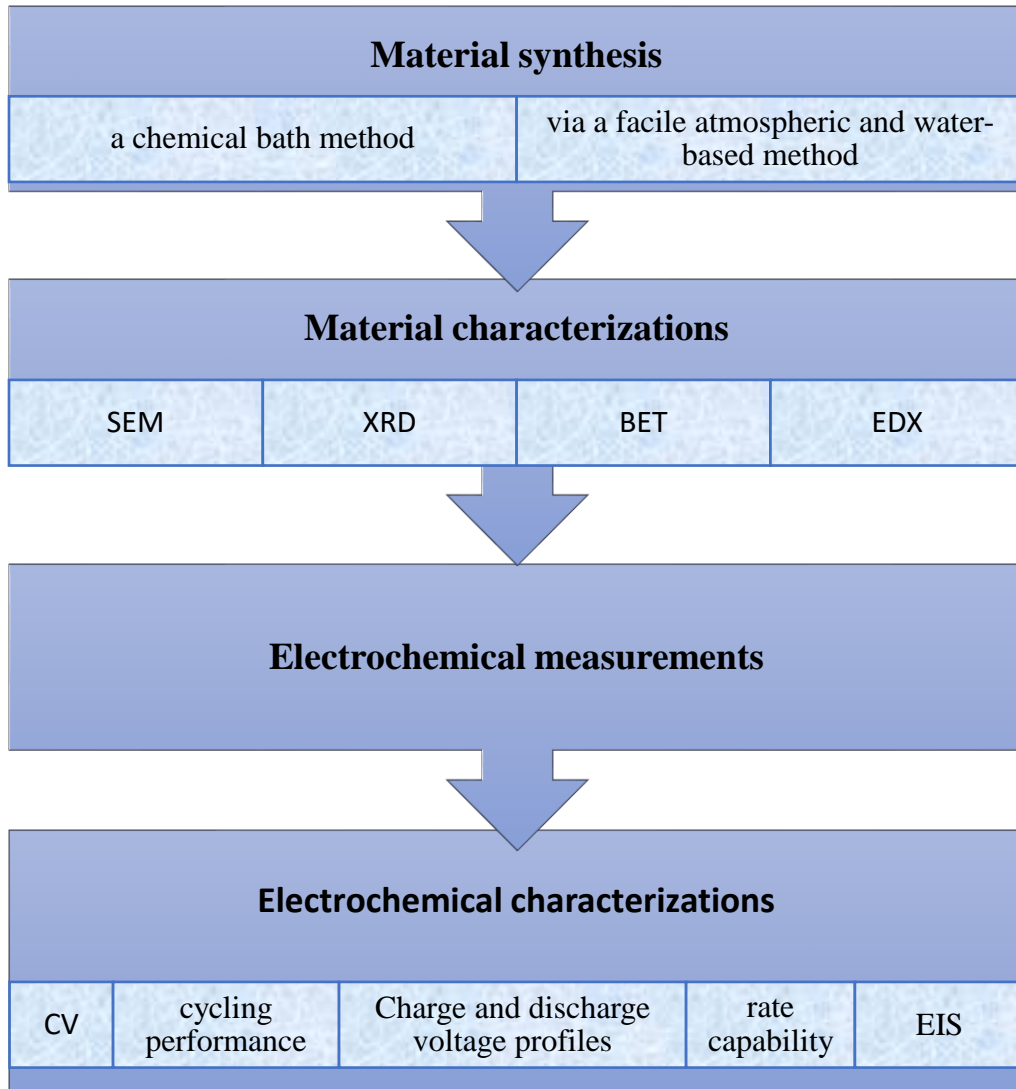


Figure 3.1 Comprehensive procedures and techniques.

3.3 Material Synthesis

It is a method for depositing thin films and nanomaterials, which was first described in 1869. It can be used to treat large batches or continuous sediments. This technique is widely used for depositing the insulating layers in thin-film photovoltaic cells. Chemical bath precipitation involves two steps, the nucleus and particle growth, and is the formation from based on the formation of a solid stage of the solution. In the chemical bath sedimentation procedure, the substrate is immersed in a solution containing precursors. This method is based on criteria such as bath temperature, time, PH of solution and molarity of concentration. In 1933 Brackman deposited lead (II) sulfide (PBS) thin film by chemical bath deposition, or solution growth method. The major advantage of CBD is that it requires in its simplest form only solution containers and substrate mounting devices. One of the drawbacks of this method is the wastage of solution after every deposition. Chemical bath deposition yields stable, adherent, uniform and hard films with good reproducibility by a relatively simple process. The growth of thin films strongly depends on growth conditions, such as duration of deposition, composition and temperature of the solution, and topographical and chemical nature of the substrate (Figure 3.2).

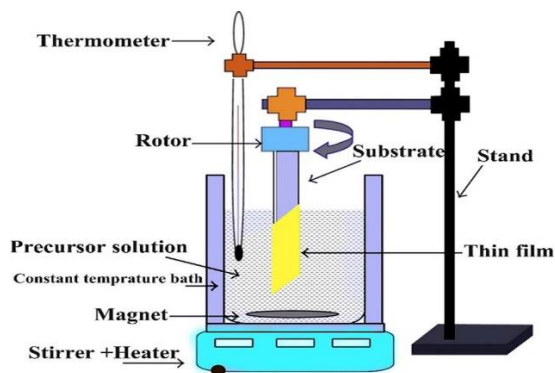


Figure 2.2 Schematic of a chemical bath deposition.

3.4 Material characterizations

3.4.1 X-Ray Diffraction

X-ray Diffraction (XRD) is one of the basic non-destructive techniques used by metal scientists and solid-state scientists to examine the physical composition of chemical substances. X-ray diffraction is one of the most important characterization tools used in solid state chemistry and materials science. An x-ray diffraction scale consists of an x-ray generator, angle instrument, detector, and computing system. During the process, the x-ray beam is generated by the generator, then the sample is doubled pending analysis. Certain diffraction patterns are then produced during this process due to the specific arrangement of atomic layers. The obtained XRD patterns with strong and weak peaks are used to determine the chemical composition, crystal structure, and particle size of the samples. To understand how these X-rays work, the illustration shown in Figure 3.3 helps in diffraction and the Prague equation that you quantify.

$$2d \sin\theta = n\lambda \quad (3-1)$$

λ is Wavelength, at a certain angle θ

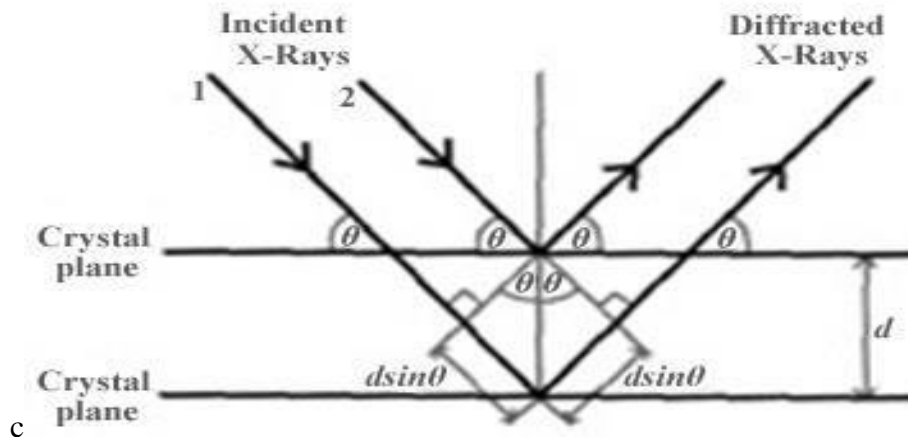


Figure 3.3 Illustration of X-ray diffraction and Bragg equation.[144]

From the illustration, we can see that the X-ray (1) scattered by the lower crystalline plane travels $2d \sin\theta$ longer than the X-ray (2) spread by the upper crystalline plane. If this distance is multiple n , of λ is correct, constructive interference occurs and the peak of the photon intensity must be noted. With known values of θ and λ , from interference analysis it is possible to determine the crystalline flat spacing d . With respect to the X-ray beam, the variation of θ is permitted to rotate the sample, and in a similar way d other crystal planes can be determined.[144] The XRD pattern is often used as a fingerprint to identify a substance, a hallmark of that crystal. To examine all the products during this research project, works the X-ray diffraction scale in (XRD, Shimadzu XRD-6000 with Cu $K\alpha$ radiation ($\lambda=1.54056 \text{ \AA}$))

3.4.2 Scanning Electron Microscope

Scanning electron microscope (SEM) is a type of electron microscope that produces images of a sample by scanning the surface with a focused beam of electrons. The electrons interact with atoms in the sample, producing various signals that contain information about the sample's surface topography and composition. The electron beam is scanned in a raster scan pattern, and the beam's position is combined with the detected signal to produce an image. SEM can achieve resolution better than 1 nanometer. Specimens can be observed in high vacuum in conventional SEM, or in low vacuum or wet conditions in variable pressure or environmental SEM, and at a wide range of cryogenic or elevated temperatures with specialized instruments. to study the structural properties and size of Nano sheets, morphological of samples. The electron beam is mostly non-destructive and can even be used to image organic materials with some additional sample preparation. The electron microscope (EM) offers a higher resolution than the optical microscope

(OM), which works with photons, because the wavelength μ of the electron is a smaller size than the photon. According to de Broglie equation

$$\lambda = \frac{h}{P} = \frac{h}{mv} \quad (3-2)$$

where $h = 6.626 \times 10^{-34}$ J.s is Planck's constant, P is the linear momentum of a particle of mass m and velocity v. An electron of a speed of 5×10^6 m/s gives a μ of 0.146 nm, which is already smaller than that of a *Dv L α* radiation ($\lambda = 0.154$ nm). Schematic Figure 2-4 illustrates the SEM process. The electron gun uses an electronic source, and it extracts a beam of electrons. And then with the electromagnets the electron beam is focused, and similarly to a small spot in the sample, the light is focused with a glass lens in OM. The name of EM scanning comes from that the sample image is created by scanning this spot of the electron beam express the region of imaging. We cannot see the electron in the sense of a photon, to collect electrons in the in the vacuum chamber a detector is used, and generates an image on a computer screen. In Figure 2-4 shows the interaction of the electronic ray with the sample is done in a more detailed view. When the sample upon bombarded with a falling electron beam, secondary electrons are emitted, and the electrons in the electron beam being that the sample is scattered are those backscattered electrons. Through the detector that collects the secondary and backscattered electrons, SEM images are created.[145, 146] Photons can be generated during the process of bombing the electronic beam, such as X-rays, whose disclosure gives information about the elemental formation of the sample near the surface[145]. These are to determine the composition of elemental by an X-ray analysis process called an X-ray spectroscopy (EDX). To examine all the products during this research project, works the (SEM) on HITACHI SU8010.

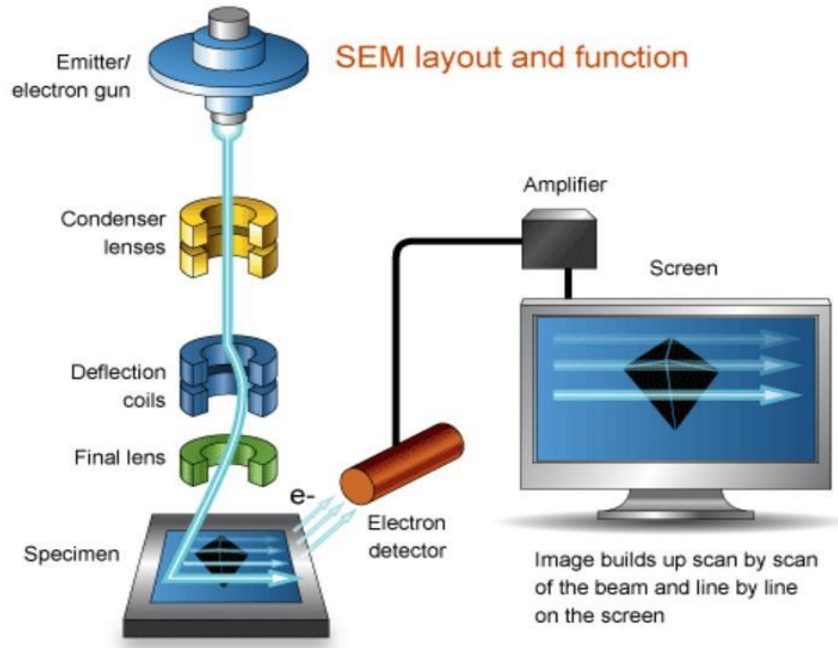


Figure 3.4 Schematic illustrating the operation and layout of a SEM [145].

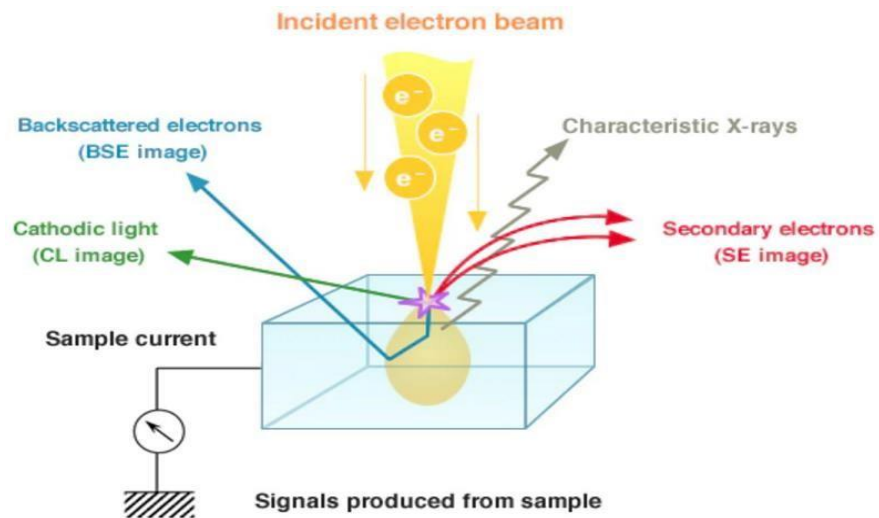


Figure 3.5 Schematic illustrating the interaction between the incident electron beam and the sample[146].

3.4.3 Brunauer-Emmett-Teller

Brunauer-Emmett-Teller (BET) is an analytical method used to evaluate the specific surface area for characterization of materials, pore size distribution, and pore size of the material by absorbing multilayer nitrogen at different relative pressures. In bulk matter, the majority of the atoms that make up the substance are found within the internal volume, and unlike the nanomaterials they are mostly made of surface atoms and with a reduced particle size. The ratio of the surface area to the total particle size increases. Thus, in nanomaterials, the reactions that take place on the surface of a substance (such as melting, oxidation, photo-dissolution, photo-excitation etc.) are more pronounced. Supposedly BET adsorption that of the material the surface is homogeneous and that adsorption happen evenly across the entire surface without preferential absorption sites. Each adsorbent site is either occupied by one adsorbent molecule (a maximum of one molecule per adsorbent site) or is not occupied.[147] The expression of total adsorption shall be expressed as a fractional surface cover. After absorption, the molecule can act as one absorption site for another gas molecule. Any interactions between other molecules are not considered (side reactions between adsorbed molecules, or non-adsorbent reactions between gas and adsorbed phase molecules, or interactions between gas phase molecules). Surface adsorption sites or adsorbed molecules (top layer) are in equilibrium with gas / vapor phase molecules called local equilibrium. The BET formula for gas absorption can be described as follows:

$$v = \frac{vm c}{(p_0 - p) + [1(c - 1)\left(\frac{p}{p_0}\right)]} \quad (3-3)$$

Here v is the adsorbed volume of gas, v_m is the adsorbed monolayer volume, p is the equilibrium gas pressure, p_0 is the saturation pressure and c are the BET constant. Can be this equation rearranged as follows as a linear function of p / p_0 :

$$\frac{1}{v[(\frac{p}{p_0})-1]} = \frac{c-1}{vmc} (\frac{p}{p_0}) + \frac{1}{vmc} \quad (3-4)$$

You can then use the y-intercept and the slope for this function to solve the constants c ($= \text{slope} / \text{intercept} + 1$) and v_m ($= 1 / (\text{slope} + \text{intercept})$). With equation (3-5), then the specified surface area (S , surface area of each unit unit) can be found in the equation

$$S = \frac{vmNA}{22,400 \times m} \quad (3-5)$$

N is the constant and is the number of Avogadro (the number of molecules per mol), A is the surface area of the cross-sectional surface of a single adsorbent gas molecule, m is the mass of nanomaterials used in the measurement and 22,400 represents the Standard Temperature and pressure (STP) volume of one mole of gas. This surface area is given in area / mass units (for example, m^2 / g), which by multiplying by the density of the material can be converted to a volume-specific surface area. The measurement of specific surface area and analysis of porosity in this research are carried out through measuring N_2 adsorption-desorption isotherms at 77 K with a Quanta chrome NOVA-3000 system [147].

3.5 Electrochemical Measurements

3.5.1 Electrode Fabrication

The electrode slurry was prepared were made by mixing the products, acetylene black (s.c) 0.02 g and polyvinylidene fluoride (PVDF) 0.003 g at a weight ratio of 8:1:1 in N-methyl pyrrolidone (NMP)150 ml. The electrode was prepared by coating the slurry onto an NiO/CC and dried in vacuum to remove the absorbed water of the electrode.

3.5.2 Electrochemical and Cell Assembly Testing

Electrochemical measurements were carried out in an electrochemical cell by using coin-type cells (CR2016) at room temperature. The composite electrode is employing as cathode without any polymer binder. Lithium foil and Celgard 3501 sheets were used as the anode and separator. The cells were assembled in an argon-filled glove box and 1.0 m LiTFSI in DOL/DME (1:1 by volume) was used as the electrolyte. In addition, 1.0 wt% LiNO₃ was used as an electrolyte additive to stabile Li anode by in situ formation of a protective layer on its surface, Cyclic voltammetry (CV) and galvanostatic charge/discharge measurement were performed on CHI660c electrochemical workstation (Chenhua, Shanghai). The relationship between current and voltage of the working electrode is measured by Cyclic Voltammetry (CV) at different scan rates. CV is used to examine the electrochemical activity of a material and the redox character can be determined by the pairs of peaks in relation to the reduction and oxidation occurred on the electrode.

3.5.3 Electrochemical Characterizations

3.5.3.1 Cyclic Voltammetry

Cyclic voltammetry (CV) is a type of potentiodynamic electrochemical measurement. The working electrode potential is ramped linearly versus time, in a cyclic voltammetry experiment. Cyclic voltammetry is generally used to study the electrochemical properties of an analytic in solution or of a molecule that is adsorbed onto the electrode. A standard CV experiment employs a cell fitted with three electrodes: reference electrode, working electrode, and counter electrode. This combination is sometimes referred to as a three-electrode setup. Electrolyte is usually added to the sample solution to ensure sufficient conductivity. The solvent, electrolyte, and material composition of the working electrode will determine the potential range that can be accessed during the experiment.

3.5.3.2 Galvanostatic cycling measurement

Galvanostat (also known as amperostat) is a control and device of measuring capable of maintaining current out of an electrolytic cell in a steady coulometric titration, ignoring changes in the load itself. An electrochemical cell charge / discharge is tested using a cell test system, it is a workstation of electrochemical that operates either as a strong air force or as a Galvanostat, recording the current or potential corresponding response. A charge / discharge cell is commonly performed under the galvanization position, in which the charge / discharge properties of the active substance may be compared to another property. Beneath a current of constant, the specified charge / discharge capacitance may be current related, the first being plotted as a loop while the cellular voltage is plotted as coordinates. Thereupon this

work, the capacity of the collected cells was fixing by re charging and discharging the tests. The analogy was performed under a constant current density, and was calculated the charge / discharge capacity (Q) by equation (3.6),

$$Q = i*t \quad (3.6)$$

where (I) is density of current and (t) is time of charging/discharging. The voltage for cutoff the sulfur composite cathode in our work is about 1.7 ~ 2.7V. The material's C rate property was too evaluated by performing tests under different densities of current for the lithium sulfur battery test.

3.5.3.3 Electrochemical Impedance Spectroscopy

The electrochemical resistance spectroscopy is one of the most sophisticated techniques in research of electrochemical. It is are techniques of electrochemical to measure a system's resistance to AC frequency dependence. It is a frequency field scale made by applying a sinusoidal disorder, and the voltage is often, on the system through an application of oscillating voltage and withdrawing a set of frequencies, the corresponding alternating current can be obtained at each frequency. Impedance at a certain frequency is related to processes occurring at time domains of the inverse frequency (such as $f = 10 \text{ Hz}$, $t = 0.1 \text{ s}$). So, impedance changes in can be measured.

Chapter Four

NiO Nanosheets Grown on Carbon Cloth as Mesoporous Cathode for High Performance Lithium-Sulfur Battery

4.1 Introduction

Transition-metal compounds are promising candidates for improving the performances of Li-S batteries owing to the high adsorption capability towards polysulfides [148, 149]. Metal oxides were introduced into carbon materials to generate a polar surface to promote the poor reaction between carbon-based non-carbon materials and polar polysulfides leading to good confinement, and freezing polysulfides from the carbon surface [150]. In the last years, due to their promising applications of nickel-based materials, nickel hydroxide ($\text{Ni}(\text{OH})_2$) and nickel oxide (NiO) have received tremendous research interest in electrochemical devices. Nickel oxide has attracted considerable attention due to its low cost, environmental friendliness, high theoretical capacity (718 mAh/g), and natural abundance [151].

In order to improve the electron transport for the conversion of the adsorbed LiPSs, carbon cloth (CC) has been used as an electronic conductive matrix for transition-metal sulfides due to its high conductivity, high flexibility strong mechanical property and light-weight [152]. However, the growth of transition-metal sulfides is accompanied with the production of pollutant hydrogen sulfide. Herein, in the present work, we demonstrate a facile chemical bath deposition method to prepare mesoporous NiO Nanosheets arrays on carbon cloth (NiO/CC) for sulfur impregnation to serve as cathode for Li-S batteries. The NiO/CC acts confinement of polysulfides. As a result,

the battery using the sulfur impregnated NiO/CC (NiO/CC/S) exhibit high specific capacity and cyclic stability.

4.2 Experimental

4.2.1 Materials

Ammonium Persulfate ((NH₄)₂S₂O₈), Nickel (II) Chloride Hexahydrate (NiCl₂·6H₂O), ammonium hydroxide (NH₄OH), carbon cloths (CC), N-methyl pyrrolidone (NMP), polyvinylidene fluoride (PVDF) were bought from Sigma-Aldrich.

4.2.2 Synthesis of NiO Nanosheets/Carbon Cloths

First, the CC was purified in ethanol and washed sequentially with deionized (DI) water. (NH₄)₂S₂O₈ (3.56 g) and NiCl₂·6H₂O (2.38 g) was dissolved in 32 mL deionized water under stirring for about 20 min, followed by the addition of 2 mL ammonium hydroxide. Subsequently, CC was immersed into the above solution for 20 min. The CC covered by the black layer were washed with DI water three times, and dried in ambient atmosphere. Finally, the dried sample was heated to 300 C° for 90 min in ambient atmosphere, then cooled to room temperature naturally. The areal loading of NiO on CC is about 3.8 mg/cm².

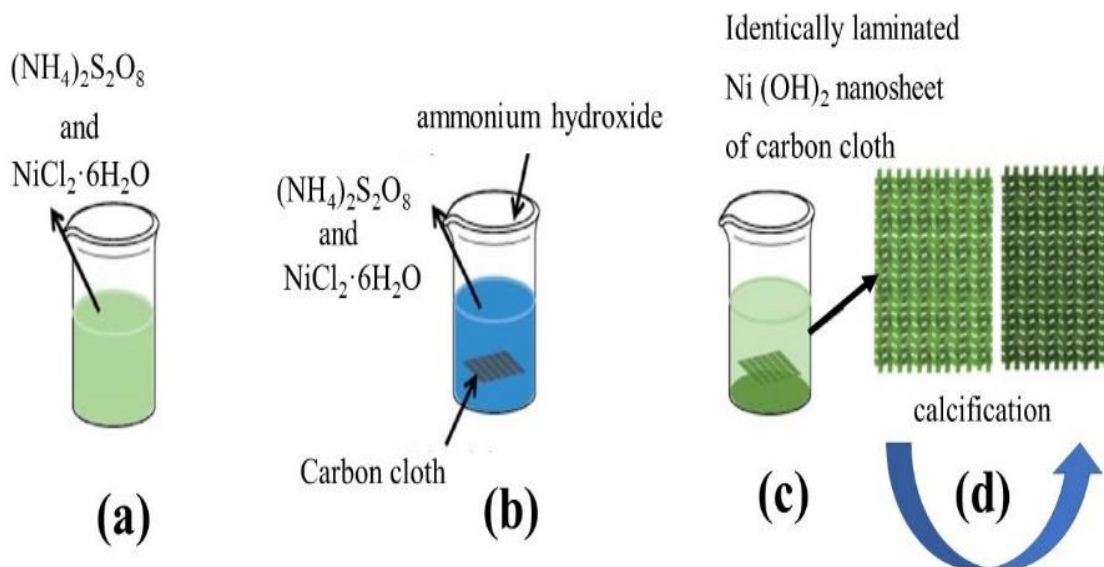


Figure 4.1 Schematic illustrating the Synthesis of NiO nanosheets/carbon cloths.

4.2.3 Preparation of NiO/CC/S

The electrode slurry was made by mixing sulfur, acetylene black and polyvinylidene fluoride at a weight ratio of 8:1:1 in N-methyl pyrrolidone (NMP). The electrode was prepared by casting the slurry onto a NiO/CC and dried at $60\text{ }^\circ\text{C}$ for 12 h in vacuum. The areal sulfur loading is $\sim 1.2\text{ mg/cm}^2$, electrode was pouched to a $\sim 1\text{ cm}^2$ pallet.

4.3 Results and Discussions

4.3.1 Physicochemical Properties of the Materials

The constituent and phase purity of the as-prepared samples were checked by X-ray diffraction (XRD), as shown in Figure 3-2. Diffraction peaks in Figure 4.2(a) from pre-fabricated precursor/carbon cloth could be assigned to $\text{Ni}(\text{OH})_2$ (JCPDS 38–0715). As shown in Figure 4.2(b), all the diffraction peaks after annealing can be indexed in NiO style with the cube-centered phase (JCPDS

47–1049), indicating that Ni (OH)₂ precursor was wholly converted to NiO. Also, the peaks at 26° and 54° can be assigned to the carbon cloth substrate [149]. No additional peaks are detected other than NiO and carbon, indicating the high purity of the product.

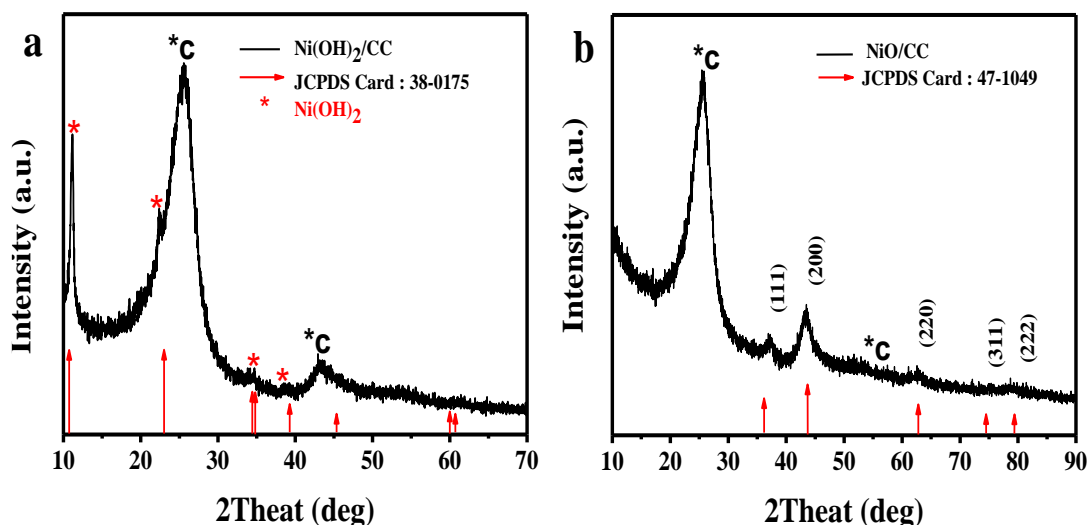


Figure 4.2 X-ray diffraction (XRD) patterns of (a) Ni (OH)₂ and (b) NiO on the carbon cloth.

According to the Brunauer–Emmett–Teller analysis, the CC and mesoporous NiO/CC composite possess specific surface area of 14.39759 and 43.8688 m² g⁻¹ and a pore volume of 0.03204 (cm³ g⁻¹) and 0.04731 cm³ g⁻¹ (Figure 4.3(a, b)), respectively. As shown in Figure 4.3 (a, b) (inset), analysis of pore size distribution indicates that the majority of pores have the diameter ranging from 1.4 to 7.75 nm and 1.7 to 18.2 nm, respectively.

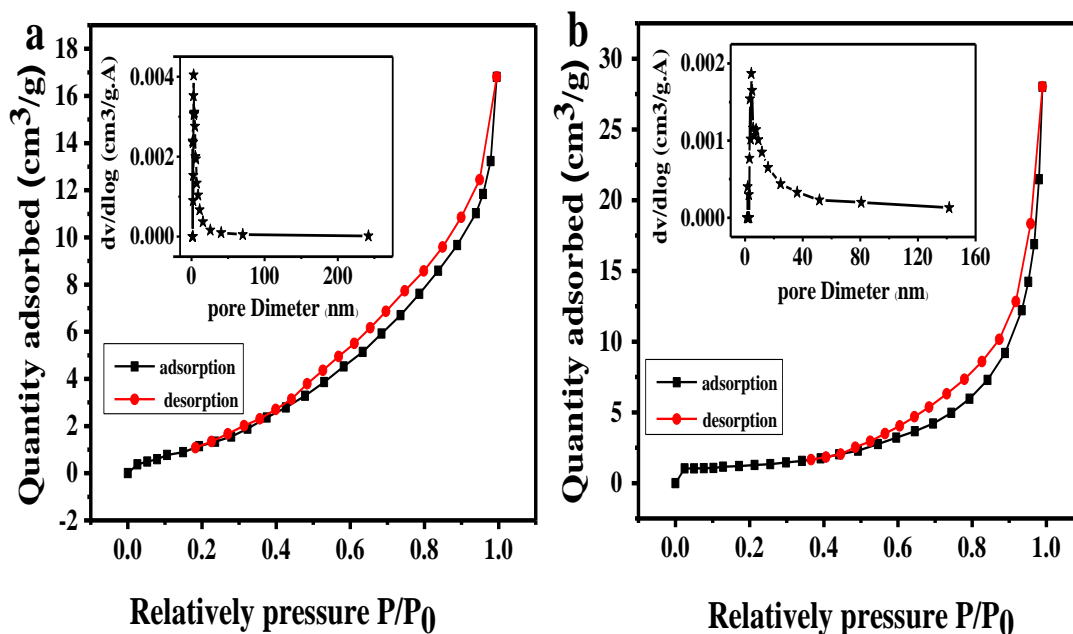


Figure 4.3 Nitrogen adsorption/desorption isotherms and pore size distribution (inset) of the (a) CC and (b) NiO/CC composite.

Figure 4.4(a) illustrates the SEM image of a well-cleaned carbon cloth with a smooth surface. In Figure 4.4(b), the surface of carbon fibers becomes rough after growth of NiO nanosheets. The carbon cloth is decorated by vertically connected NiO Nanosheets, creating a porous nanostructure with open space and electro active surface. Energy dispersive spectroscopy (EDS) analysis was carried out in a representative region (Figure 4.4(d)). The mapping results of O (Figure 4.4(e)) and Ni (Figure 4.4(f)) indicates the homogeneous decoration of NiO nanosheets on CC fibers.

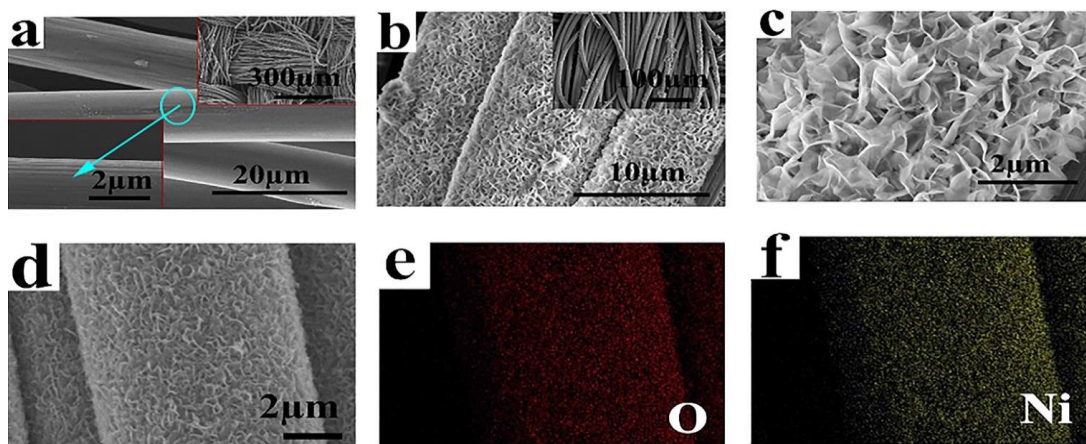


Figure 4.4 SEM images of (a) Pure carbon cloth, (b) NiO Nanosheets grown on carbon cloth (inset, low magnification image), and (c) micro structure of NiO Nanosheets. (d) Typical SEM image for a selected region of the NiO/CC composites, and the corresponding elemental mapping of (e) O and (f) Ni.

4.3.2 Electrochemical Performance of the S/NiO/CC and S/CC Composite

The electrochemical performances of Li-S cells based on NiO/CC/S cathode compared to those based on CC/S cathode are evaluated, in which the areal loading of sulfur and electrolyte volume in each cell are $\sim 1.2 \text{ mg cm}^2$ and $30 \text{ }\mu\text{L}$, respectively. The galvanostatic charge–discharge profiles of NiO/CC/S and CC/S composite electrodes are shown in Figure 4.5(a) at 0.1C. Two clear reaction plateaus are observed in the discharge curve of NiO/CC/S composite electrode. Importantly, the NiO/CC/S composite electrode exhibits high specific discharge capacity of 1154.8 mAh/g , higher than that of CC/S electrode (887 mAh g^{-1}). As shown in Figure 4.5(b), at the current densities of 0.5, 1, 2, 3, 4 and 5 mA cm^2 , the specific capacities of 1008.8, 761.6, 596.5, 526.2, 442.2 and 416.9 mAh g^{-1} can be achieved, respectively, indicating

excellent rate performance. Besides, a capacity of $1004.4 \text{ mAh g}^{-1}$ is observed when the current density reduces back to 0.5 mA cm^{-2} , indicating high reversibility of the NiO/CC/S composite electrode after high-rate cycling. Figure 4.5(c) presents the cycling performance of the NiO/CC/S and CC/S composite electrode at a current density of 2 mA cm^{-2} (about 1C). The initial discharge capacity of the composite electrode is 661.9 mAh/g , and the capacity remains at 520 mAh/g after 300 cycles with a decay rate of 0.07% per cycle and Coulombic efficiency of 98.7% , higher than that of the pure CC loaded with sulfur (about 300 mAh/g).

Carbon materials compared to TMO as additives of sulfur are superior in electronic conductivity under normal conditions; however, the S / NiO / CC compound offers good modifying performance (Figure 4.6(a)). At a current density of 0.2 C , the initial capacitance of the S / NiO / CC electrode is 1046.6 mAh/g and the S / NiO / CC electrode continues to provide a larger discharge capacity of 908.4 mAh/g even after 100 cycles. While the S / CC electrode shows an initial specific capacitance of 810.1 mAh/g , after 100 cycles this specific capacitance value fades to 413.9 mAh/g (Figure 4.6(b)). Moreover, the S / CC electrode during the electrochemical reaction suffers from severe polarization. It can be seen that the S / NiO / CC electrode exhibits a stable electrochemical process, a feature of the discharge / charge [82]. Figure 4.6(c, d, e) shows the spin performance of Li-S cells using a modified NiO / CC / S electrode with a current density of 1.1 mA cm^{-2} , 2.5 mA cm^{-2} and 3 mA cm^{-2} between 2.7 V and 1.7 V at room temperature. The cells with the modified NiO / CC / S electrode exhibit a distinct initial discharge capacity of $1359.09 \text{ mAh g}^{-1}$ and 656.5 and 650.4 mAh g^{-1} , respectively.

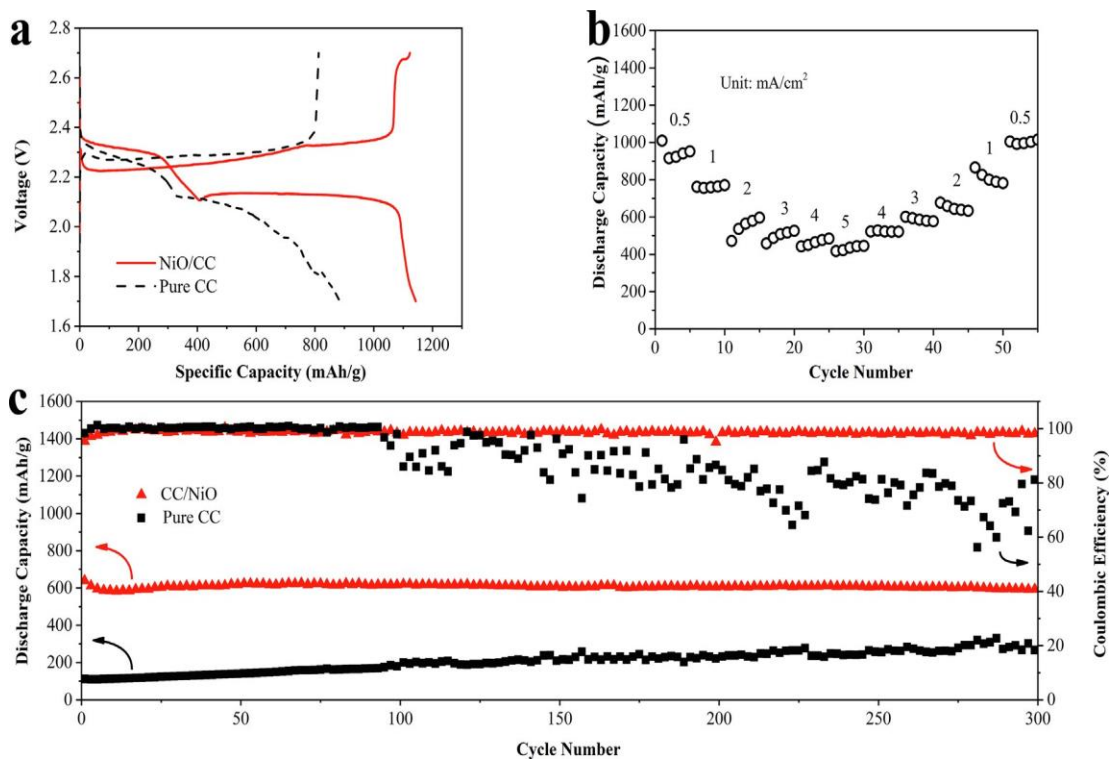


Figure 4.5 (a) Charge and discharge voltage profiles of NiO/CC/S and CC/S composite electrodes for the first cycle at 0.1C. (b) Rate performance of NiO/CC/S composite electrode at various current densities. (c) Cycle capacity and Coulombic efficiency of NiO/CC/S and CC/S composite electrodes at a current density of 2.0 mA cm² (~1C).

Cells with the modified NiO / CC / S electrode maintain discharge capabilities of 600.6, 511.4 and 502.03 mAh g⁻¹, after 140 cycles, 300 cycles, 250 cycles, the columbic efficiency is 99.69, 99.95 and 99.81%, respectively. In comparison, the CC/S modified electrode was tested at 1.1 mA cm² for 140 cycles as shown in Figure 4.6(f). After 140 cycles, the cell discharge capacity remained 325 mAh/g with a Colombian efficiency above 82.15%, much lower than the NiO / CC / S electrode.

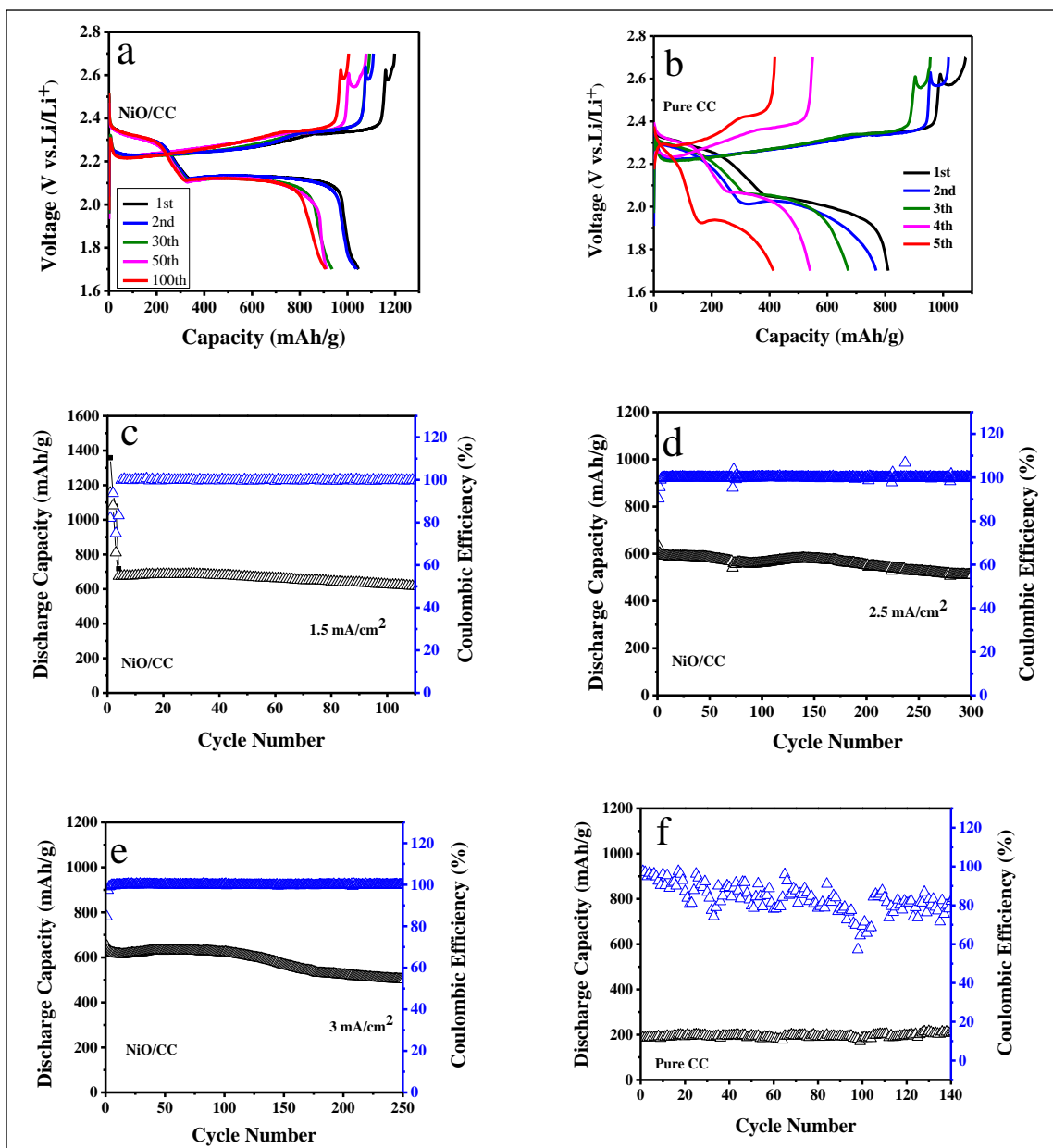


Figure 4.6 Electrochemical performance of the S/NiO/CC and S/CC composites (sulfur loading: 1.5–3.0 mg cm⁻²). (a, b) Comparison of discharge–charge profiles of the S/NiO/CC and S/CC composites at 0.2 C rate. (c) Cycle capacity and Coulombic efficiency of NiO/CC/S and CC/S composite electrodes at a current density of 1.5 mA cm⁻². (d) Cycle capacity and Coulombic efficiency of NiO/CC/ at a current density of 2.5 mA cm⁻². (e) Cycle capacity and Coulombic efficiency of NiO/CC/S at a current density of 3.0 mA cm⁻² and (f) Cycle capacity and Coulombic efficiency of CC/S composite electrodes.

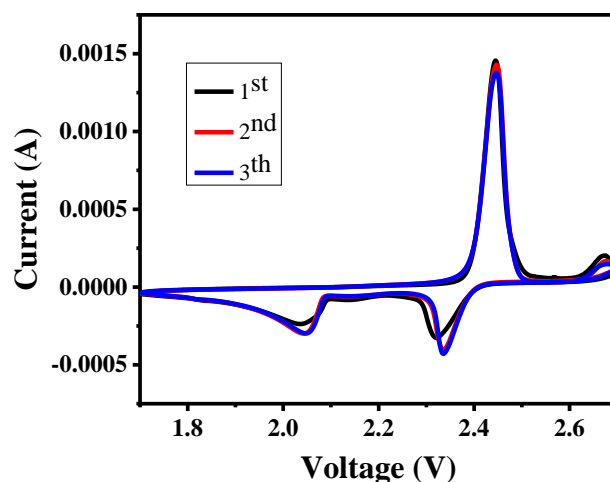


Figure 4.7 CVs of the NiO /CC /S electrodes at a scan rate of 0.1 mV s^{-1} between 1.7 and 2.7 V.

The electrochemical properties of the NiO / CC /S cathode of Li-S cells. Cyclic voltmeter measurement was carried out in the potential range 1.7 ~ 2.7 V (versus Li / Li⁺) at a rate of 0.1 mV/s. Cyclic voltammograms (CVs) of the NiO/CC/S electrode are shown in Figure 4.7. Visibly, the first cycle differs slightly from the other cycles of electrode, especially for the cathodic branch. In the first cycle the cathodic peak voltage at 2.31 volts in the first lithiation cycle is shifted to 2.33 volts in the subsequent cycles. This, as a result of structural and compositional changes of the active sulfur material, results in continuous formation at different chain lengths of Li polysulfide. The NiO/CC/S electrode after the first cycle, detects two cathodic peaks at 2.33 and 2.05 V. The peak of 2.33 versus Li / Li⁺ is related by the corresponding as the highly soluble polysulfides (Li₂S_x, 4 ≤ x ≤ 8) of sulfur, and the peak at about 2.05 V versus Li/Li⁺ is attributed to the conversion of long chain polysulfides into Li₂S₂ /Li₂S non-soluble. Opposite anode peak at 2.45 V, which can be assigned to convert Li₂S₂/Li₂S to sulfur. Showing stable CV

profiles after the first cycle. Besides, the peak sites in the NiO/CC/S composite cathode of the second and third cycle are almost unchanged, indicating excellent electrochemical reflection and stability.

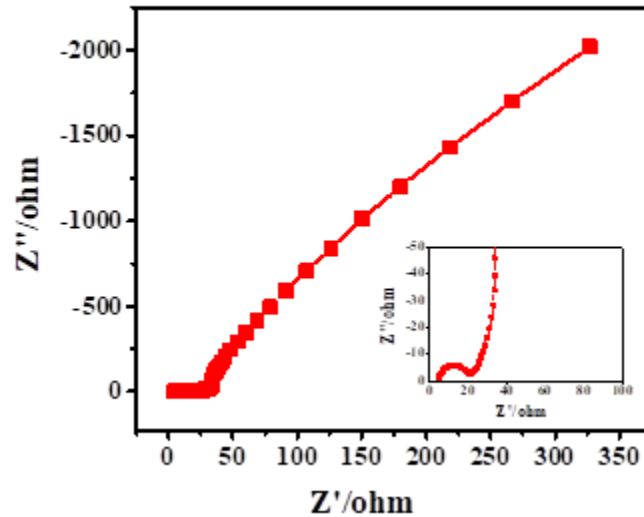


Figure 4.8 EIS of the hollow NiO/CC/S composites electrode.

Figure 4.8 shows the EIS spectra of the electrode of NiO/S/CC before cycling tests. In the inset Figure 3.8 the equivalent circuit approved to fit Nyquist diagrams and resistance values obtained after fitting is shown. At the high-frequency end, the series resistance of electrolyte and electrode (R_s), which can be obtained through the intersection of the front end of the semicircles with the Z axis has been evaluated, which value (4.7Ω), This reveals an improved conductivity of the NiO/CC/S electrode since the same electrolyte was used for every coin cell. The charge transfer resistance (R_{ct}) results in a semicircle in the high frequency region in parallel to a double-layer electrode capacitor at the electrolyte-electrode interface. The R_{ct} value is apparent at ($\sim 22.1 \Omega$), Due to the microstructure of NiO, which provides a high surface area for polysulfides adsorption and superior electrical conductivity to

enhance the charge transfer reaction. Straight lines describe at the low-frequency end of a Warburg resistor of specified length (Z_w) by ion diffusion within the electrode. The straight line of NiO in the Nyquist diagram is tilted at an angle of greater than 45, indicating that the porous NiO structure can facilitate the transport of electrolyte ions.

4.4 Conclusion

In summary, the NiO/CC/S composite cathode is obtained through a simple chemical method. The three-dimensional porous electrode possesses advantages including robust mechanical strength, large surface area, promoted electronic and ionic transport and entrapment of polysulfides. Vertical NiO sheets decorating the vertically connected piece of carbon cloth were very effective in trapping polysulfides in the Li-S battery on the cathode side. Battery performance is further improved, through porous grid structure and S-interaction. Specifically, by inserting a thin carbon cloth on the side of the cathode through the addition of more Neo-nanoparticles, the dissolution of the polysulfides was effectively impeded and the modifier capacity and long-term stability were effectively enhanced.

As a result, the NiO/CC/S composite cathode delivers a high initial capacity of 1154.8 mAh g⁻¹ at 0.1C and 1046.6 mAh g⁻¹ at 0.2C compared to the CC/S electrode. Even at higher rate of 1C, a specific capacity of 661.9 mAh g⁻¹ can be obtained, with a low decay rate of 0.07% per cycle over 300 cycles. It showed better rate performance and capacity recovery and coulombic efficiency performance compared to the S electrode. Most of the sulfur cathode problems arise from poor polysulfide shuttle conductance. Therefore, the NiO nanosheets' was important for the physical and chemical confinement of the polysulfides, to overcome the insulating nature of sulfur materials.

Carbon paper can act as a scaffold for electrically conducting various Hollow NiO. Shown in the CV and GCD curves are two cathodic peaks, the first peak (plateau) at 2.33 V can be attributed to the electrochemical configuration of S_8 to Li_2S_4 which can be reduced to Li_2S at the second peak (plateau) at 2.05 V. The reverse reactions occurred against the anode peak at 2.45 V, which can be assigned to convert Li_2S_2/Li_2S into sulfur. Which indicates great potential as an advanced electrode for next generation energy storage device.

Chapter Five

Mesoporous Nanoparticles as Cathode Additive for Li-S Battery

5.1 Introduction

The transition metal oxides (TMOs, (M_xO_y) , $M = \text{Co, Mn, Ni, Fe, etc.}$) are promising as cathode materials for Li-S applications and they also considered distinct poles for the development of the next generation of lithium-sulfur batteries due to many advantages such as low cost, high stability and high theoretical capacity [148, 153]. In recent years, ternary transition metal oxides like, Mn-Co oxide [154], Ni-Mn oxide [155, 156] Fe-Mn oxide[157],Ni-Co oxide[158],Co-Zn oxide [159], have attracted considerable attention to the storage of electrochemical energy, because of their contribution to the oxidation and reduction process combined for both metal ions. So, it is important to benefit from multi-component metal oxide materials in Lithium-sulfate batteries[160, 161] . For instance, ternary NiCo_2O_4 is one of the most promising electrode materials for superconductors due to high electrical conductivity and electrochemical activity compared to binary NiO and Co_3O_4 , which have been widely verified [162]. Also these features prefer to apply of NiCo_2O_4 as a cathode material to (Li-S), but there are only a limited number of these studies to date [163, 164]. For example, the NiCo_2O_4 trio is one of the most promising high-performance electrodes for energy storage due to low cost, natural abundance, environmental friendliness, high electrical conductivity and electrochemical activity compared to NiO and Co_3O_4 , which have been widely verified in the worldwide [165]. Recently, NiCo_2O_4 has been prepared in a wide range of forms, with nanostructures NiCo_2O_4 ,

including nanowires, nanostructures, slabs, nanoparticles and investigated for their electrochemical performance [164]. All these results indicate that the electrochemical properties of electrode materials are highly dependent on their size and shape. Therefore, it is necessary to develop an easy, low-cost and scalable method for assembling high-performance nanostructure materials with the desired shape and size NiCo_2O_4 is preferred as a cathode over (Li-S), but only a limited number of such studies are available now [164]. Here in this work, we illustrate a strategy for synthesizing NiCo_2O_4 nanoparticles via a low-temperature solution of sodium citrate (TSC) followed by heat treatment, which has shown good battery performance, it is expected that electrochemical activity and stability in these hybrid nanostructures will be greatly enhanced. As a result, NiCo_2O_4 exhibits high discharge capacity, good bike stability and excellent rate capability. Also, NiCo_2O_4 electrode material has a potential application that makes it a good anode material for high power applications in Li-S.

5.2 Experimental Section

5.2.1 Materials Synthesis

Synthesis of NiCo_2O_4 nanoparticles. All of the purchased chemicals with grade analytical and used without any pretreatment were bought from Sigma-Aldrich. For the preparation of the NiCo_2O_4 nanoparticles with hybrid nanostructure, 0.8 mmol of $\text{Ni}(\text{NO}_3)_2 \cdot 6\text{H}_2\text{O}$, 1.6 mmol of $\text{Co}(\text{NO}_3)_2 \cdot 6\text{H}_2\text{O}$, 2.0 mmol of hexamethylenetetramine (HMT) and 0.4 mmol of trisodium citrate dihydrate (TSC) were added into 40 mL of deionized (DI) water, followed by ultrasound for 30 minutes. The above solution was kept in the oil bath at $90\text{ }^\circ\text{C}$ for 6 hours with agitation. After cooling naturally to room temperature, the black

precipitate was collected by centrifugation and washed with DI water and ethanol for several times. Lastly, the precipitate was dried for 6 h at 150 C°, and was heated to 500 C° for 3 hours in the air at a heating rate of 1 C min⁻¹ to obtain NiCo₂O₄ nanoparticles. Details about characterization and battery assemble can be found in the supplementary material.

5.2.2 Materials Characterization

Using the advanced X-Ray Diffractometer of Bruker D8 with Cu K α radiation ($\lambda = 1.5406 \text{ \AA}$) at a voltage of 40 kV and a current of 40 mA, X-ray diffraction patterns (XRD) were obtained [44]. The N₂ adsorption-desorption were determined by BET measurements using a Quanta chrome instrument surface area analyzer. The nanostructures and morphological properties of nanomaterials prepared by scanning electron microscopy (SEM).

5.2.3 Electrochemical Measurements

Standard 2025 metal cells were assembled to assess the electrochemical performance of powder samples. Coin cells were assembled in a very pure Argon-filled glove box using pure lithium as reference electrodes with Celgard 2400 membrane as separation and 1 mol L⁻¹ LiPF₆ as electrolyte. Working electrodes were prepared from 70 wt% of the active substances, 20 wt% of conductive black carbon (Super-P-Li), and 10 wt% of the polymer bond (polyvinylidene fluoride, PVDF). The 1 M LiPF₆ electrolyte solution was dissolved in a mixture of ethylene carbonate and diethyl carbonate in a 1:1 volume. Cyclic voltammetry (CV) was performed under a scan rate of 0.2 mV·s⁻¹ within a voltage window of 1.7 to 2.7 volts. All discharge and charge measurements were performed at room temperature on the LAND CT-2001A system (Wuhan, China).

5.3 Results and Discussion

Typical SEM images with different magnification are shown in Figure 5.1. It is worth noting that the entire nanoparticle surface is covered by nanostructures. These porous nanostructures can provide abundant adsorption sites for the interaction between NiCo_2O_4 and soluble polysulfides. Moreover, these structures are useful in enhancing electrolyte infiltration and ionic transfer.

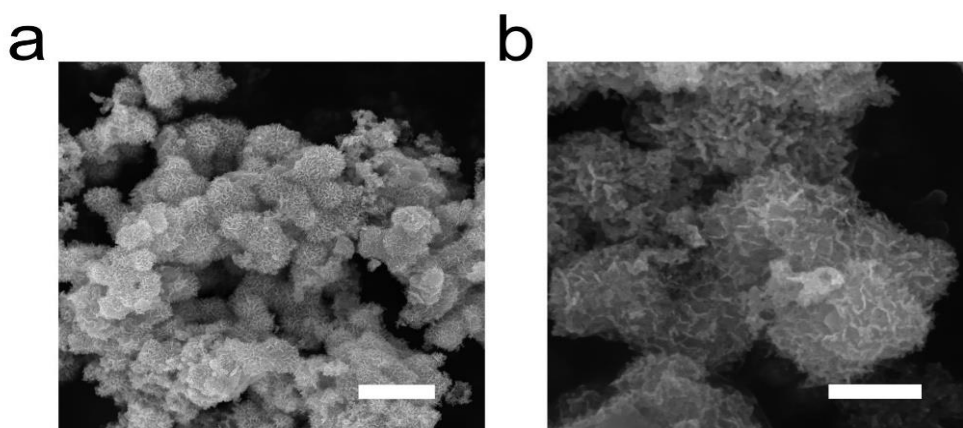


Figure 5.1 SEM images of NiCo_2O_4 nanoparticles. The scale bars are (a) 1 μm and (b) 300 nm, respectively.

X-ray diffraction (XRD) measurement was performed to examine crystal information of NiCo_2O_4 product as shown in Figure 5.2a. The specific diffraction peaks of the spinel NiCo_2O_4 phase (JCPDS card 20-0781) can be well identified. No additional peaks of potential impurities have been observed, suggesting a high purity of NiCo_2O_4 product. The specific surface area and pore size distribution of the selected sample were investigated by conducting nitrogen (N_2) adsorption–desorption isotherm measurements. As shown in Figure 4-2b, the N_2 adsorption–desorption curve of porous NiCo_2O_4 can be assigned to the IV-H2 type isotherm, indicating the mesoporous nature of the

particle structure. According to the Brunauer-Emmett-Teller analysis, the NiCo₂O₄ nanoparticles possess a very high surface area of 59.99 m²g⁻¹. The inset of Figure 5.2b shows the pore-size distribution plot calculated by the Barrett Joyner-Halenda method of the adsorption branch. The average pore size distribution and volume are 10.66 nm and 0.26 cm³g⁻¹, respectively.

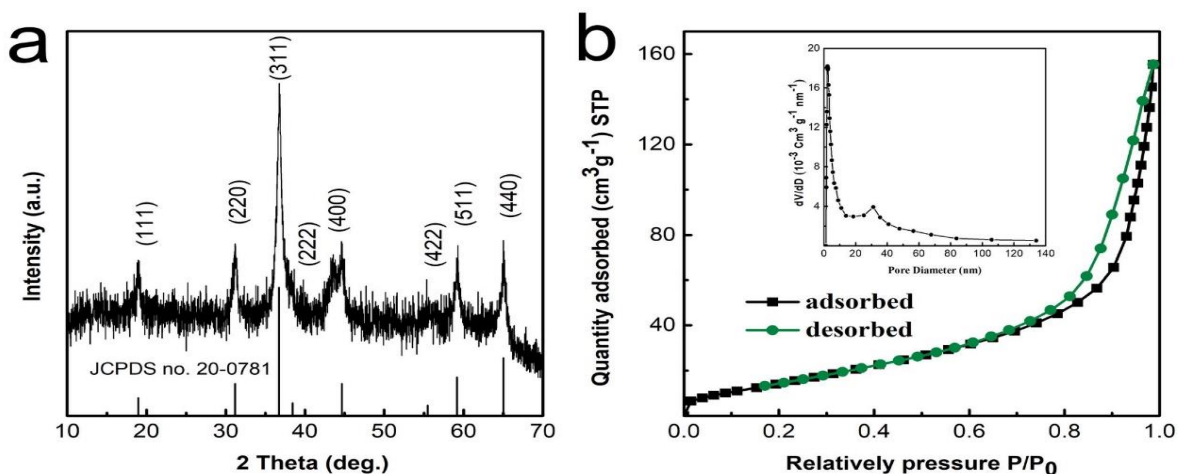


Figure 5.2 (a) XRD patterns and (b) N₂ adsorption-desorption isotherm and pore size distribution curve (inset) for NiCo₂O₄ sample.

Figure 5.3a shows the features of the charge/discharge curves at 0.1 C in the range of 1.7 to 2.7 V, in which a high capacity of 1399.8 mAh g⁻¹ can be obtained. The typical plateaus at \approx 2.35 and 2.12 V in the discharge curve represent reduction of S₈ to Li₂S_x ($4 \leq x \leq 8$) and transition from Li₂S₄ to Li₂S₂/Li₂S, respectively. After fully discharged, the electrode was charged to 2.7 V and a long charging plateau was found in the charging curve of approximately 2.2 to 2.35 V. The plateau is associated with the oxidation processes involving the overall consumption of Li₂S_n ($1 \leq n \leq 8$).

As shown in Figure 5.3b, we have also studied rate performance to understand the electrochemical behavior of NiCo₂O₄ based cathode. As the current density increases from 0.2 C to 1.0 C (0.2, 0.5, 0.7, 1.0 C), the cell shows a good rated

with average discharge capacities of 972, 946.7, 767, and 544.6 mAh/g, respectively, indicating that the exclusively designed NiCo₂O₄ nanostructures has great potential as a high-rate cathode material. Moreover, when the current density is again reduced to 0.2 C, the average discharge capacity of 764.3 mAh/g, can be recovered. Figure 5.3c shows cyclic performance of the electrode with NiCo₂O₄ at 0.5 C. After activation at 0.1 C for 3 cycles, the NiCo₂O₄ based electrode obtains a capacity of 692.5 mAh/g after 59 cycles, then slowly decreased until it stabilized at 464.2 mAh/g after 200 cycles.

To reveal the electrochemical mechanism, the CV curves of the NiCo₂O₄ electrode at rates of 0.3, 0.5 and 0.7 mV s⁻¹ in the potential range of 1.7 ~ 2.7 V (vs. Li/Li⁺) are shown in Figure 4-3d. Two cathodic peaks of about 2.2 and 1.9 V can be observed, associated to formation of soluble high-order polysulfides (Li₂S_x, 4 ≤ x ≤ 8) from sulfur and conversion of long-chain polysulfides to Li₂S₂/Li₂S, respectively. A sharp anodic peak can be observed at about 2.5 V, which can be assigned to transformation from Li₂S₂/Li₂S to S. Combining the linear relationship between peak current and square root at different scan rate, the Li⁺ diffusion coefficient of peaks at 2.5, 2.2 and 1.9 V in the NiCo₂O₄ based battery are calculated to be 0.9×10⁻⁷, 0.1×10⁻⁷ and 0.5×10⁻⁷ cm² s⁻¹, respectively, based on the Randles-Sevcik equation, indicating facilitated ionic transport due to the porous nanostructures.

In this study, NiCo₂O₄ nanoparticles was prepared via a facile atmospheric and water-based method and designed as cathode additive for Li-S batteries. The mesoporous NiCo₂O₄ nanoparticles can provide abundant adsorption sites to confine polysulfides and facilitate the ionic transport. As a result, the cells with NiCo₂O₄ nanoparticles show an initial specific capacity of 1399.8 mAh/g at the current density of 0.1 C and reversible high-rate performances. This work may

provide a promising method for preparing high-performance cathodes of Li-S batteries.

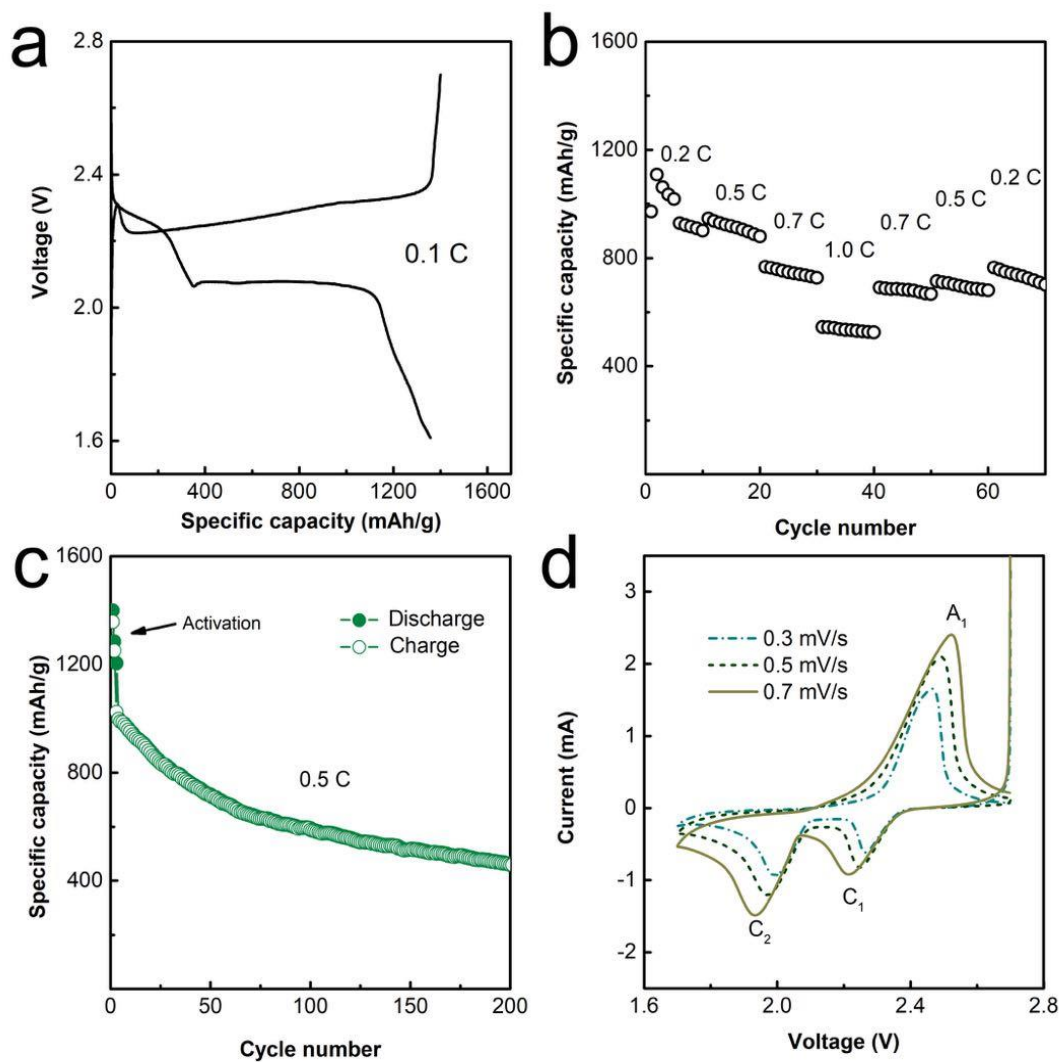


Figure 5.3 Electrochemical performances of the NiCo₂O₄/sulfur composites electrode. (a) The discharge/charge profiles. (b) Rate capability. (c) Cycle performance at 0.5 C. (d) CV curves at different scan rate.

5.4 Conclusions

Li-S as one of the most promising energy storage devices due to their high theoretical capacity and high theoretical density are promising alternatives to LIBs. However, the challenges in developing the marketing process of lithium-sulfur battery must be overcome. In this thesis, the work focused on essential chemistry of lithium-sulfur batteries. In particular, studies have mainly been conducted on the development of different transitional nickel oxide nanostructures to improve the electrochemical performance of (Li-S). Work in Chapter 3 focused on a combination of NiO Nanosheets arrays on hierarchical carbon nanoparticles was briefly obtained by chemical bath precipitation method (CBD). Corresponding NiO Nanosheets products without significant morphological change were subsequently obtained through annealing, for sulfur inoculation as a cathode material of Li-S. Corresponding NiO Nanosheets products without major morphological change were subsequently obtained through annealing, with a large surface area ($43.8688 \text{ m}^2/\text{g}$) and pore size ($0.04731 \text{ cm}^3/\text{g}$), while CC porous carbon has a specific surface area of $14.39759 \text{ m}^2/\text{g}$) and a pore volume of $0.03204 \text{ (cm}^3/\text{g)}$. Such a porous nickel oxide and carbon nanostructure provides several favorable properties to form a distinct cathode structure for Li-S batteries. The conduction limitations of pure sulfur can be overcome by nanostructures with high surface area. In addition, it can provide the conductive nickel oxide microstructure with medium-porous Nano scale sheets connected to each other and form a grid with separators with open space and electrically active surface, thus enhancing the charge transfer interaction between lithium ions and sulfur materials, effective storage of variable volume, and shuttle restriction polysulfide.

The transport pathways for electrons and lithium ions can be greatly shortened by reducing the size of the sulfur particles, which leads to an increased use of sulfur. By confining the sulfur to a large number of small spaces, the sulfur loss can be suppressed by medium porous NiO sheets and porous carbon paper. NiO Nanosheets arrays on with sulfur at 80% -impregnated carbon cloth demonstrated high capacity and good contents when used as a cathode material for Li-S, the NiO/CC/S composite cathode delivers a high initial capacity of 1154.8 mAh/g at 0.1C and 1046.6 mAh/g at 0.2C compared to the CC/S electrode. Even at higher rate of 1C, a specific capacity of 661.9 mAh/g can be obtained, with a low decay rate of 0.07% per cycle over 300 cycles. It showed better rate performance and capacity recovery and CMP performance compared to the S electrode. Which indicates great potential as an advanced electrode for next generation energy storage devices.

Next, we investigated another particle based on nickel materials. The work in Chapter 4 focused on hollow NiCo_2O_4 as sulfur hosts for Li-S. The NiCo_2O_4 with hybrid nanostructure is manufactured in a simple atmospheric and water-based method. With a relatively high surface area ranging from $59.99 \text{ m}^2\text{g}^{-1}$, average pore size distribution and volume are 10.66 nm and $0.26 \text{ cm}^3\text{g}^{-1}$, respectively. NiCo_2O_4 products with infinitesimal structures showed can provide abundant adsorption sites to confine polysulfides and facilitate the ionic transport. As a result, an initial capacity of 1399.8 mAh/g at a current density of 0.1 C. and reversible high-rate performances. The cyclic performance of the electrode with NiCo_2O_4 at 0.5 C. After activation at 0.1 C for 3 cycles, the NiCo_2O_4 based electrode obtains a capacity of 692.5 mAh/g after 59 cycles, then slowly decreased until it stabilized at 464.2 mAh/g after 200 cycles. Prepared Nano composites are evaluated as electrode as a cathode

material for Li-S, where high capacities are provided with stable stability for cycles.

5.5 Recommendations for Study Future

Although from the most promising results obtained, more needs to be done before large-scale Li-S batteries are produced. Many aspects are strongly encouraged, for future study. Appropriate dispersion of the active sulfur: During recycling, the sulfur turns into a soluble poly sulfide, although if the sulfur does not have sufficient contact with the conducting agents the use of the active substance will be low, which weakens the specific capacity. Therefore, pole manufacturing must be improved.

Effective absorption materials: The currently developed carbon frames appear to be well suited to absorb sulfur, although the higher carbon content in the cathode area reduces energy density and is still unsatisfactory.

References

- [1] Zu C-X, Li H, Science E. Thermodynamic analysis on energy densities of batteries[J]. *Energy & Environmental Science*, 2011, 4(8):2614–2624.
- [2] Bruce P G, Freunberger S A, Hardwick L J, et al. Li–O₂ and Li–S batteries with high energy storage [J]. *Nature materials*, 2012, 11(1):19–29.
- [3] Manthiram A, Murugan A V, Sarkar A, et al. Nanostructured electrode materials for electrochemical energy storage and conversion [J]. *Energy & Environmental Science*, 2008, 1(6):621–638.
- [4] Goodenough J B. Rechargeable batteries: challenges old and new [J]. *Journal of Solid State Electrochemistry*, 2012, 16(6):2019–2029.
- [5] Armand M, Tarascon J-M. Building better batteries[J]. *nature*, 2008, 451(7179):652–657.
- [6] Walter M, Kovalenko M V, Kravchyk K V. Challenges and benefits of post-lithium-ion batteries[J]. *New Journal of Chemistry*, 2020, 44(5):1677–1683.
- [7] Nilta N, Wu F, Lee J T, et al. Li-ion battery materials: present and future[J]. *Materials today*, 2015, 18(5):252–264.
- [8] Ritchie A, Giwa C, Lee J, et al. Future cathode materials for lithium rechargeable batteries[J]. *Journal of power sources*, 1999, 80(1-2):98–102.
- [9] Lim L. Development of Porous Carbon for High Performance Lithium-Sulphur Batteries [D]; University of Waterloo, 2016.
- [10] Manthiram A, Fu Y, Chung S-H, et al. Rechargeable lithium–sulfur batteries[J]. *Chemical reviews*, 2014, 114(23):11751–11787.
- [11] Scheers J, Fantini S, Johansson P. A review of electrolytes for lithium–sulphur batteries[J]. *Journal of Power Sources*, 2014, 255:204–218.

- [12] Yin Y X, Xin S, Guo Y G, et al. Lithium–sulfur batteries: electrochemistry, materials, and prospects[J]. *Angewandte Chemie International Edition*, 2013, 52(50):13186–13200.
- [13] Ji X, Lee K T, Nazar L F. A highly ordered nanostructured carbon–sulphur cathode for lithium–sulphur batteries[J]. *Nature materials*, 2009, 8(6):500–506.
- [14] Yang Y, Zheng G, Cui Y. Nanostructured sulfur cathodes[J]. *Chemical Society Reviews*, 2013, 42(7):3018–3032.
- [15] Barghamadi M, Kapoor A, Wen C. A review on Li-S batteries as a high efficiency rechargeable lithium battery[J]. *Journal of the Electrochemical Society*, 2013, 160(8):A1256.
- [16] Zhang S S. Role of LiNO₃ in rechargeable lithium/sulfur battery[J]. *Electrochimica Acta*, 2012,70:344–348.
- [17] Zhang S S. Liquid electrolyte lithium/sulfur battery: fundamental chemistry, problems, and solutions[J]. *Journal of Power Sources*, 2013, 231:153.
- [18] Huang X, Sun B, Li K, et al. Mesoporous graphene paper immobilised sulfur as a flexible electrode for lithium–sulfur batteries[J]. *Journal of Materials Chemistry A*, 2013, 1(43):13484–13489.
- [19] Han S-C, Song M-S, Lee H, et al. Effect of multiwalled carbon nanotubes on electrochemical properties of lithium/sulfur rechargeable batteries[J]. *Journal of the electrochemical society*, 2003, 150(7):A889.
- [20] Cheon S-E, Choi S-S, Han J-S, et al. Capacity fading mechanisms on cycling a high-capacity secondary sulfur cathode[J]. *Journal of the Electrochemical Society*, 2004, 151(12):A2067.
- [21] Liang X, Liu Y, Wen Z, et al. A nano-structured and highly ordered polypyrrole-sulfur cathode for lithium–sulfur batteries[J]. *Journal of Power Sources*, 2011, 196(16):6951–6955.
- [22] Zhang F, Dong Y, Huang Y, et al. Preparation and performance of a sulfur/graphene composite for rechargeable lithium-sulfur battery;

- proceedings of the Journal of Physics: Conference Series, F, 2012 [C]. IOP Publishing.
- [23] Huang J-Q, Zhang B, Xu Z-L, et al. Novel interlayer made from Fe₃C/carbon nanofiber webs for high performance lithium–sulfur batteries[J]. Journal of Power Sources, 2015, 285:43–50.
- [24] Hou Y, Li J, Gao X, et al. 3D dual-confined sulfur encapsulated in porous carbon nanosheets and wrapped with graphene aerogels as a cathode for advanced lithium sulfur batteries[J]. Nanoscale, 2016, 8(15):8228–8235.
- [25] Niu X-Q, Wang X-L, Xie D, et al. Nickel hydroxide-modified sulfur/carbon composite as a high-performance cathode material for lithium sulfur battery[J]. ACS applied materials & interfaces, 2015, 7(30):16715–16722.
- [26] Li J, Guo J, Deng J, et al. Enhanced electrochemical performance of lithium-sulfur batteries by using mesoporous TiO₂ spheres as host materials for sulfur impregnation[J]. Materials Letters, 2017, 189:188–191.
- [27] Song M-K, Cairns E J, Zhang Y J N. Lithium/sulfur batteries with high specific energy: old challenges and new opportunities[J]. Nanoscale, 2013, 5(6):2186–2204.
- [28] Zheng J, Gu M, Wang C, et al. Controlled nucleation and growth process of Li₂S₂/Li₂S in lithium-sulfur batteries[J]. Journal of the Electrochemical Society, 2013, 160(11):A1992.
- [29] Cheon S-E, Ko K-S, Cho J-H, et al. Rechargeable lithium sulfur battery I. Structural change of sulfur cathode during discharge and charge[J]. Journal of the Electrochemical Society, 2003, 150(6):A796.
- [30] Xiao J, Wang D, Xu W, et al. Optimization of air electrode for Li/air batteries[J]. Journal of The Electrochemical Society, 2010, 157(4):A487.
- [31] Bai X. Fabrication of Mesoporous Conductive Carbon as Cathode Materials For High Performance Lithium Sulfur Battery [D]; UCLA, 2016.
- [32] Cao R, Xu W, Lv D, et al. Anodes for Rechargeable Lithium-Sulfur batteries[J]. Advanced Energy Materials, 2015, 5(16):1402273.

- [33] Tao T, Lu S, Fan Y, et al. Anode improvement in rechargeable lithium–sulfur batteries[J]. *Advanced materials*, 2017, 29(48):1700542.
- [34] Zheng S, Chen Y, Xu Y, et al. In situ formed lithium sulfide/microporous carbon cathodes for lithium-ion batteries[J]. *ACS nano*, 2013, 7(12):10995–11003.
- [35] Lee S-K, Oh S-M, Park E, et al. Highly Cyclable Lithium–Sulfur Batteries With a Dual-Type Sulfur Cathode and a Lithiated Si/SiO_x Nanosphere Anode[J]. *Nano letters*, 2015, 15(5):2863–2868.
- [36] Duan B, Wan W, Zhao H, et al. Li-B alloy as anode material for lithium/sulfur battery[J]. *ECS Electrochemistry Letters*, 2013, 2(6):A47-A51.
- [37] Wang W, Wang X, Tan L, et al. In situ sulfur deposition route to obtain sulfur–carbon composite cathodes for lithium–sulfur batteries[J]. *Journal of Materials Chemistry A*, 2014, 2(12):4316–4323.
- [38] Xin S, Gu L, Zhao N-H, et al. Smaller sulfur molecules promise better lithium–sulfur batteries[J]. *Journal of the American Chemical Society*, 2012, 134(45):18510–18513.
- [39] Choi H, Zhao X, Kim D-S, et al. A mesoporous carbon–sulfur composite as cathode material for high rate lithium sulfur batteries[J]. *Materials Research Bulletin*, 2014, 58:199–203.
- [40] An T, Deng D, Lei M, et al. MnO modified carbon nanotubes as a sulfur host with enhanced performance in Li/S batteries[J]. *Journal of Materials Chemistry A*, 2016, 4(33):12858–12864.
- [41] Wang H, Yang Y, Liang Y, et al. Graphene-wrapped sulfur particles as a rechargeable lithium–sulfur battery cathode material with high capacity and cycling stability[J]. *Nano letters*, 2011, 11(7):2644–2647.
- [42] Brun N, Sakaushi K, Yu L, et al. Hydrothermal carbon-based nanostructured hollow spheres as electrode materials for high-power lithium–sulfur batteries[J]. *Physical Chemistry Chemical Physics*, 2013, 15(16):6080–6087.

- [43] Choudhury S, Ebert T, Windberg I T, et al. Hierarchical Porous Carbon Cathode for Lithium–Sulfur Batteries Using Carbon Derived from Hybrid Materials Synthesized by Twin Polymerization[J]. *Particle & Particle Systems Characterization*, 2018, 35(12):180036464.
- [44] Li Z, Zhang J, Lou X W. Hollow carbon nanofibers filled with MnO₂ nanosheets as efficient sulfur hosts for lithium–sulfur batteries[J]. *Angewandte Chemie*, 2015, 127(44):13078–13082.
- [45] Ji X, Nazar L F. Advances in Li–S batteries[J]. *Journal of Materials Chemistry*, 2010, 20(44):9821–9826.
- [46] Manthiram A, Fu Y, Su Y-S. Challenges and prospects of lithium–sulfur batteries[J]. *Accounts of chemical research*, 2013, 46(5):1125–1134.
- [47] Guo J, Xu Y, Wang C. Sulfur-impregnated disordered carbon nanotubes cathode for lithium–sulfur batteries[J]. *Nano letters*, 2011, 11(10):4288–4294.
- [48] Qiu Y, Li W, Li G, et al. Polyaniline-modified cetyltrimethylammonium bromide-graphene oxide-sulfur nanocomposites with enhanced performance for lithium-sulfur batteries[J]. *Nano Research*, 2014, 7(9):1355–1363.
- [49] Han K, Shen J, Hayner C M, et al. Li₂S-reduced graphene oxide nanocomposites as cathode material for lithium sulfur batteries[J]. *Journal of Power Sources*, 2014, 251:331–337.
- [50] Liang X, Hart C, Pang Q, et al. A highly efficient polysulfide mediator for lithium–sulfur batteries[J]. *Nature communications*, 2015, 6(1):1–8.
- [51] Wu F, Chen J, Li L, et al. Improvement of rate and cycle performance by rapid polyaniline coating of a MWCNT/sulfur cathode[J]. *The Journal of Physical Chemistry C*, 2011, 115(49):24411–24417.
- [52] Li D, Han F, Wang S, et al. High sulfur loading cathodes fabricated using peapodlike, large pore volume mesoporous carbon for lithium–sulfur battery[J]. *ACS applied materials & interfaces*, 2013, 5(6):2208–2213.
- [53] Li W, Zheng G, Yang Y, et al. High-performance hollow sulfur nanostructured battery cathode through a scalable, room temperature, one-step, bottom-up

- approach[J]. Proceedings of the National Academy of Sciences, 2013, 110(18):7148–7153.
- [54] Wu F, Chen J, Chen R, et al. Sulfur/polythiophene with a core/shell structure: synthesis and electrochemical properties of the cathode for rechargeable lithium batteries[J]. The Journal of Physical Chemistry C, 2011, 115(13):6057–6063.
- [55] Wei W, Wang J, Zhou L, et al. CNT enhanced sulfur composite cathode material for high rate lithium battery[J]. Electrochemistry Communications, 2011, 13(5):399–402.
- [56] Fu Y, Su Y-S, Manthiram A, et al. Sulfur–carbon nanocomposite cathodes improved by an amphiphilic block copolymer for high-rate lithium–batteries[J]. ACS applied materials & interfaces, 2012, 4(11):6046–6052.
- [57] Xiao L, Cao Y, Xiao J, et al. A soft approach to encapsulate sulfur: polyaniline nanotubes for lithium-sulfur batteries with long cycle life[J]. Advanced materials, 2012, 24(9):1176–1181.
- [58] Gao H, Lu Q, Liu N, et al. Facile preparation of an ultrathin sulfur-wrapped polyaniline nanofiber composite with a core–shell structure as a high performance cathode material for lithium–sulfur batteries[J]. Journal of Materials Chemistry A, 2015, 3(14):7215–7218.
- [59] Chen H, Dong W, Ge J, et al. Ultrafine sulfur nanoparticles in conducting polymer shell as cathode materials for high performance lithium/batteries[J]. Scientific reports, 2013, 3(1):1–6.
- [60] Zhou W, Yu Y, Chen H, et al. Yolk–shell structure of polyaniline-coated sulfur for lithium–sulfur batteries[J]. Journal of the American chemical society, 2013, 135(44):16736–16743.
- [61] Oschmann B, Park J, Kim C, et al. Copolymerization of polythiophene and sulfur to improve the electrochemical performance in lithium–sulfur batteries[J]. Chemistry of Materials, 2015, 27(20):7011–7017.

- [62] Zhao S, Chen H, Li J, et al. Synthesis of polythiophene/graphite composites and their enhanced electrochemical performance for aluminum ion batteries[J]. *New Journal of Chemistry*, 2019, 43(37):15014–15022.
- [63] Yin L, Wang J, Lin F, et al. Polyacrylonitrile/graphene composite as a precursor to a sulfur-based cathode material for high-rate rechargeable Li–S batteries[J]. *Energy & Environmental Science*, 2012, 5(5):6966–6972.
- [64] Konarov A, Gosselink D, Doan T N L, et al. Simple, scalable, and economical preparation of sulfur–PAN composite cathodes for Li/S batteries[J]. *Journal of Power Sources*, 2014, 259:183–187.
- [65] Tang Z, Jiang J, Liu S, et al. Polyaniline-coated activated carbon aerogel/sulfur composite for high-performance lithium-sulfur battery[J]. *Nanoscale research letters*, 2017, 12(1):1–9.
- [66] Yang Y, Yu G, Cha J J, et al. Improving the performance of lithium–sulfur batteries by conductive polymer coating[J]. *ACS nano*, 2011, 5(11):9187–9193.
- [67] Wang J, Lu L, Shi D, et al. A Conductive Polypyrrole-Coated, Sulfur–Carbon Nanotube Composite for Use in Lithium–Sulfur batteries[J]. *ChemPlusChem*, 2013, 78(4):318.
- [68] Liang X, Zhang M, Kaiser M R, et al. Split-half-tubular polypyrrole@ sulfur@ polypyrrole composite with a novel three-layer-3D structure as cathode for lithium/sulfur batteries[J]. *Nano Energy*, 2015, 11:587–599.
- [69] Seh Z W, Li W, Cha J J, et al. Sulphur–TiO₂ yolk–shell nanoarchitecture with internal void space for long-cycle lithium–sulphur batteries[J]. *Nature communications*, 2013, 4(1):1–6.
- [70] Tao X, Wang J, Ying Z, et al. Strong sulfur binding with conducting magnéli-phase Ti_nO_{2n–1} nanomaterials for improving lithium–sulfur batteries[J]. *Nano letters*, 2014, 14(9):5288–5294.
- [71] Ji X, Evers S, Black R, et al. Stabilizing lithium–sulphur cathodes using polysulphide reservoirs[J]. *Nature communications*, 2011, 2(1):1–7.

- [72] Zhang L P, Wang Y F, Gou S Q, et al. All inorganic frameworks of tin dioxide shell as cathode material for lithium sulfur batteries with improved cycle performance[J]. *The Journal of Physical Chemistry C*, 2015, 119(52):28721–28727.
- [73] Ponraj R, Kannan A G, Ahn J H, et al. Improvement of cycling performance of lithium–sulfur batteries by using magnesium oxide as a functional additive for trapping lithium polysulfide[J]. *ACS applied materials & interfaces*, 2016, 8(6):4000–4006.
- [74] Dong K, Wang S, Zhang H, et al. Preparation and electrochemical performance of sulfur-alumina cathode material for lithium-sulfur batteries[J]. *Materials Research Bulletin*, 2013, 48(6):2079–2083.
- [75] Long H, Shi T, Hu H, et al. Growth of hierarchal mesoporous NiO nanosheets on carbon cloth as binder-free anodes for high-performance flexible lithium-ion batteries[J]. *Scientific reports*, 2014, 4(1):1–9.
- [76] Preetham P, Roy A, Raj K A, et al. Investigation of NiO/CNF Coating on Glass Fiber Separator as Polysulfide Migration Inhibitors for High-Energy Lithium–Sulfur Batteries [M]. *Advances in Energy Research*, Vol 1. Springer. 2020: 379-86.
- [77] Li H, Gu S, Tao B, et al. Highly wrinkled NiO nanosheet-based hierarchical structure/reduced fluorographene composite for enhanced performance of lithium-sulfur battery[J]. *Journal of the Taiwan Institute of Chemical Engineers*, 2020, 111:205–211,
- [78] Guo J-W, Wu M-S. Carbon paper with attached hollow mesoporous nickel oxide microspheres as a sulfur-hosting material for rechargeable lithium-sulfur batteries[J]. *Electrochimica Acta*, 2019, 327:135028.
- [79] Xie D, Su Q, Yuan W, et al. Synthesis of porous NiO-wrapped graphene nanosheets and their improved lithium storage properties[J]. *The Journal of Physical Chemistry C*, 2013, 117(46):24121–24128.

- [80] Wang J, Liang J, Wu J, et al. Coordination effect of network NiO nanosheet and a carbon layer on the cathode side in constructing a high-performance lithium–sulfur battery[J]. *Journal of Materials Chemistry A*, 2018, 6(15):6503–6509.
- [81] Wei T Y, Chen C H, Chien H C, et al. A cost-effective supercapacitor material of ultrahigh specific capacitances: spinel nickel cobaltite aerogels from an epoxide-driven sol–gel process[J]. *Advanced materials*, 2010, 22(3):347–351.
- [82] Xia X. Hollow NiCo₂O₄ nanocages as sulfur host for advanced lithium-sulfur batteries[J]. *Materials Research Express*, 2019, 6(9):095309.
- [83] Zhang G, Lou X W J A M. General solution growth of mesoporous NiCo₂O₄ nanosheets on various conductive substrates as high-performance electrodes for supercapacitors[J]. *Advanced materials*, 2013, 25(7):976–979.
- [84] Meher S K, Rao G R. Ultralayered Co₃O₄ for high-performance supercapacitor applications[J]. *The Journal of Physical Chemistry C*, 2011, 115(31):15646–15654.
- [85] Zhang Y, Ru Y, Gao H-L, et al. Sol-gel synthesis and electrochemical performance of NiCo₂O₄ nanoparticles for applications[J]. *Journal of Electrochemical Science and Engineering*, 2019, 9(4):243–253.
- [86] Xiao D, Zhang H, Chen C, et al. Interwoven NiCo₂O₄ Nanosheet/Carbon Nanotube Composites as Highly Efficient Lithium– Sulfur Cathode Hosts[J]. *ChemElectroChem*, 2017, 4(11):2959–2965.
- [87] Luo J, Zheng J J I. Novel NiCo₂O₄ nanofibers prepared via electrospinning method as host materials for perfect polysulfide inhibition[J]. *Ionics*, 2021, 27(2):651–656.
- [88] Liu Y T, Han D D, Wang L, et al. NiCo₂O₄ nanofibers as carbon-free sulfur immobilizer to fabricate sulfur-based composite with high volumetric capacity for lithium–sulfur battery [J]. *Advanced Energy Materials*, 2019, 9(11):1803477.

- [89] Iqbal A, Ghazi Z A, Khattak A M, et al. Efficient sulfur host based on NiCo₂O₄ hollow microtubes for advanced Li-S batteries[J]. *Journal of Solid State Chemistry*, 2017, 256:189–195.
- [90] Xiong S, Xie K, Diao Y, et al. Properties of surface film on lithium anode with LiNO₃ as lithium salt in electrolyte solution for lithium–sulfur batteries[J]. *Electrochimica Acta*, 2012, 83:78–86.
- [91] Lin Z, Liu Z, Fu W, et al. Phosphorous pentasulfide as a novel additive for high-performance lithium-sulfur batteries[J]. *Advanced Functional Materials*, 2013, 23(8):1064–1069.
- [92] Zu C, Manthiram A. Stabilized lithium–metal surface in a polysulfide-rich environment of lithium–sulfur batteries[J]. *The journal of physical chemistry letters*, 2014, 5(15):2522–2527.
- [93] Liang C, Dudney N, Howe J. Carbon/sulfur nanocomposites and additives for high-energy lithium sulfur batteries; proceedings of the Vehicle Technologies Program Annual Merit Review and Peer Evaluation Meeting, Washington DC, F, 2011 [C].
- [94] Xiong S, Kai X, Hong X, et al. Effect of LiBOB as additive on electrochemical properties of lithium–sulfur batteries[J]. *Ionics*, 2012, 18(3):249–254.
- [95] Wu F, Qian J, Chen R, et al. An effective approach to protect lithium anode and improve cycle performance for Li–S batteries[J]. *ACS applied materials & interfaces*, 2014, 6(17):15542–15549
- [96] Kim H, Wu F, Lee J T, et al. In situ formation of protective coatings on sulfur cathodes in lithium batteries with LiFSI-based organic electrolytes[J]. *Advanced energy materials*, 2015, 5(6):1401792.
- [97] Xiong S, Xie K, Blomberg E, et al. Analysis of the solid electrolyte interphase formed with an ionic liquid electrolyte for lithium-sulfur batteries[J]. *Journal of Power Sources*, 2014, 252:150–155.

- [98] Wu F, Zhu Q, Chen R, et al. Ionic liquid-based electrolyte with binary lithium salts for high performance lithium–sulfur batteries[J]. *Journal of Power Sources*, 2015, 296:10–17.
- [99] Wu F, Zhu Q, Chen R, et al. A safe electrolyte with counterbalance between the ionic liquid and tris (ethylene glycol) dimethyl ether for high performance lithium-sulfur batteries[J]. *Electrochimica Acta*, 2015, 184:356–363.
- [100] Zheng J, Gu M, Chen H, et al. Ionic liquid-enhanced solid state electrolyte interface (SEI) for lithium–sulfur batteries[J]. *Journal of Materials chemistry A*, 2013, 1(29):8464–8470.
- [101] Ma G, Wen Z, Jin J, et al. The enhanced performance of Li–S battery with P14YRTFSI-modified electrolyte[J]. *Solid State Ionics*, 2014, 262:174–178.
- [102] Bresser D, Passerini S, Scrosati B. Recent progress and remaining challenges in sulfur-based lithium secondary batteries—a review[J]. *Chemical communications*, 2013, 49(90):10545–10562.
- [103] Zhang S S, Tran D T. How a gel polymer electrolyte affects performance of lithium/sulfur batteries[J]. *Electrochimica Acta*, 2013, 114:296–302.
- [104] Hassoun J, Scrosati. Moving to a solid-state configuration: a valid approach to making lithium-sulfur batteries viable for practical applications[J]. *Advanced Materials*, 2010, 22(45):5198–5201.
- [105] Jeong S, Lim Y, Choi Y, et al. Electrochemical properties of lithium sulfur cells using PEO polymer electrolytes prepared under three different mixing conditions[J]. *Journal of Power Sources*, 2007, 174(2):745–750.
- [106] Villaluenga I, Wujcik K H, Tong W, et al. Compliant glass–polymer hybrid single ion-conducting electrolytes for lithium batteries[J]. *Proceedings of the National Academy of Sciences*, 2016, 113(1):52–57.
- [107] Nagao M, Imade Y, Narisawa H, et al. All-solid-state Li–sulfur batteries with mesoporous electrode and thio-LISICON solid electrolyte[J]. *Journal of Power Sources*, 2013, 222:237–242.

- [108] Nagao M, Suzuki K, Imade Y, et al. All-solid-state lithium–sulfur batteries with three-dimensional mesoporous electrode structures[J]. *Journal of Power Sources*, 2016, 330:120–126.
- [109] Yamada T, Ito S, Omoda R, et al. All solid-state lithium–sulfur battery using a glass-type P_2S_5 – Li_2S electrolyte: benefits on anode kinetics[J]. *Journal of The Electrochemical Society*, 2015, 162(4):A646.
- [110] Agostini M, Aihara Y, Yamada T, et al. A lithium–sulfur battery using a solid, glass-type P_2S_5 – Li_2S electrolyte[J]. *Solid State Ionics*, 2013, 244:48–51.
- [111] Trevey J E, Jung Y S, Lee S-H J E A. High lithium ion conducting Li_2S – GeS_2 – P_2S_5 glass–ceramic solid electrolyte with sulfur additive for all solid-state lithium secondary J]. *Electrochimica Acta*, 2011, 56(11):4243–4247.
- [112] Kamaya N, Homma K, Yamakawa Y, et al. A lithium superionic conductor[J]. *Nature materials*, 2011, 10(9):682–686.
- [113] Su Y-S, Manthiram A. A new approach to improve cycle performance of rechargeable lithium–sulfur batteries by inserting a free-standing MWCNT interlayer[J]. *Chemical communications*, 2012, 48(70):8817–8819.
- [114] Li Z, Yuan L, Yi Z, et al. Confined selenium within porous carbon nanospheres as cathode for advanced Li–Se batteries[J]. *Nano Energy*, 2014, 9:229–236.
- [115] Chung S H, Manthiram A. A natural carbonized leaf as polysulfide diffusion inhibitor for highperformance lithium–sulfur battery cells [J]. *ChemSusChem*, 2014, 7(6):1655–1661.
- [116] Chung S H, Manthiram A. Carbonized eggshell membrane as a natural polysulfide reservoir for highly reversible li-S batteries[J]. *Advanced materials*, 2014, 26(9):1360–1365.
- [117] Wang X, Wang Z, Chen L. Reduced graphene oxide film as a shuttle-inhibiting interlayer in a lithium–sulfur battery[J]. *Journal of Power Sources*, 2013, 242:65–69.

- [118] Zhang K, Qin F, Fang J, et al. Nickel foam as interlayer to improve the performance of lithium–sulfur battery[J]. *Journal of Solid State Electrochemistry*, 2014, 18(4):1025–1029.
- [119] Ma G, Wen Z, Wang Q, et al. Enhanced performance of lithium sulfur battery with self-assembly polypyrrole nanotube film as the functional interlayer[J]. *Journal of Power Sources*, 2015, 273:511–516.
- [120] Balach J, Jaumann T, Klose M, et al. Mesoporous carbon interlayers with tailored pore volume as polysulfide reservoir for high-energy lithium–sulfur batteries[J]. *The Journal of Physical Chemistry C*, 2015, 119(9):4580–4587.
- [121] Su Y-S, Manthiram A. Lithium–sulphur batteries with a microporous carbon paper as a bifunctional interlayer[J]. *Nature communications*, 2012, 3(1):1–6.
- [122] Chung S H, Manthiram A. Bifunctional separator with a light-weight carbon-coating for dynamically and statically stable lithium-sulfur batteries [J]. *Advanced Functional Materials*, 2014,24(33):5299–5306.
- [123] Balach J, Jaumann T, Klose M, et al. Functional mesoporous carbon-coated separator for longlife, high-energy lithium–sulfur batteries[J]. *Advanced Functional Materials*, 2015, 25(33):5285–5291.
- [124] Ma G, Huang F, Wen Z, et al. Enhanced performance of lithium sulfur batteries with conductive polymer modified separators[J]. *Journal of Materials Chemistry A*, 2016, 4(43):16968–16974.
- [125] Li G, Jing H, Su Z, et al. A hydrophilic separator for high performance lithium sulfur batteries[J]. *Journal of Materials Chemistry A*, 2015, 3(20):11014–11020.
- [126] Li J, Huang Y, Zhang S, et al. Decoration of silica nanoparticles on polypropylene separator for lithium–sulfur batteries[J]. *ACS applied materials & interfaces*, 2017, 9(8):7499–7504.
- [127] Ghazi Z A, He X, Khattak A M, et al. MoS₂/Celgard separator as efficient polysulfide barrier for long-life lithium–sulfur batteries[J]. *Advanced Materials*, 2017, 29(21):1606817.

- [128] Liu J, Yuan L, Yuan K, et al. SnO₂ as a high-efficiency polysulfide trap in lithium–sulfur batteries[J]. *Nanoscale*, 2016, 8(28):13638–13645.
- [129] Balach J, Jaumann T, Klose M, et al. Improved cycling stability of lithium–sulfur batteries using a polypropylene-supported nitrogen-doped mesoporous carbon hybrid separator as polysulfide adsorbent[J]. *Journal of Power Sources*, 2016, 303:317–324.
- [130] Chang C H, Chung S H, Manthiram A. Effective stabilization of a high-loading sulfur cathode and a lithium-metal anode in Li-S batteries utilizing SWCNT-modulated separators[J]. *Small*, 2016, 12(2):174–179.
- [131] Zhou X, Liao Q, Tang J, et al. A high-level N-doped porous carbon nanowire modified separator for long-life lithium–sulfur batteries[J]. *Journal of Electroanalytical Chemistry*, 2016, 768:55–61.
- [132] Zhou G, LI L, Wang D W, et al. A flexible sulfur-graphene-polypropylene separator integrated electrode for advanced Li–batteries[J]. *Advanced Materials*, 2015, 27(4):641–647.
- [133] Vizintin A, Patel M U, Genorio B, et al. Effective separation of lithium anode and sulfur cathode in lithium–sulfur batteries[J]. *ChemElectroChem*, 2014, 1(6):1040–1045.
- [134] Yao H, Yan K, Li W, et al. Improved lithium–sulfur batteries with a conductive coating on the separator to prevent the accumulation of inactive S-related species at the cathode–separator interface[J]. *Energy & Environmental Science*, 2014, 7(10):3381–3390.
- [135] Qian X, Jin L, Zhao D, et al. Ketjen black-MnO composite coated separator for high performance rechargeable lithium-sulfur battery[J]. *Electrochimica Acta*, 2016, 192:346–356.
- [136] Zhang Z, Lai Y, Zhang Z, et al. Al₂O₃-coated porous separator for enhanced electrochemical performance of lithium sulfur batteries[J]. *Electrochimica Acta*, 2014, 129:55–61.

- [137] Tang H, Yao S, Mi J, et al. Ketjen Black/Mg_{0.6}Ni_{0.4}O composite coated separator for lithium-sulfur batteries with enhanced electrochemical performance[J]. *Materials Letters*, 2017, 186:127–130.
- [138] Li W, Hicks-Garner J, Wang J, et al. V₂O₅ polysulfide anion barrier for long-lived Li–S batteries[J]. *Chemistry of Materials*, 2014, 26(11):3403–3410.
- [139] Wang Q, Wen Z, Yang J, et al. Electronic and ionic co-conductive coating on the separator towards high-performance lithium–sulfur batteries[J]. *Journal of Power Sources*, 2016, 306:347–353.
- [140] Song R, Fang R, Wen L, et al. A trilayer separator with dual function for high performance lithium–sulfur batteries[J]. *Journal of Power Sources*, 2016, 301:179–186.
- [141] Wu F, Ye Y, Chen R, et al. Systematic effect for an ultralong cycle lithium–sulfur battery[J]. *Nano letters*, 2015, 15(11):7431–7439.
- [142] Cai W, Li G, He F, et al. A novel laminated separator with multi functions for high-rate dischargeable lithium–sulfur batteries[J]. *Journal of Power Sources*, 2015, 283:524–529.
- [143] Huang J-Q, Zhang Q, Peng H-J, et al. Ionic shield for polysulfides towards highly-stable lithium–sulfur batteries[J]. *Energy & environmental science*, 2014, 7(1):347–353.
- [144] Epp J. X-ray diffraction (XRD) techniques for materials characterization [M]. *Materials characterization using nondestructive evaluation (NDE) methods*. Elsevier. 2016: 81-124.
- [145] Ali A S. Application of nanomaterials in environmental improvement [M]. *Nanotechnology and the Environment*. IntechOpen. 2020.
- [146] Inkson B. Scanning electron microscopy (SEM) and transmission electron microscopy (TEM) for materials characterization [M]. *Materials characterization using nondestructive evaluation (NDE) methods*. Elsevier. 2016: 17-43.

- [147] Brame J A, Griggs C S. Surface area analysis using the Brunauer-Emmett-Teller (BET) method: scientific operation procedure series: SOP-C [J]. 2016,
- [148] Liu X, Huang J Q, Zhang Q, et al. Nanostructured metal oxides and sulfides for lithium–sulfur batteries[J]. *Advanced materials*, 2017, 29(20):1601759.
- [149] Zhao M, Peng H J, Zhang Z W, et al. Activating inert metallic compounds for high-rate lithium–sulfur batteries through in situ etching of extrinsic metal[J]. *Angewandte Chemie International Edition*, 2019, 58(12):3779–3783 .
- [150] Zheng G, Zhang Q, Cha J J, et al. Amphiphilic surface modification of hollow carbon nanofibers for improved cycle life of lithium sulfur batteries[J]. *Nano letters*, 2013, 13(3):1265–1270.
- [151] Lv X, Lei T, Wang B, et al. An Efficient Separator with Low Li-Ion Diffusion Energy Barrier Resolving Feeble Conductivity for Practical Lithium–Sulfur Batteries[J]. *Advanced Energy Materials*, 2019, 9(40):1901800.
- [152] Meng Z, Zhang S, Wang J, et al. Nickel-based-hydroxide-wrapped activated carbon cloth/sulfur composite with tree-bark-like structure for high-performance freestanding sulfur cathode[J]. *ACS Applied Energy Materials*, 2018, 1(4):1594–1602.
- [153] Rui X, Lu Z, Yu H, et al. Ultrathin V_2O_5 nanosheet cathodes: realizing ultrafast reversible lithium storage[J]. *Nanoscale*, 2013, 5(2):556–560.
- [154] Zhao X, Yu R, Tang H, et al. Formation of Septuple-Shelled $(Co_{2/3}Mn_{1/3})(Co_{5/6}Mn_{1/6})_2O_4$ Hollow Spheres as Electrode Material for Alkaline Rechargeable Battery[J]. *Advanced Materials*, 2017, 29(34):1700550.
- [155] Liu E-H, Li W, Li J, et al. Preparation and characterization of nanostructured NiO/MnO₂ composite electrode for electrochemical supercapacitors[J]. *Materials Research Bulletin*, 2009, 44(5):1122–1126.
- [156] Tian D, Lu X, Nie G, et al. Direct growth of Ni–Mn–O nanosheets on flexible electrospun carbon nanofibers for high performance supercapacitor applications[J]. *Inorganic Chemistry Frontiers*, 2018, 5(3):635–642.

- [157] Hao S, Zhang B, Feng J, et al. Nanoscale ion intermixing induced activation of Fe₂O₃/MnO₂ composites for application in lithium ion batteries[J]. *Journal of Materials Chemistry A*, 2017, 5(18):8510–8518.
- [158] Wang R, Yan X. Superior asymmetric supercapacitor based on Ni-Co oxide nanosheets and carbon nanorods[J]. *Scientific reports*, 2014, 4(1):1–9.
- [159] Chen H, Jiang G, Yu W, et al. Electrospun carbon nanofibers coated with urchin-like ZnCo₂O₄ nanosheets as a flexible electrode material[J]. *Journal of Materials Chemistry A*, 2016, 4(16):5958–5964.
- [160] Gao G, Wu H B, Lou X W. Citrate-assisted growth of NiCo₂O₄ nanosheets on reduced graphene oxide for highly reversible lithium storage[J]. *Advanced Energy Materials*, 2014, 4(14):1400422.
- [161] Yuan C, Wu H B, Xie Y, et al. Mixed transition-metal oxides: design, synthesis, and energy-related applications[J]. *Angewandte Chemie International Edition*, 2014, 53(6):1488–1504.
- [162] Hu L, Wu L, Liao M, et al. Electrical transport properties of large, individual NiCo₂O₄ nanoplates[J]. *Advanced Functional Materials*, 2012, 22(5):998–1004.
- [163] Chen Y, Qu B, Hu L, et al. High-performance supercapacitor and lithium-ion battery based on 3D hierarchical NH₄F-induced nickel cobaltate nanosheet–nanowire cluster arrays as self-supported electrodes[J]. *Nanoscale*, 2013, 5(20):9812–9820.
- [164] Li L, Cheah Y, Ko Y, et al. The facile synthesis of hierarchical porous flower-like NiCo₂O₄ with superior lithium storage properties[J]. *Journal of Materials chemistry A*, 2013, 1(36):10935–10941.
- [165] Cui B, Lin H, Li J B, et al. Core–ring structured NiCo₂O₄ nanoplatelets: synthesis, characterization, and electrocatalytic applications[J]. *Advanced Functional Materials*, 2008, 18(9):1440–1447.

Research Results Obtained During the Study for Doctoral Degree

- [1] S. Abualela, X. Lv, Y. Hu, M. Dirar Abd-Alla. NiO nanosheets grown on carbon cloth as mesoporous cathode for High-performance lithium-sulfur battery [J]. *Materials Letters*. 2020, 127622, 268. (SCI, IF:3.204).
- [2] S. Abualela, X. Lv, Y. Hu, Mu. Dirar Abd-Alla, S. S. Ewakeel, A. K. Mohamed. Mesoporous NiCo₂O₄ nanoparticles as cathode additive for high-performance lithium sulfur battery [C]. In *Journal of Physics: Conference Series*, vol. 1707, no. 1, p. 012006. IOP Publishing, 2020 (EI, Conference)
- [3] Azza Osman, Mubarak Dirar Abd-Alla, Sohad S. Ewakeel, S. Abualela, and Adam Khalifa Mohamed. Process Photocatalytic Treatment of Rhodamine 6G in Wastewater Using Nickel Oxide (NiO) [J]. *Materials Research Express*. Under review (SCI, IF:1.609).
- [4] Nisreen A. Elthair, Eltayeb M. Mustafa, S. Abualela, and Abdelrahman A. Elbadawi. The Structural, Electrical and Optical Properties of Zn_{0.5}Li_{2x}Mn_{0.5-x}Fe₂O₄ by Co-Precipitation Method [J]. *RSC Advances*. Under review (SCI, IF:3.245).
- [5] Adam Khalifa Mohamed, Liu Dan¹, Song Kai, Elsiddig Eldaw, S. Abualela. Evaluating the suitability of groundwater for drinking purposes in the North Chengdu Plain, China [C]. *The 1st International Symposium on Water Resource and Environmental Management (WREM 2018)*. Online (EI, Conference).